Physics of the atmosphere

Lecture 4

THE TROPICS

B. Legras, legras@lmd.ens.fr,
http://www.lmd.ens.fr/legras/

2023

I Mean state and seasonal cycle

II The monsoon

III ENSO

IV Madden-Julian mode

V Equatorial waves

VI Tropical cyclones

Circulation générale de L'atmosphère

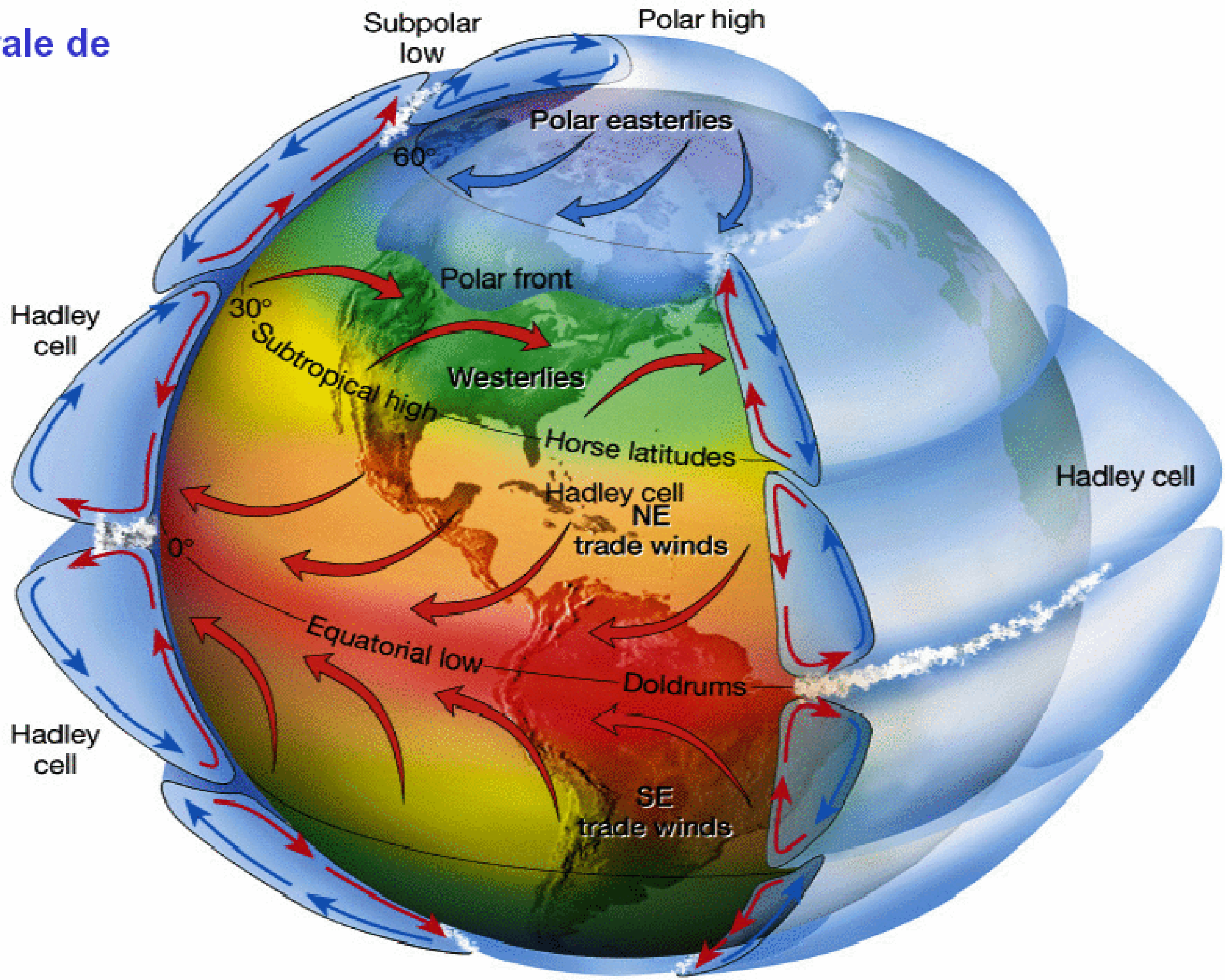

The tropics are homing the Hadley circulation : ascending motion near the equator l'équateur, descending motion at 30 N/S and trade wind easterlies near the ground.

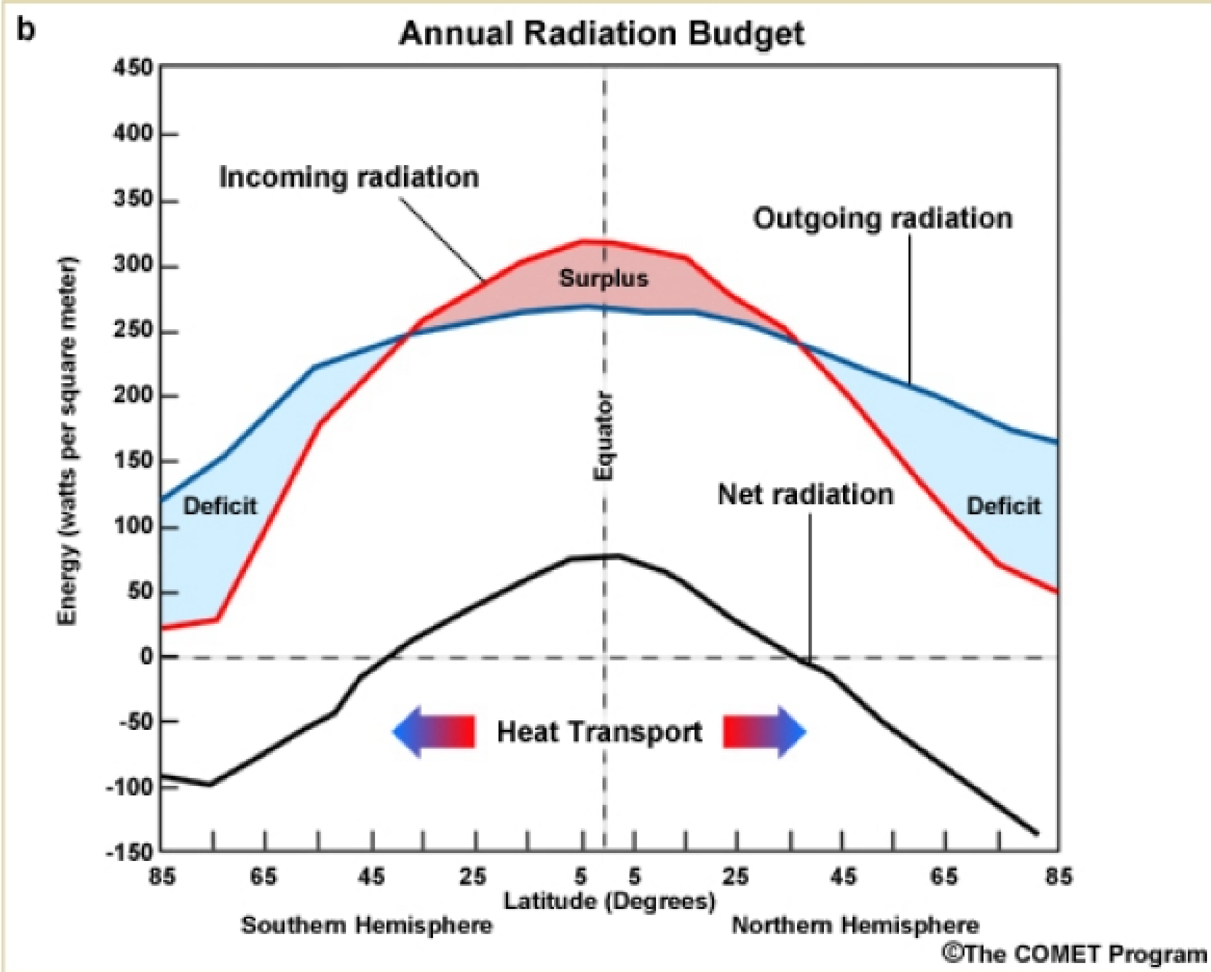

The tropics are the region where the radiative budget is positive

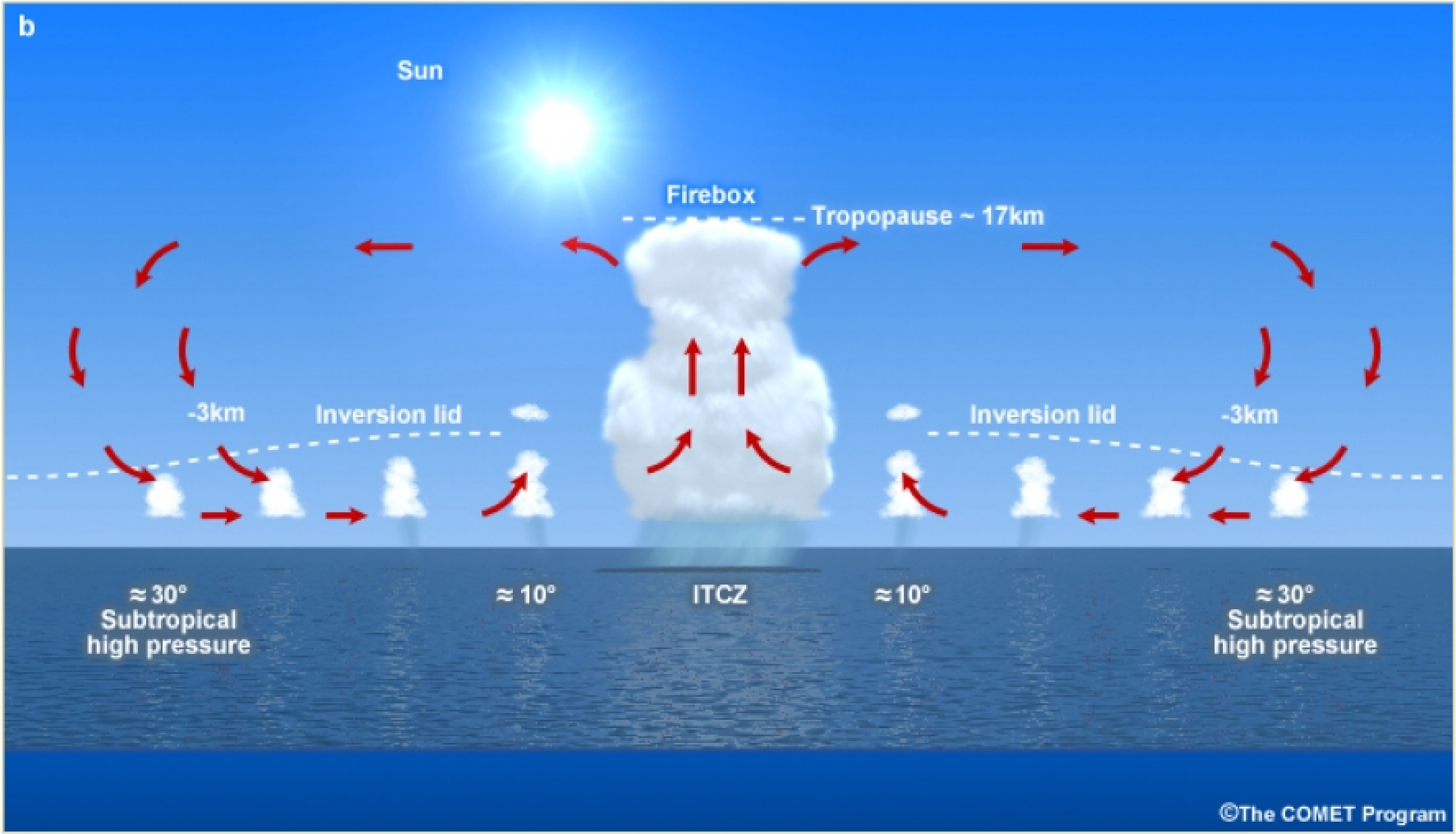
b
Sun
Firebox
Tropopause ~ 17km
-3km
Inversion lid
Inversion lid
-3km
≈ 30°
Subtropical
high pressure
≈ 10°
ITCZ
≈ 10°
≈ 30°
Subtropical
high pressure
©The COMET Program

Observations (1)

Distribution in latitude of wi
and temperature

- reinforcement of winter jets
- easterlies on the equator
- transport to the summer hemisphere
- weak temperature gradient in tl tropical zone

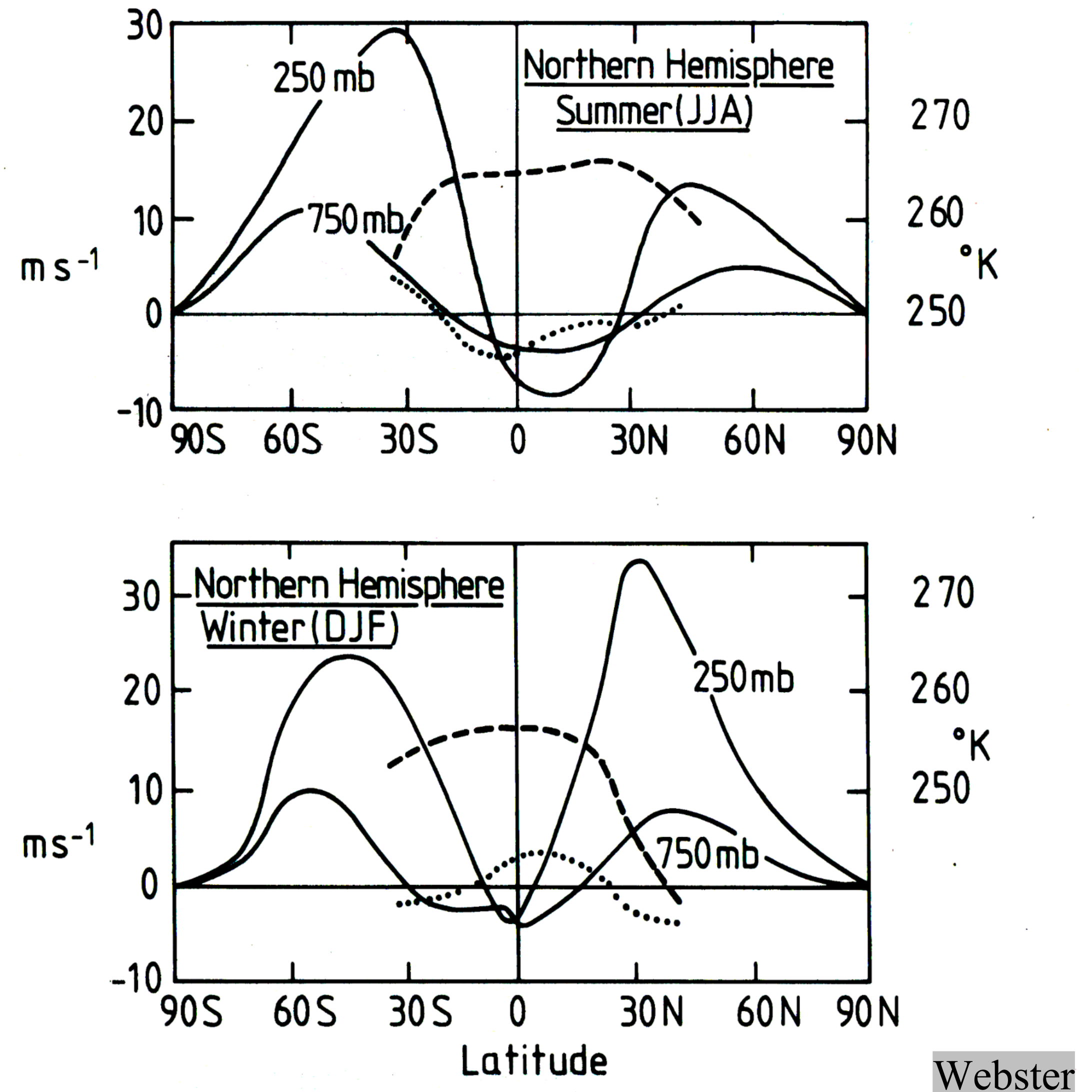

Fig. 9.1. The latitudinal distribution of the zonally averaged structure of the atmosphere for summer and winter. Solid lines refer to the 250 and 750 mb zonal wind fields, dashed curves to the 500 mb temperature field and dotted lines to the 250 mb meridional component of the wind.

Solid: zonal wind
Dotted: meridional wind at 250 hPa
Hash: temperature à 500 hPa

Observations (2)

Meridional section of the temperature

Very weak gradient in the tropical zone

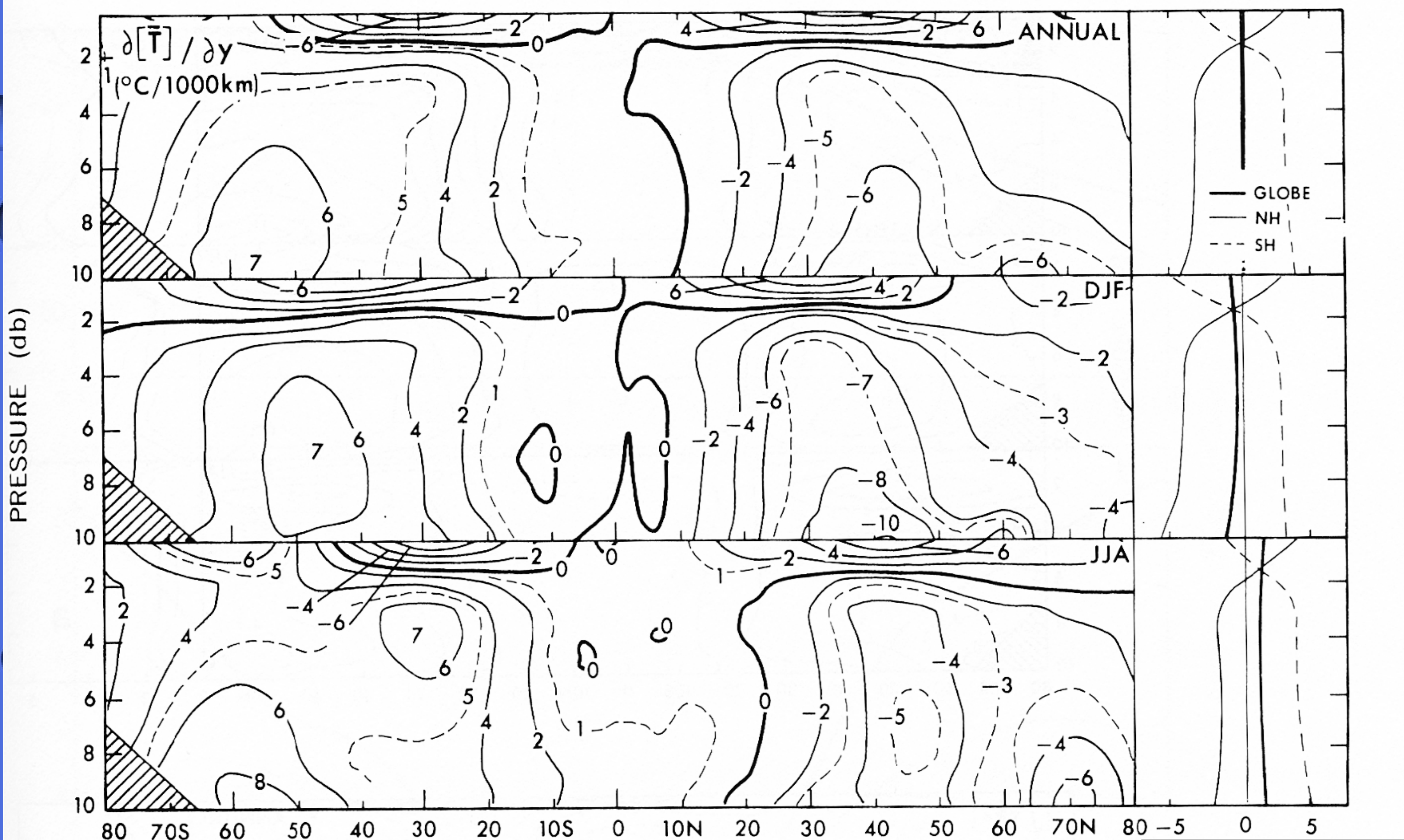

Peixoto & Oort, fig7.7

Observations (3)

Méridian section of the temperature variance

Weak variations in the tropical zone

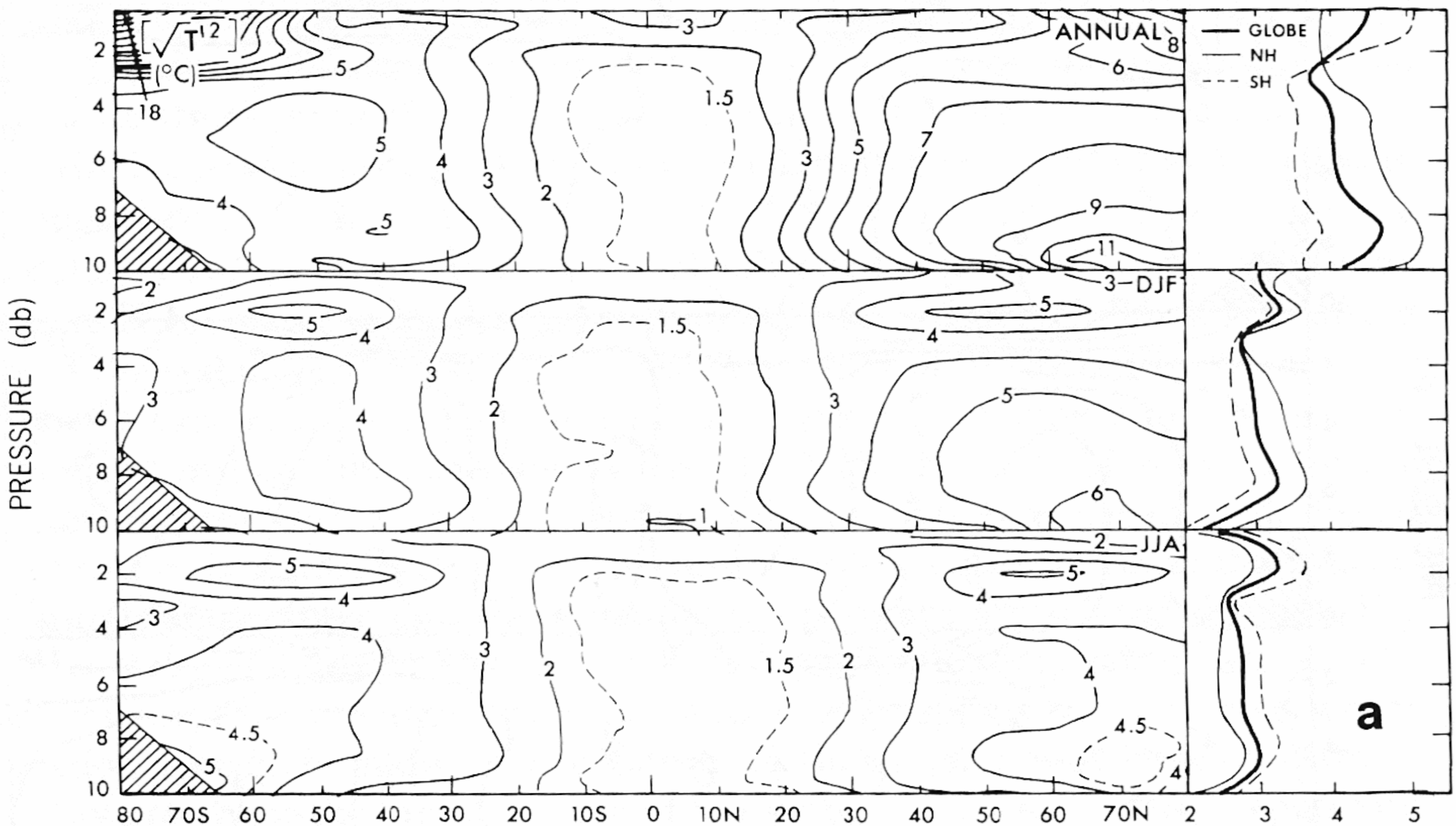

Peixoto & Oort, fig7.8

Observations (4)

Surface pressure variations are small and dominated by tides

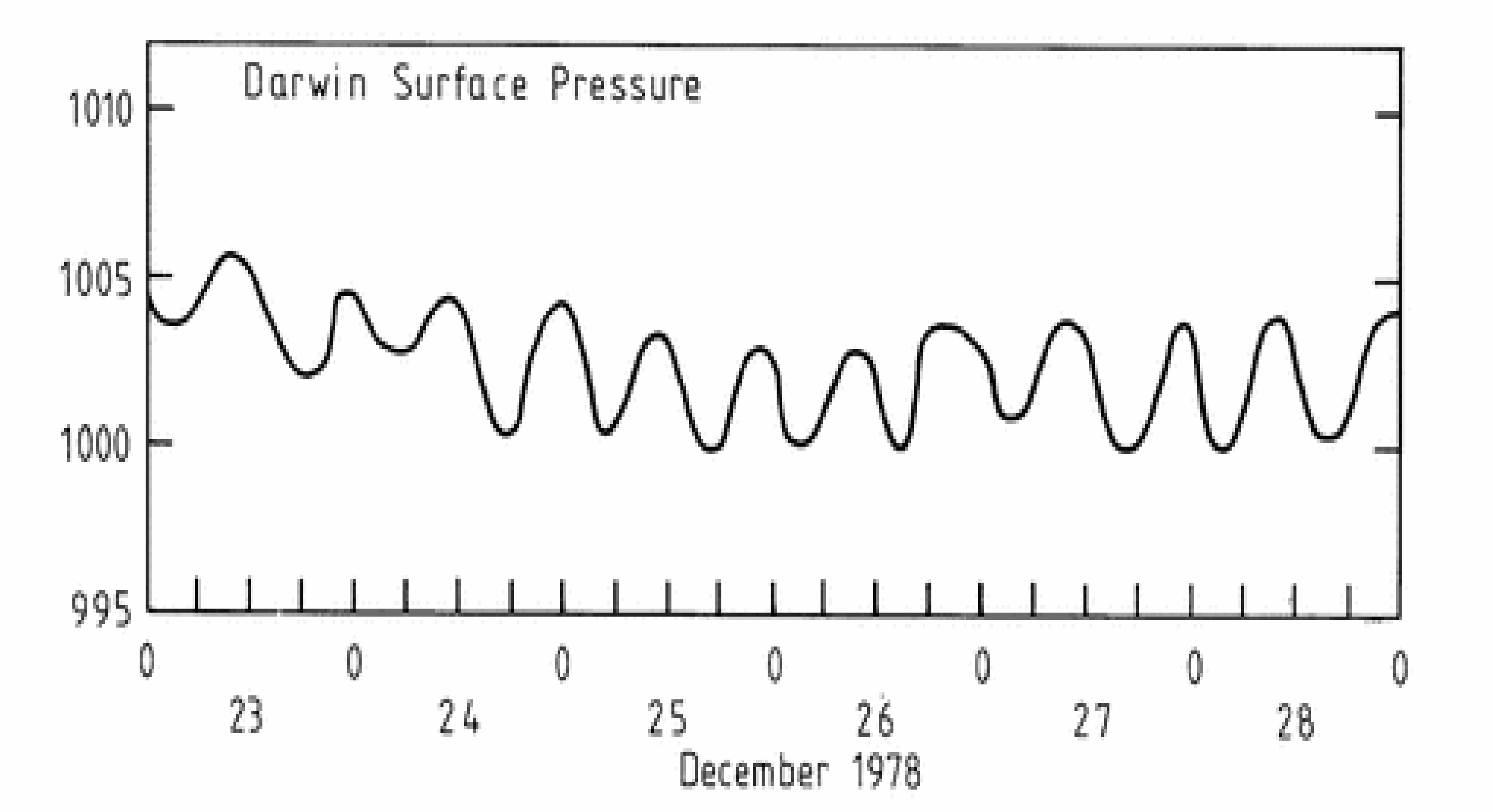

Webster, fig9.10

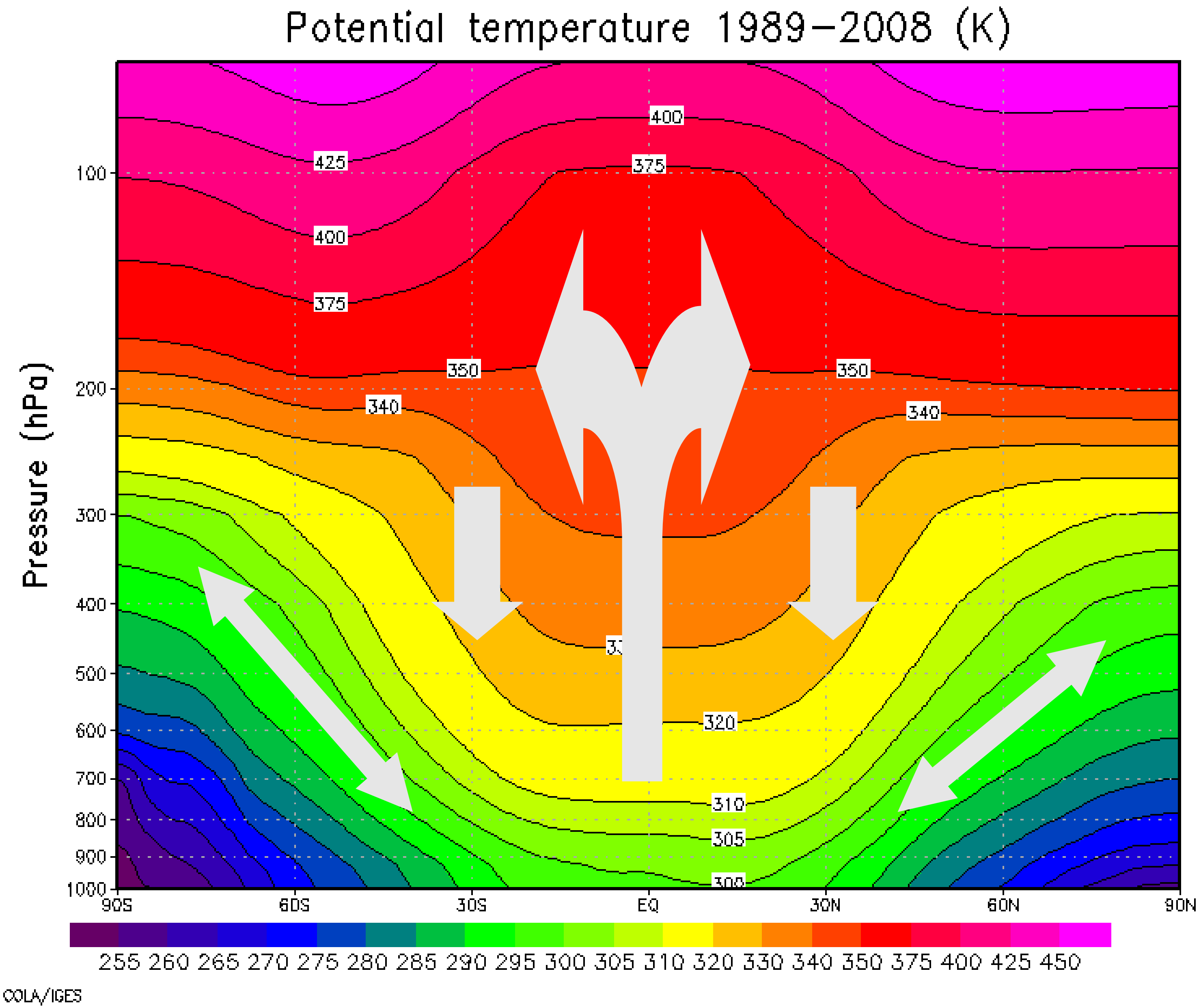

Tropical tropopause at 100 hPa (380K ou 17,5 km)

In the extra-tropical regions, adiabatic motion along isentropic surfaces can move air parcels between the ground and the tropopause. Within the tropics, horizontal temperature gradients are small and any vertical motion must be associated with heat exchange as it crosses isentropic surfaces

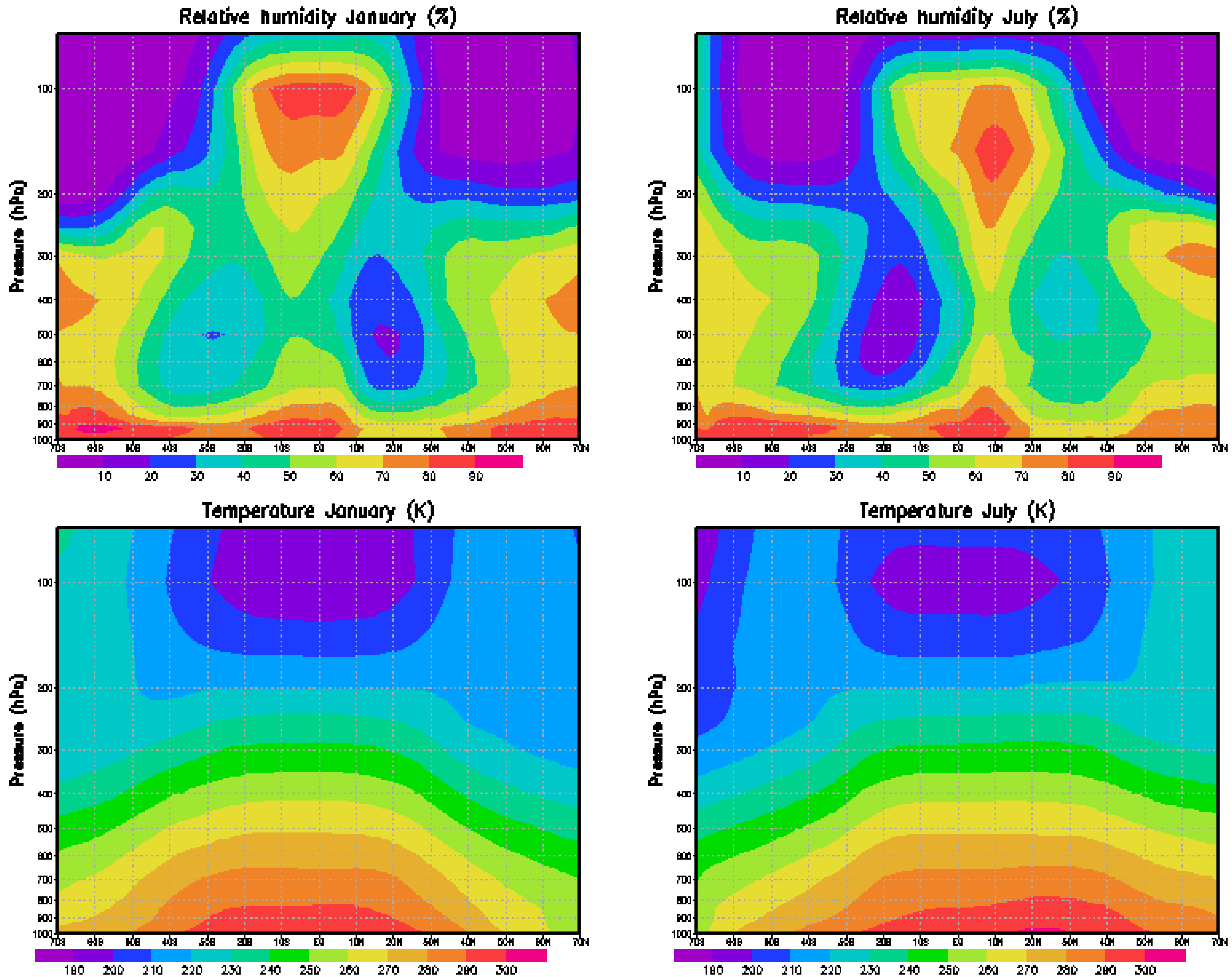

Relative moisture $H=r/r_S$

Deep convection in the tropics

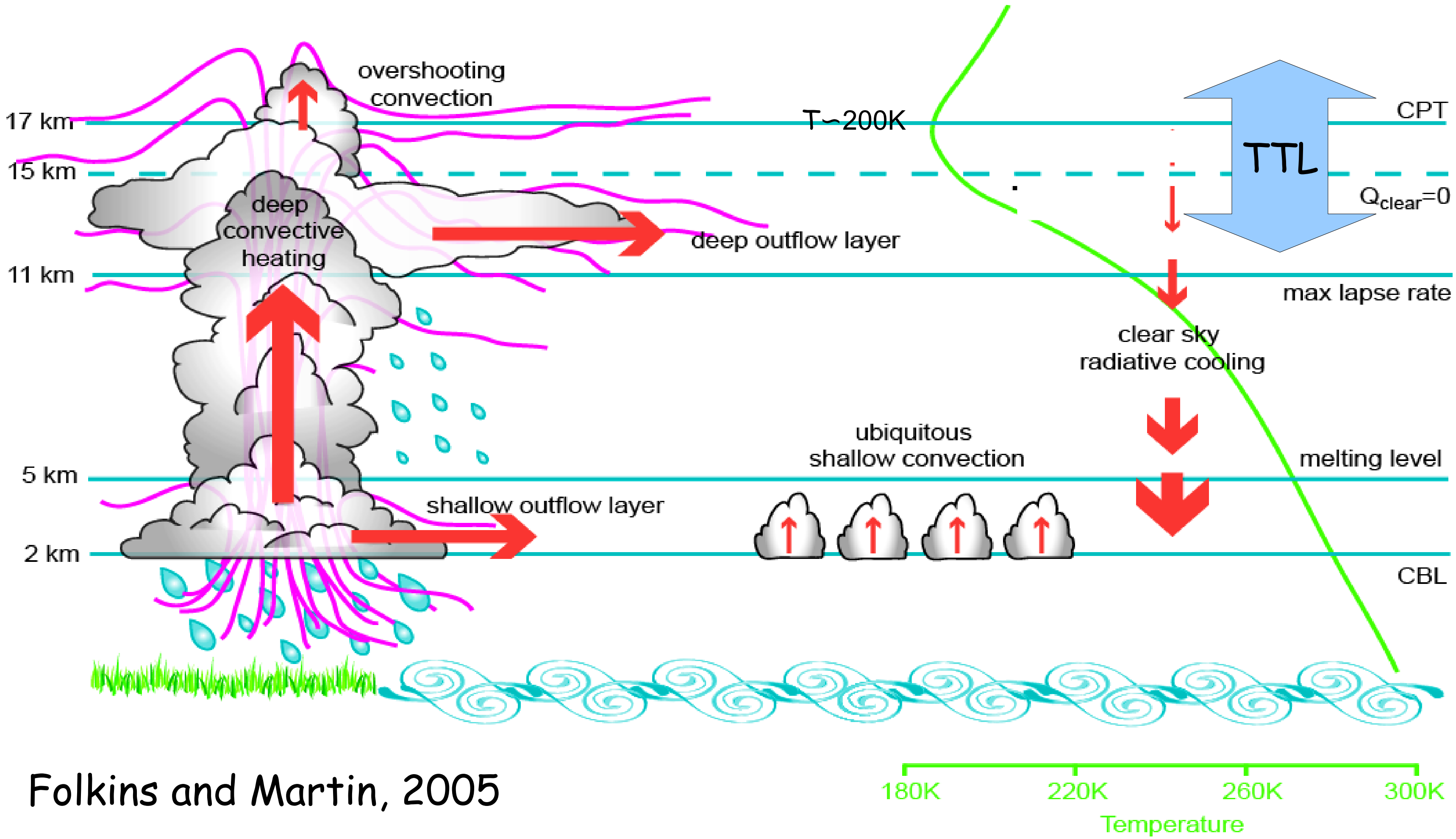

Folkins and Martin, 2005

Injection of the air by convection in the upper troposphere. Moisture in the middle tropical troposphere is regulated by the descent of the air detrained by clouds, evaporation of precipitations and exchanges with the mid-latitudes.

Water vapour
25 kg/m²
on average

Liquid water
80 g/m²
on average

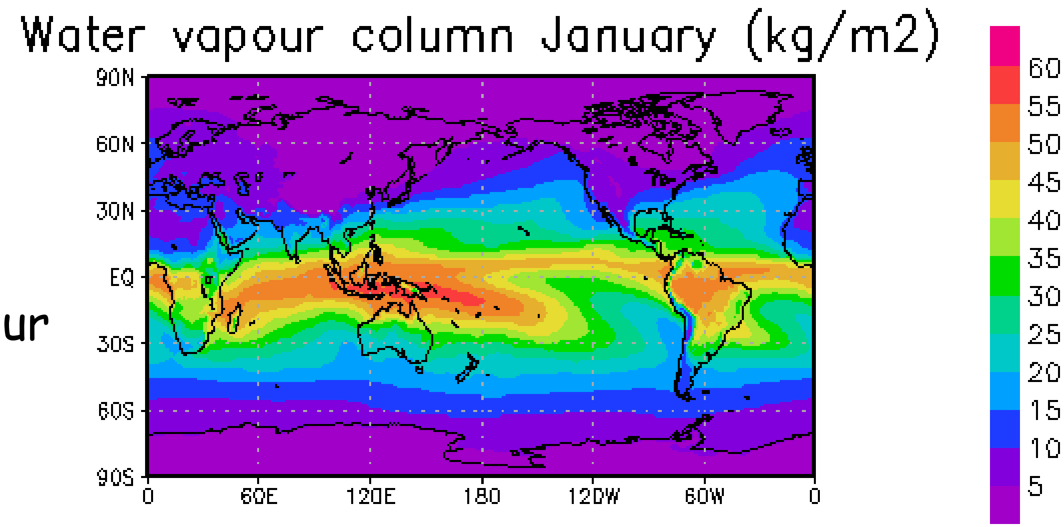

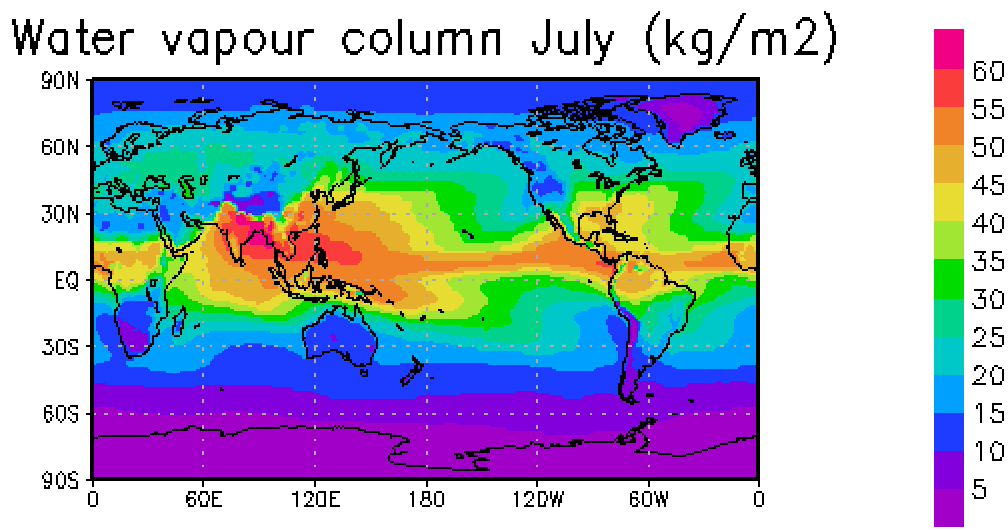

ECMWF ERA-Interim 1989-2008

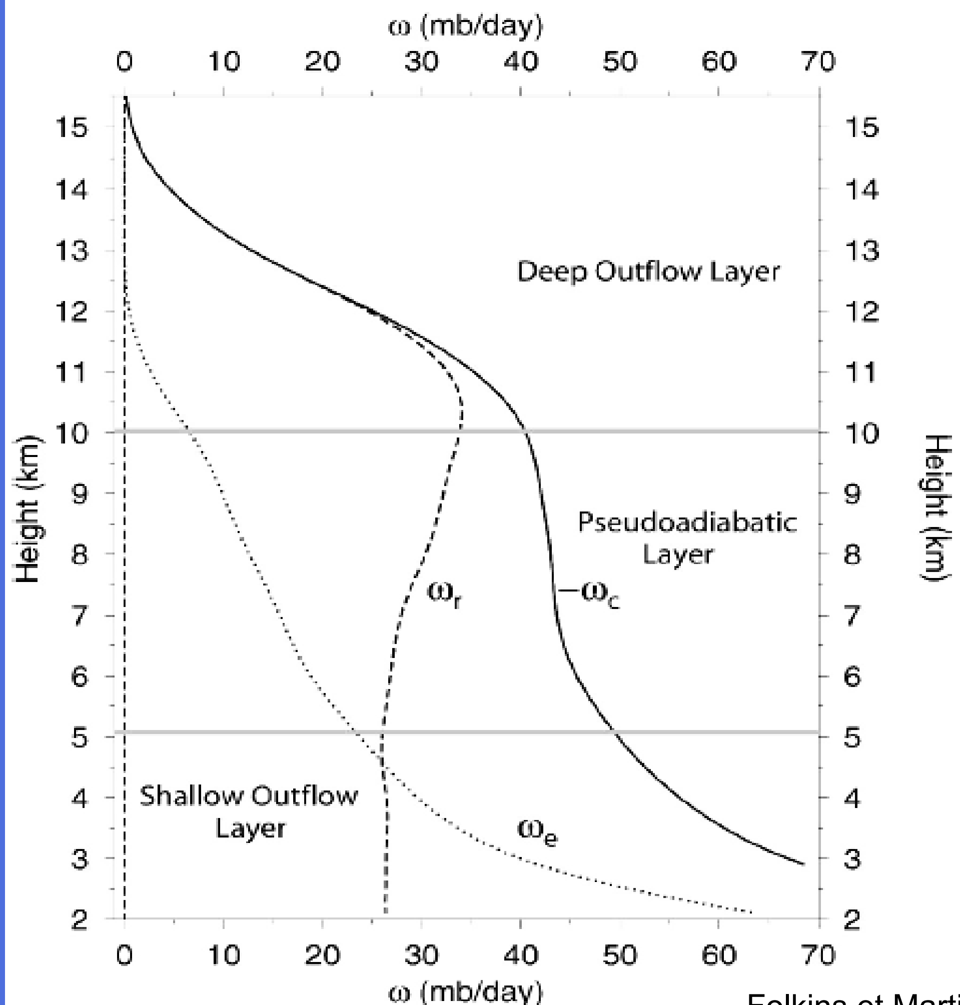

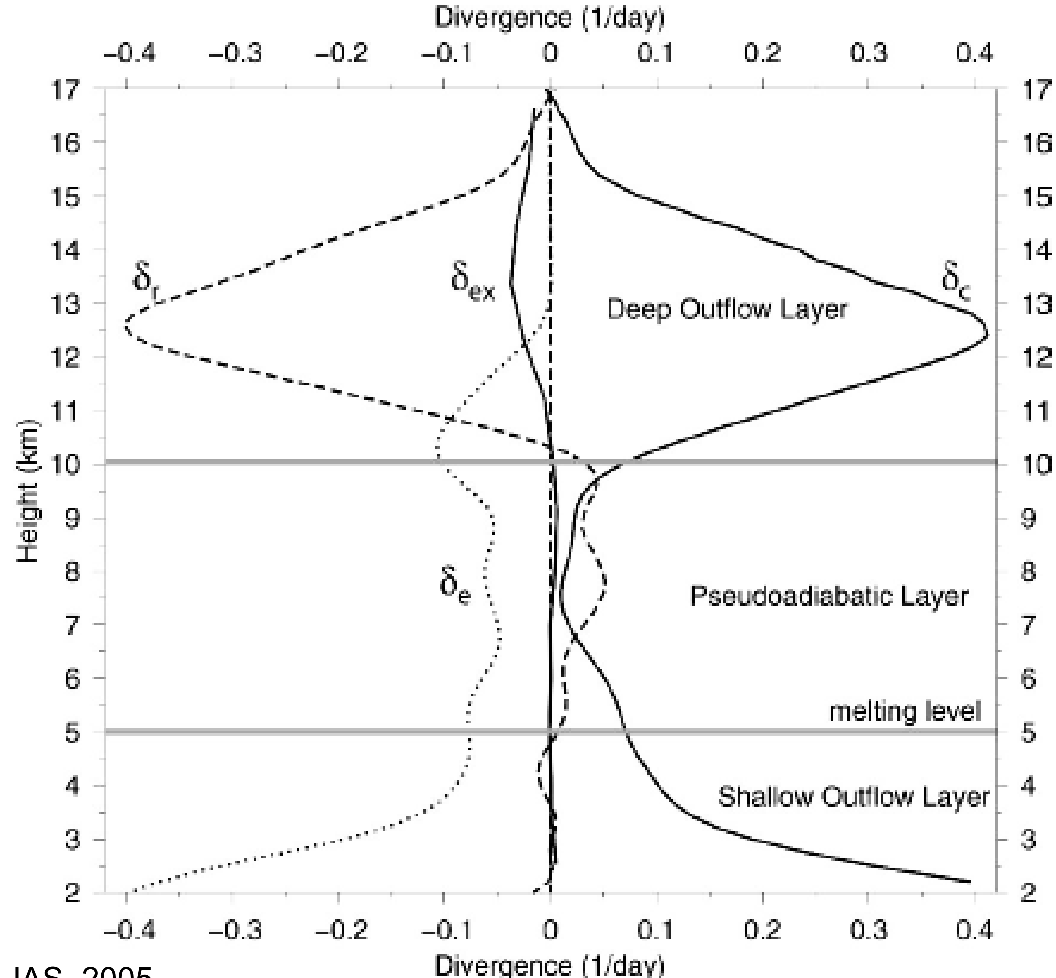

Folkins et Martin, JAS, 2005

Radiative, evaporative and radiative mass flux (over 20S-20N)

Radiative, evaporative and convective divergence (over 20S-20N)

$$\omega_r = \frac{Q_r}{\sigma} \qquad \omega_e = \frac{-Le}{c_p \sigma} \qquad \omega_c + \omega_r + \omega_e = 0$$

Q_r : radiative heating

e : evaporation

$$\sigma : \text{static stability } = -\frac{(\Gamma_d - \Gamma)}{\rho g} = \frac{T}{\theta}\frac{\partial \theta}{\partial p} = \frac{1}{c_p}\frac{\partial}{\partial p}(c_p T + g z)$$

$$\delta = -\frac{\partial \omega}{\partial p}$$

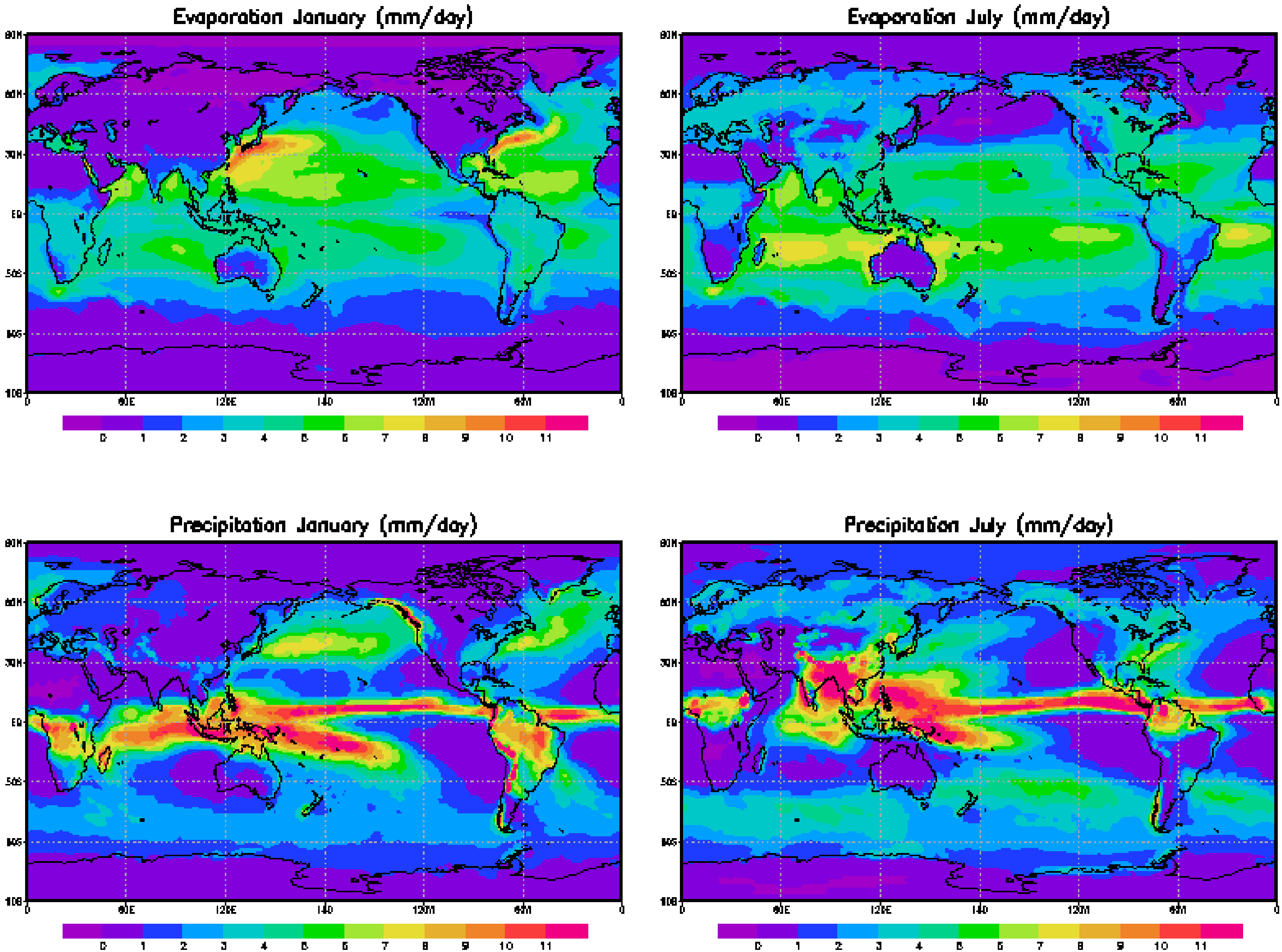

ECMWF ERA-Interim 1989-2008

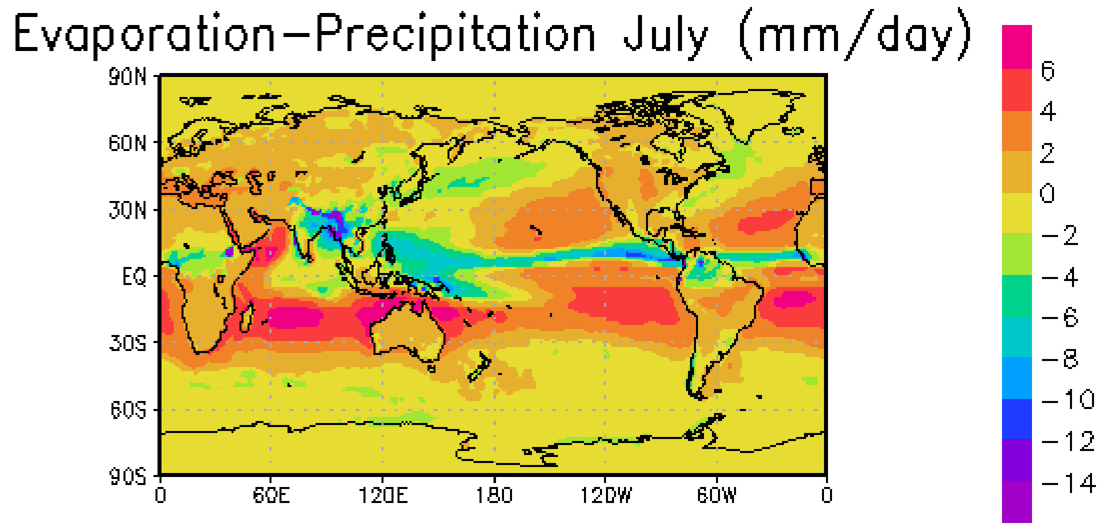

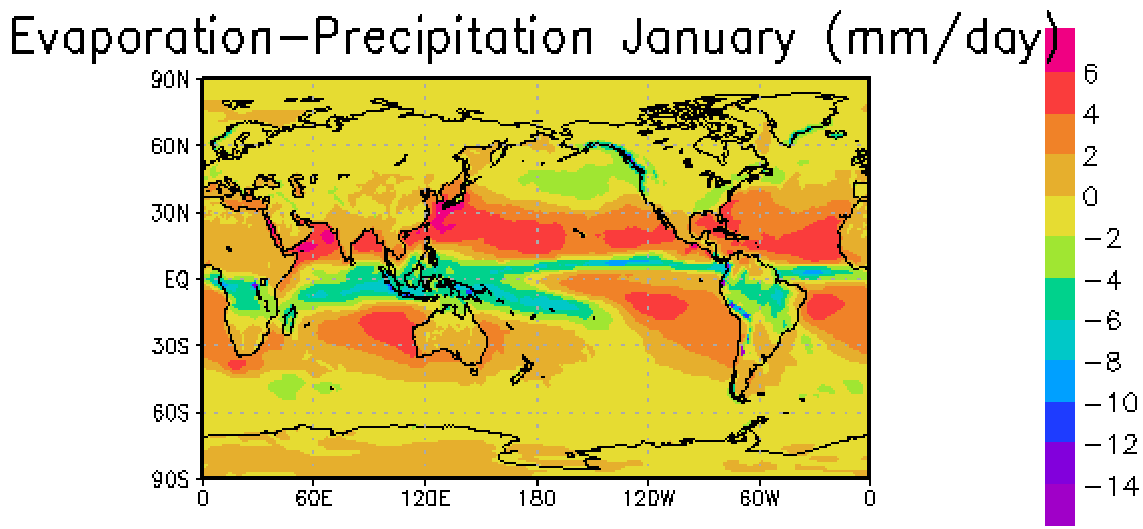

$E \sim C\,|V|\,(1 - H)\,r_s$ where H is relative moisture r/r_s above the surface.

E is contrained by the net radiative flux at the surface.

E is mainly distributed in the winter subtropical domain

Transport towards the ITCZ and convergence due to the trade winds and of the lower branch of the monsoon circulation.

II.3 Meridian Hadley circulation in the tropical region

Vertical velocity
$\omega = Dp/Dt$

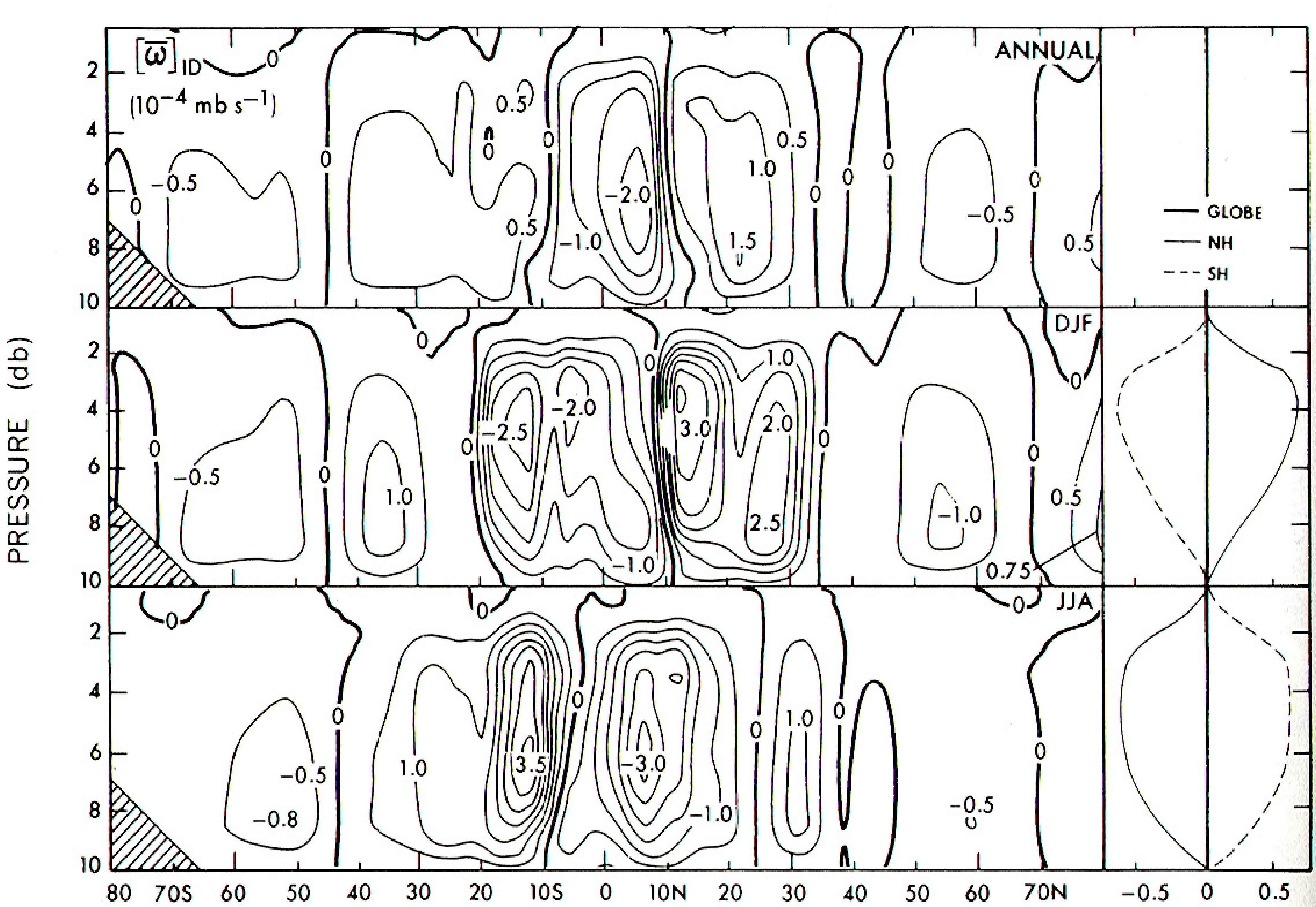

OLR in January and July

January
2001

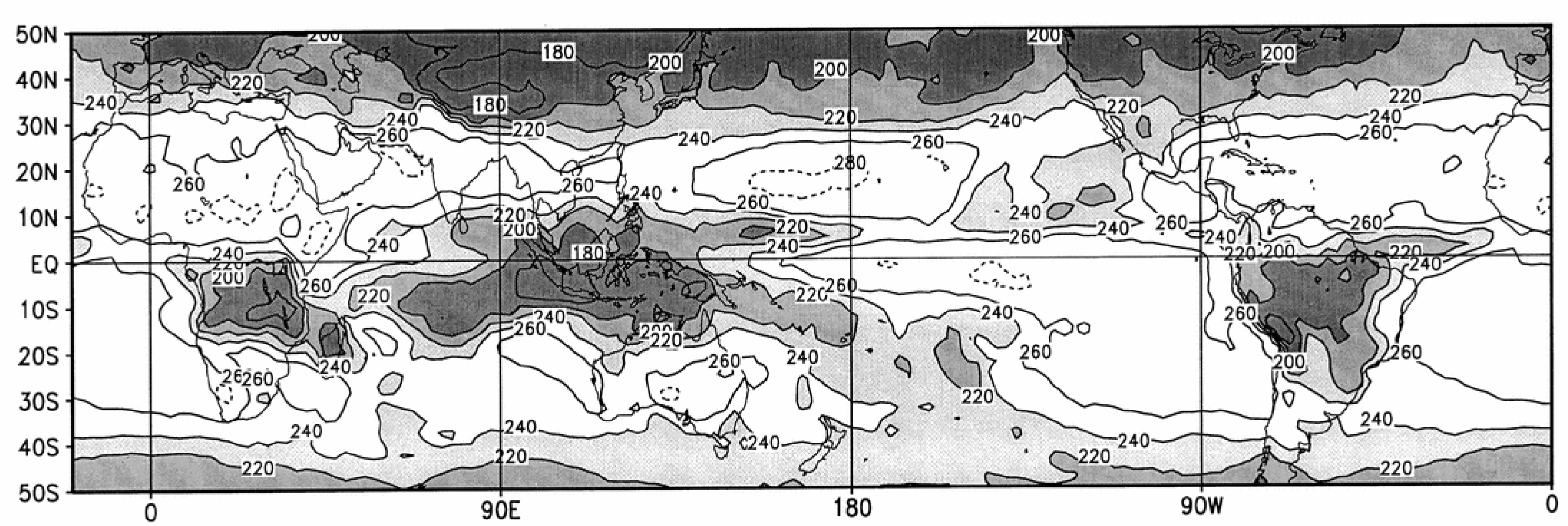

July
2001

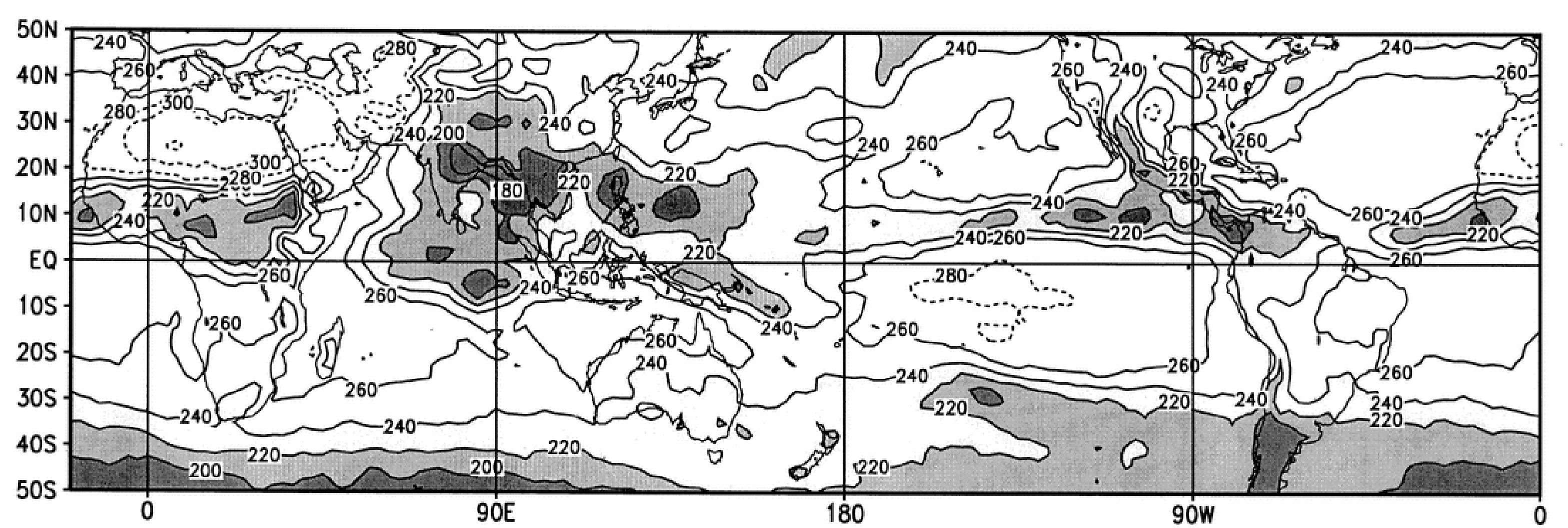

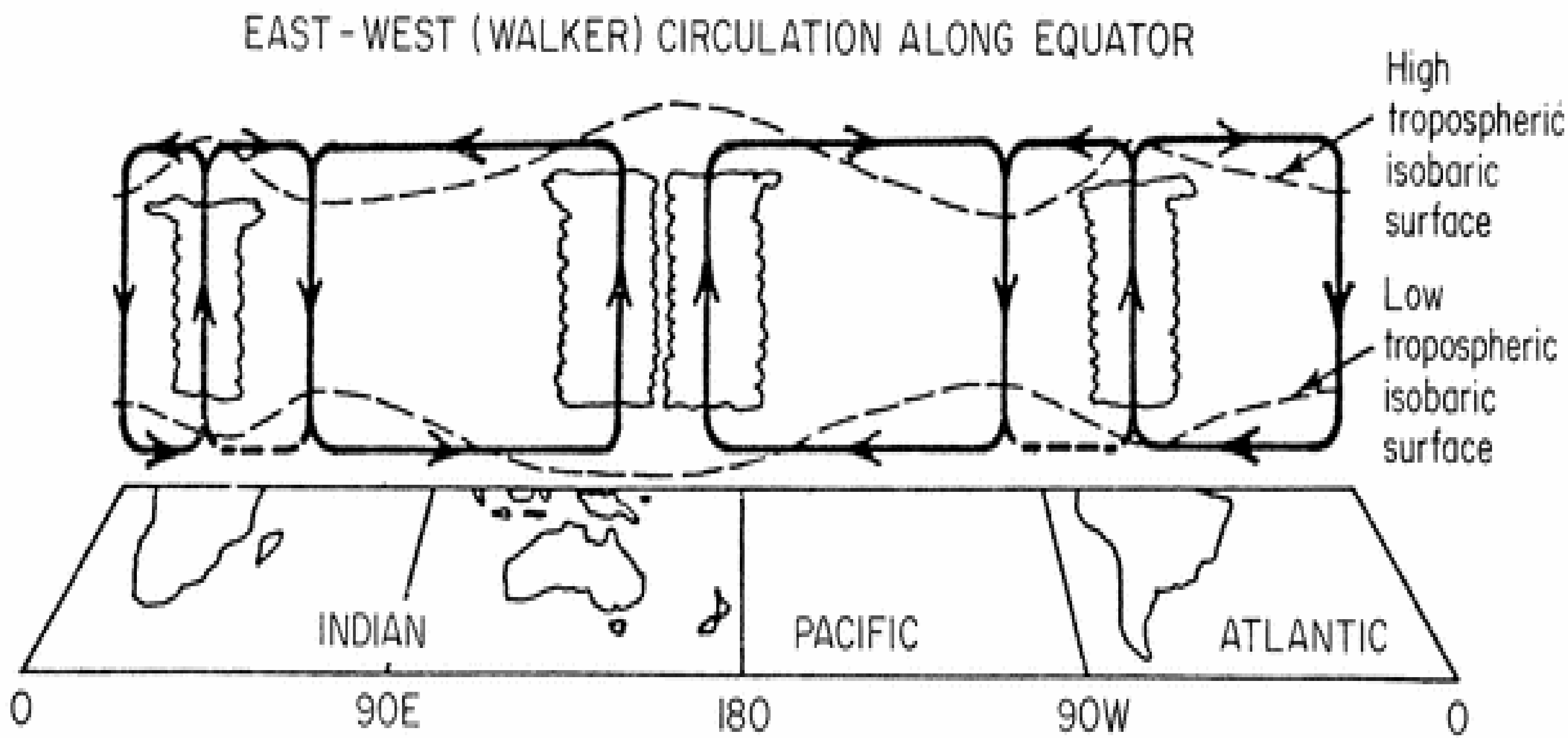

Fig. 9.4 Schematic view of the equatorial symmetric planetary scale features. Regions

The special conditions of the tropical region (15S-15N) (1)

- Small horizontal temperature variations
- Geopotential fluctuations and vertical velocities (excluding convective systems) are an order of magnitude lower than at temperate latitudes
- Strong convection/mesoscale/large-scale circulation interaction
- In convective zones, precipitation of the order of 2 cm / day or 20 kg per m^2, or (with $L = 2.5\ 10^6$ J kg^{-1}), a heating of the column of $5\ 10^7$ J m^{-2} day^{-1}. Assuming this heat is evenly distributed in the mass column $p_0/g \approx 10^4$ kg m^{-2}, the heating per unit mass of air is $J/cp \approx 5$ K day^{-1}. In practice, the unevenly distributed heating is 2 to 4 times larger, resulting in average speeds of the order of 3 to 5 cm s^{-1}, much stronger than outside convective systems. Locally, within convective towers, the ascent can reach several m s^{-1}
- Convergence of moisture in the convection zone (precipitation far exceeds local evaporation)

I Mean state and seasonal cycle

II The monsoon

III ENSO

IV Madden-Julian mode

V Equatorial waves

VI Tropical cyclones

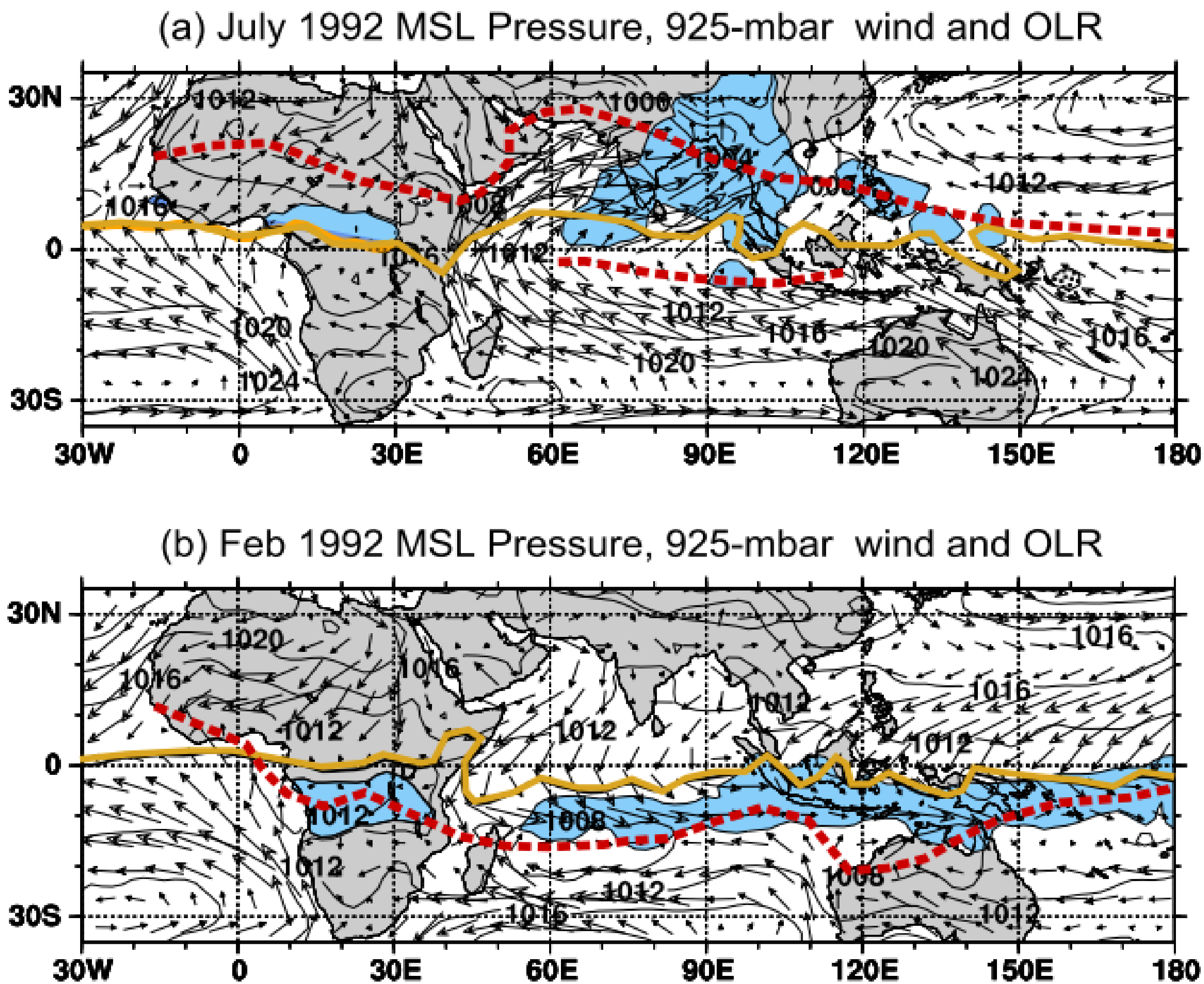

The monsoons, in Asia, Australia and Africa

Surface pressure and winds at 935 hPa 935 hPa. In blue : OLR < 200 W/m2.

Line of semi-permanent surface depressions in red

Webster

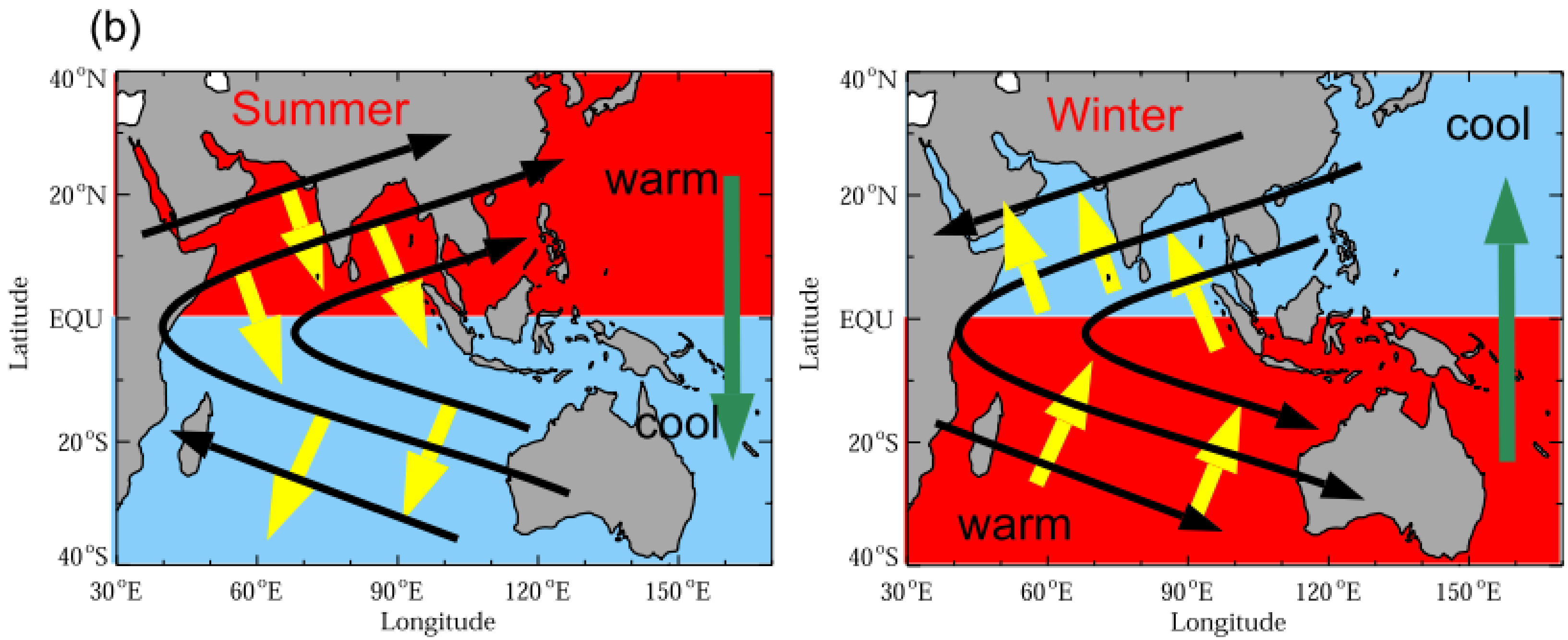

Wind and heat transport induced in the surface layer of the ocean (Ekman effect)

Divergent circulation of the monsoons in Asia and Australia

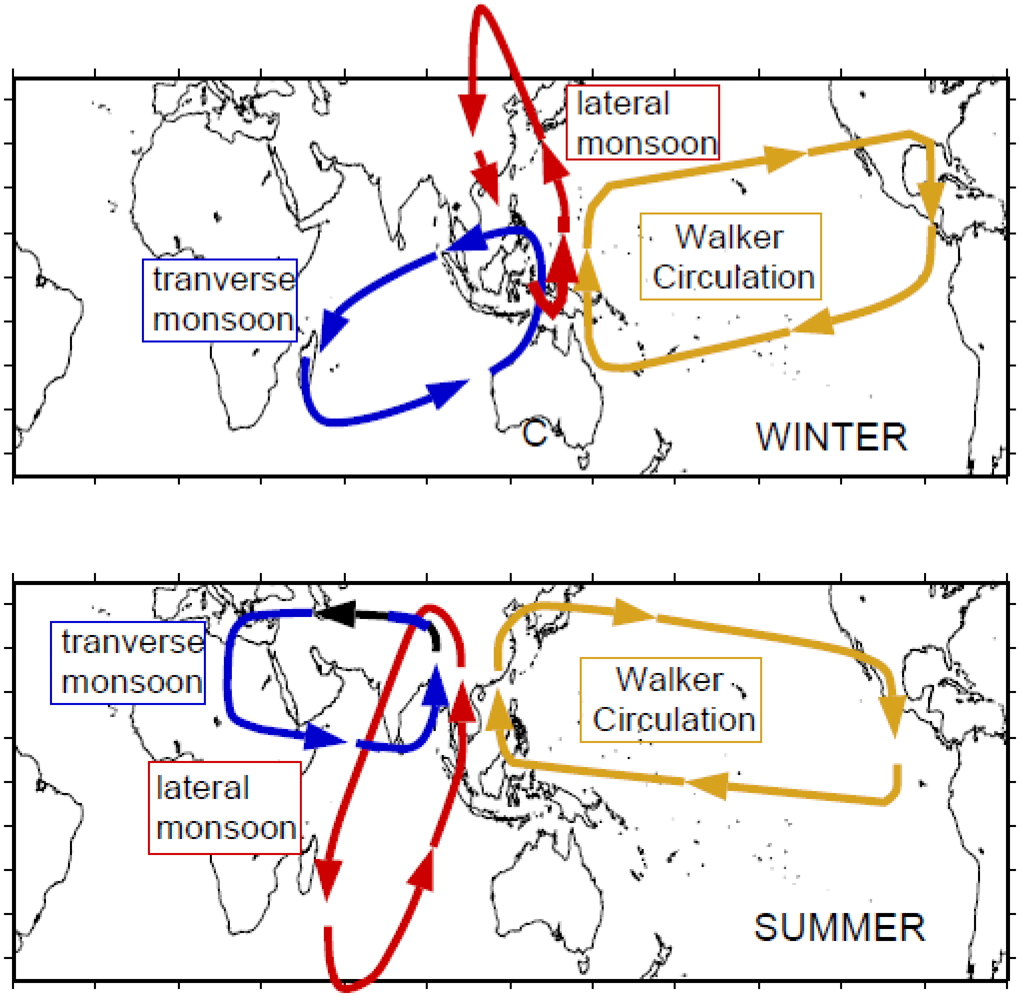

Winter:

	TM	LM	WC
Mass	12	18	15
LH	49	61	17
Rad	20	21	8

Summer:

	TM	LM	WC
Mass	25	25	18
LH	72	56	20
Rad	36	20	9

Webster

Figure 5: Synthesis of the summer and winter monsoon divergent wind circulations. Three major components are identified: the transverse monsoon, the lateral monsoon and the Walker Circulation. The lower tropospheric mass flux and the latent and radiative heating gradients associated with each circulation are given in the table in units of Gkg s^{-1} and W m^{-2} per 1000 km, respectively.

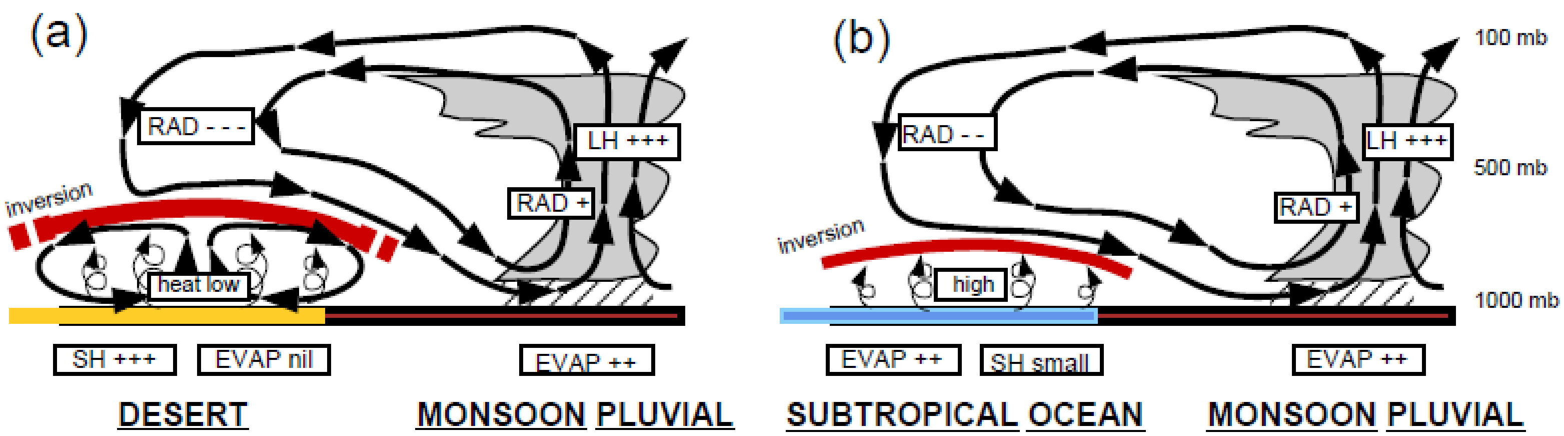

Monsoon circulation : coupling with subsidence and energetic conversions

Fluctuations of rain over India : alternation of active and inactive phases.

Quasi bi-weekly modulation.

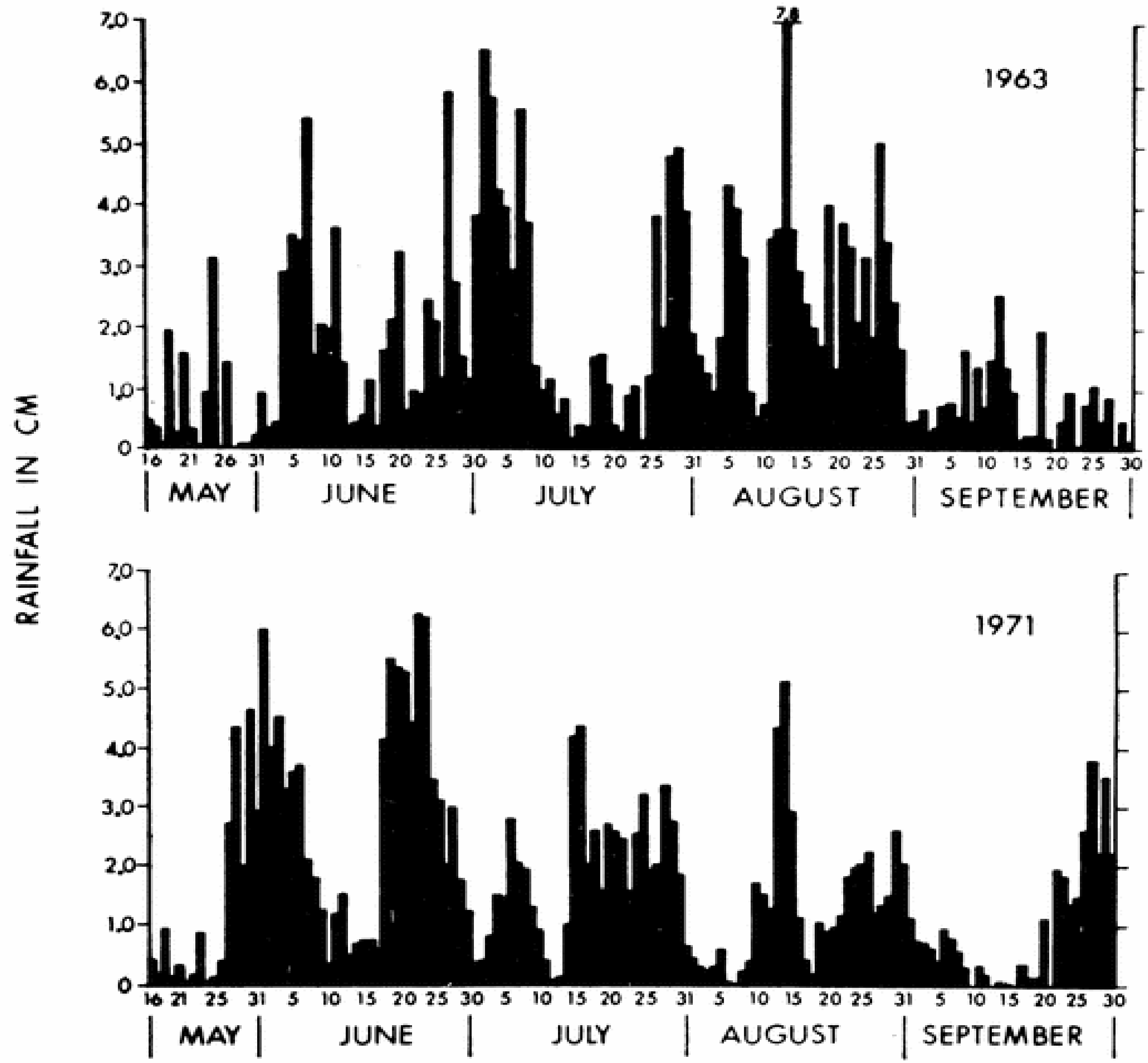

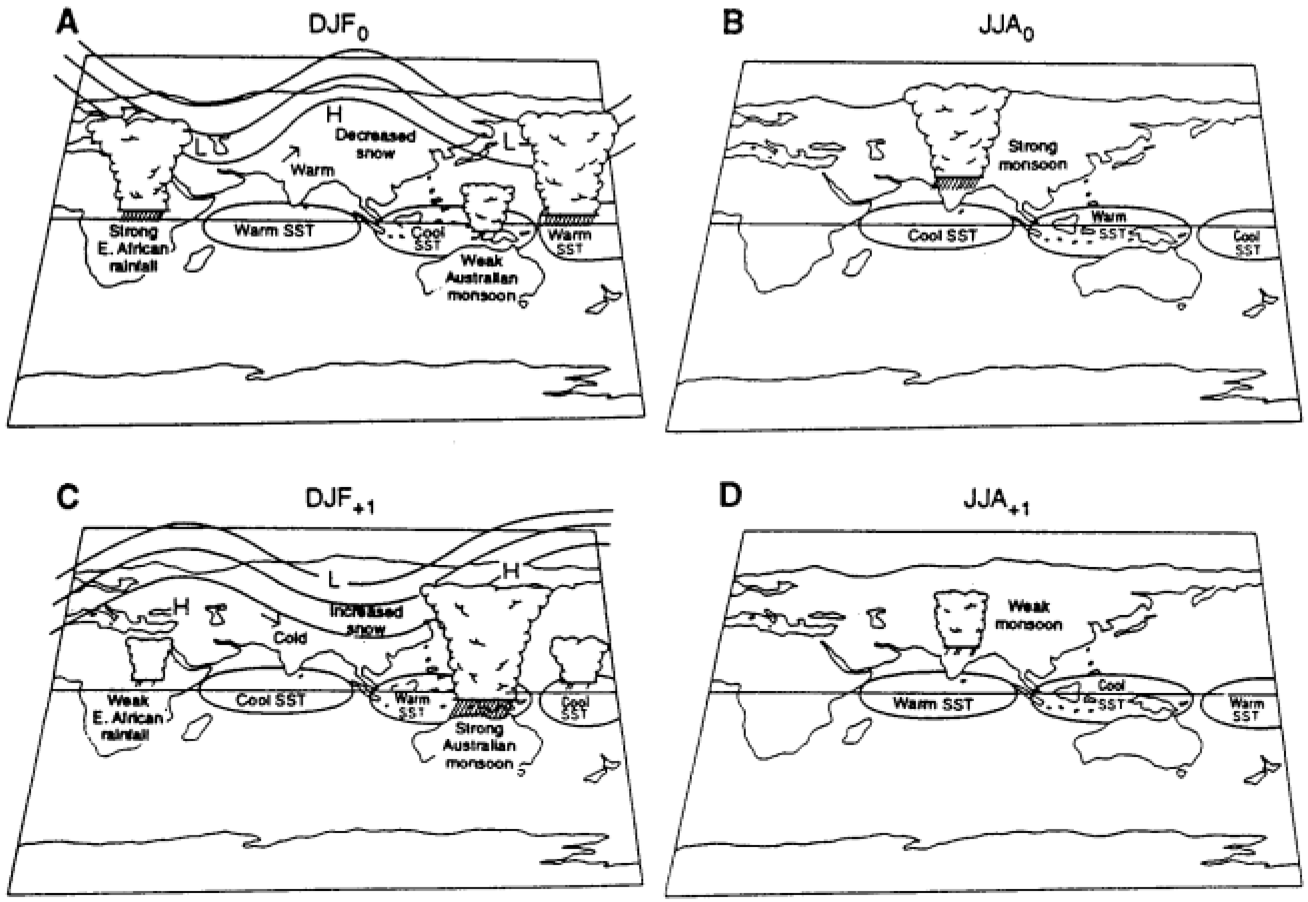

Bi-annual variability of the monsoon coupling the sea surface temperature (SST) and the snow cover of the Tibetan plateau (TP)

A : winter, warm SST, jet moved to the north, little amount of snow on the TP

B : summer, low pressure enhanced by dry and warm TP, intense monsoon, formation of cold surface water

C : winter, cold SST, jet moved to the south, au sud, a lot of snow over the TP

D : summer, low pressure weakened by moist and cold TP, weak monsoon, formation of warm surface water

Warm event in the Indian ocean

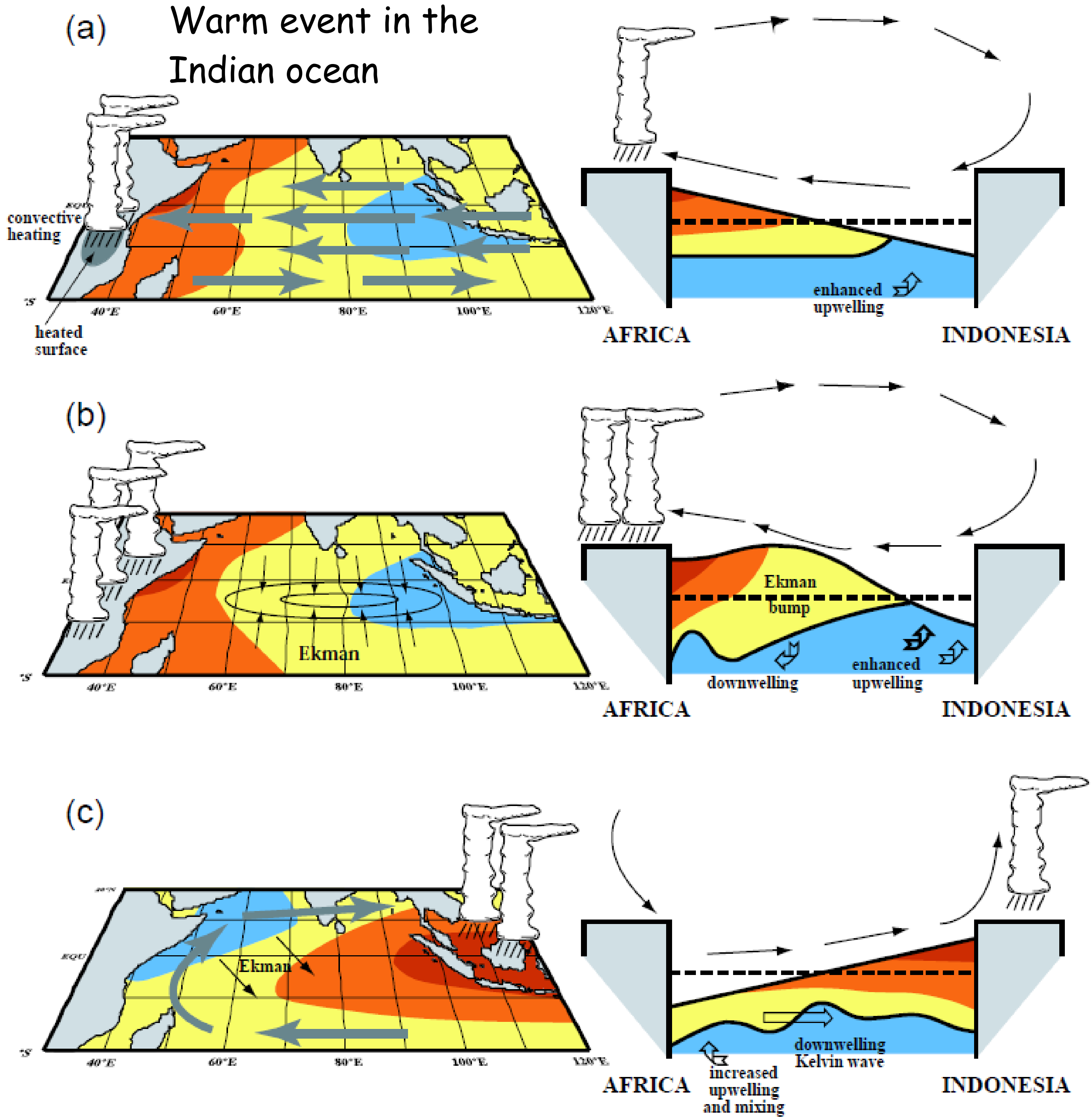

Webster

Coupling between the Asian monsoon and the African monsoon via the easterly jet

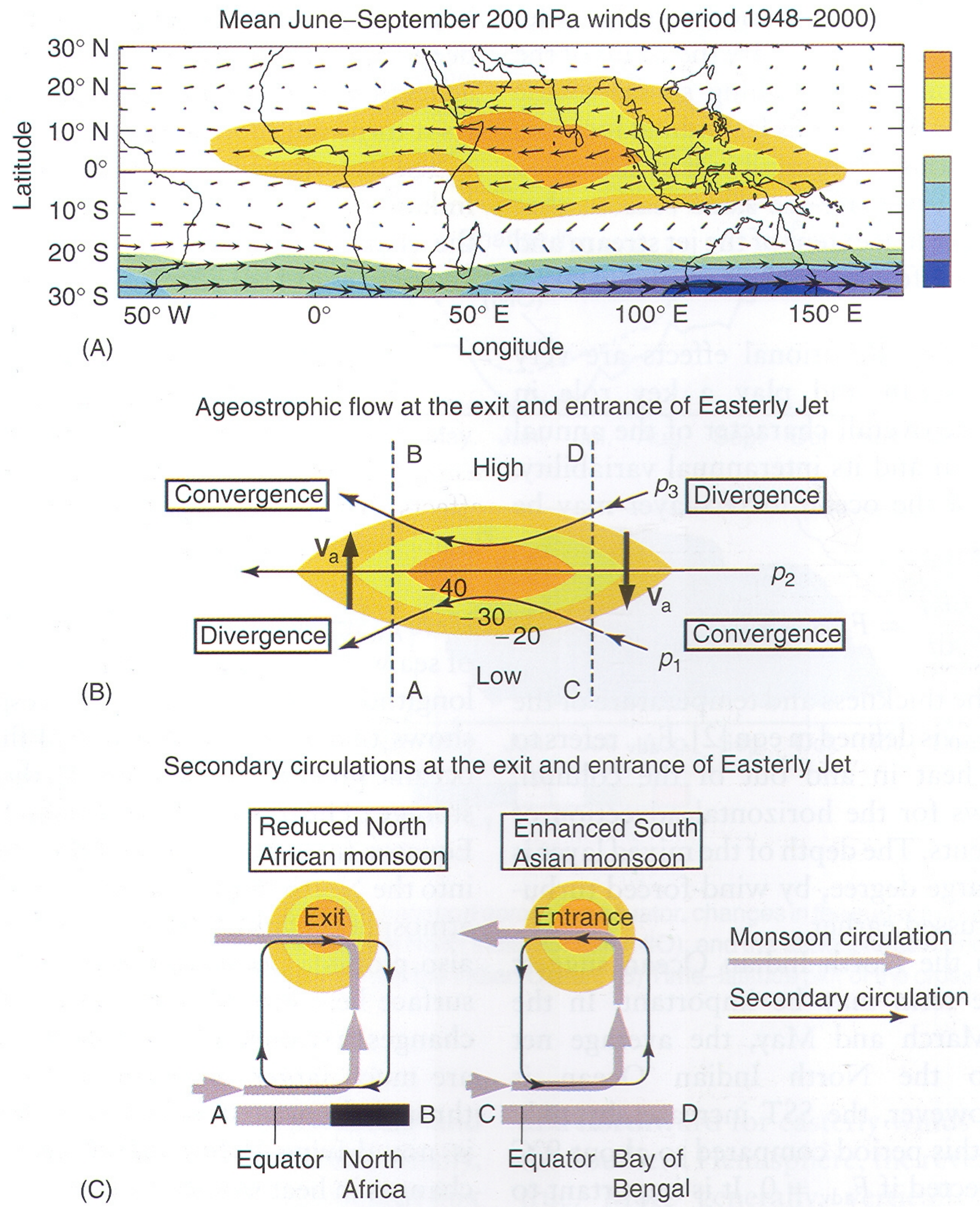

Anticyclone in the upper troposphere

Temperature and geopotential

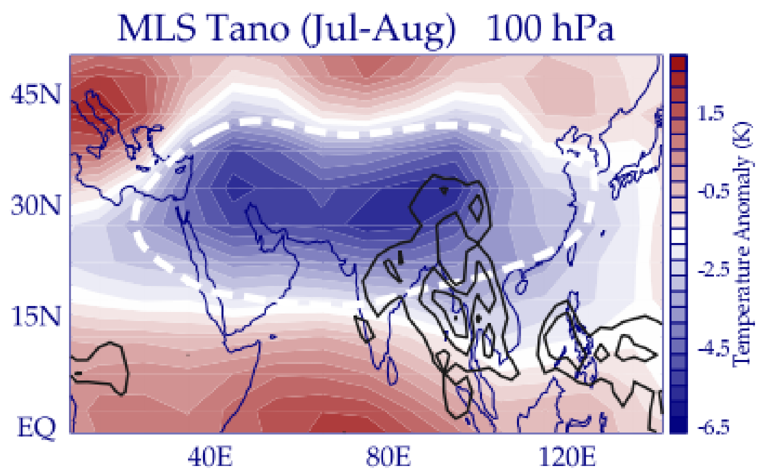

Geopotential 150 hPa

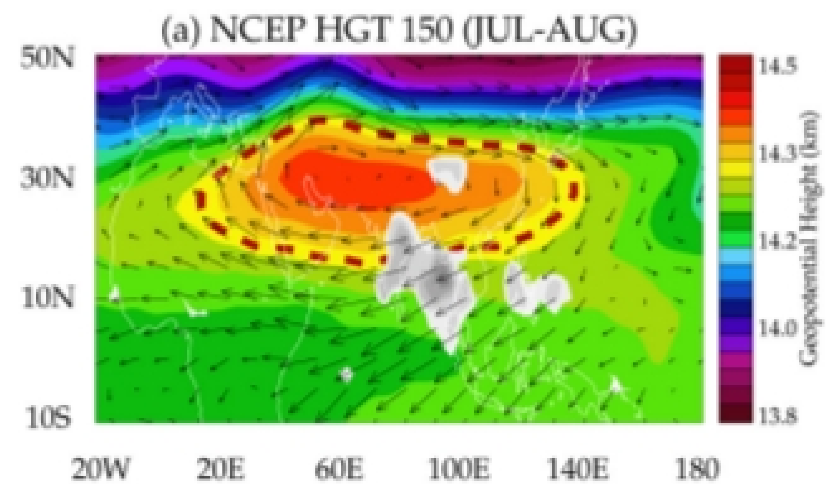

Trapping of ground emitted compound

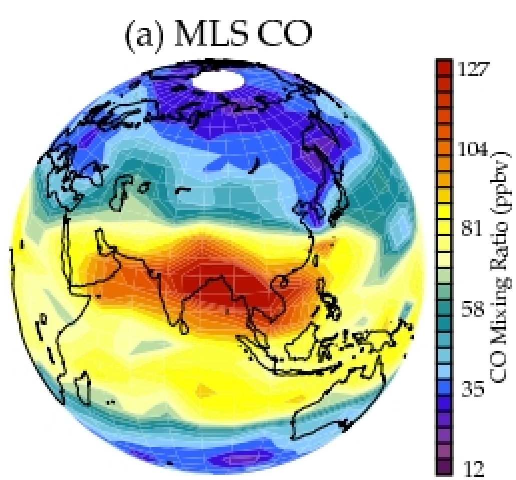

Ventilation of the convective sources

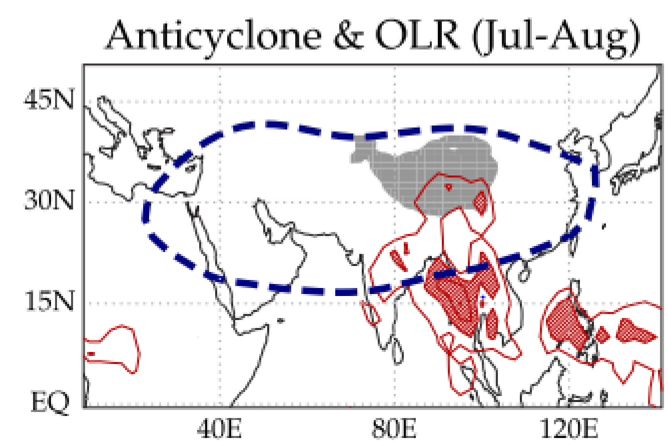

Park et al., 2006, 2008

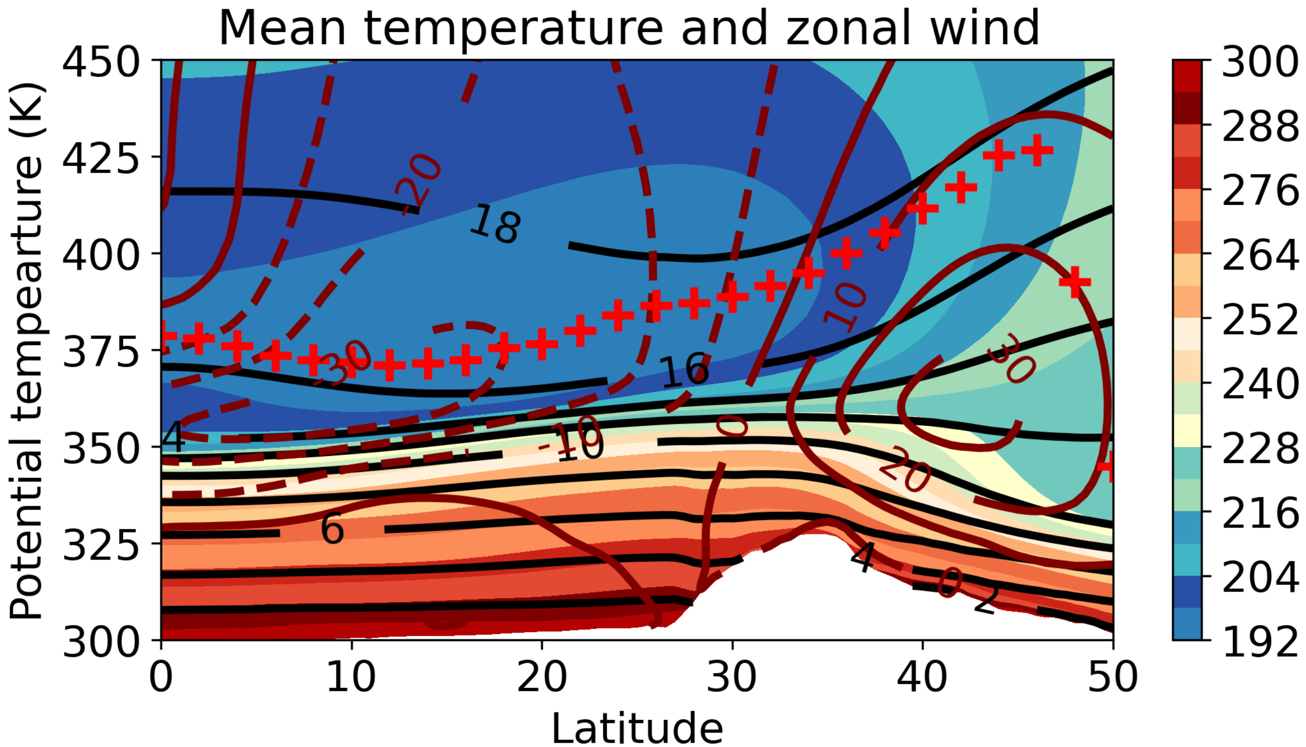
Mean temperature and zonal wind
Potential tempearture (K)
Latitude

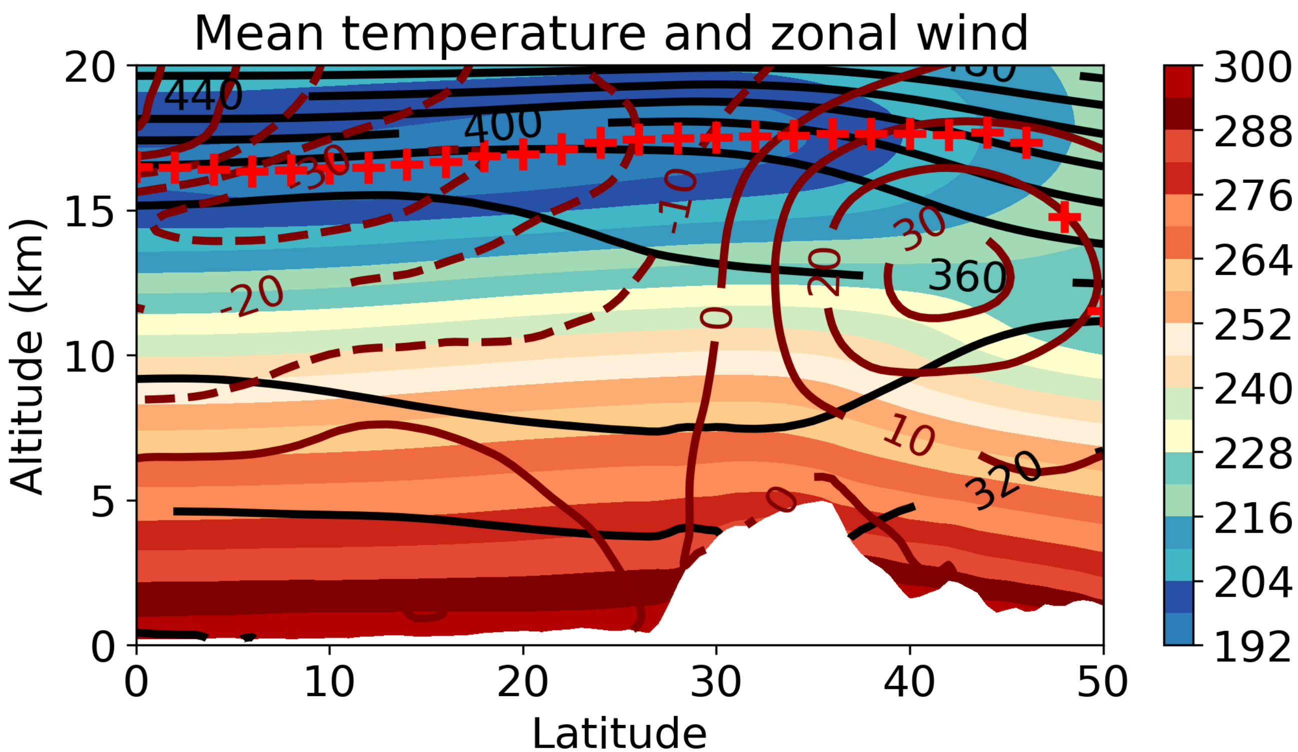
Mean temperature and zonal wind
Altitude (km)
Latitude

Bi-weely oscillation of the Asian monsoon anticyclone

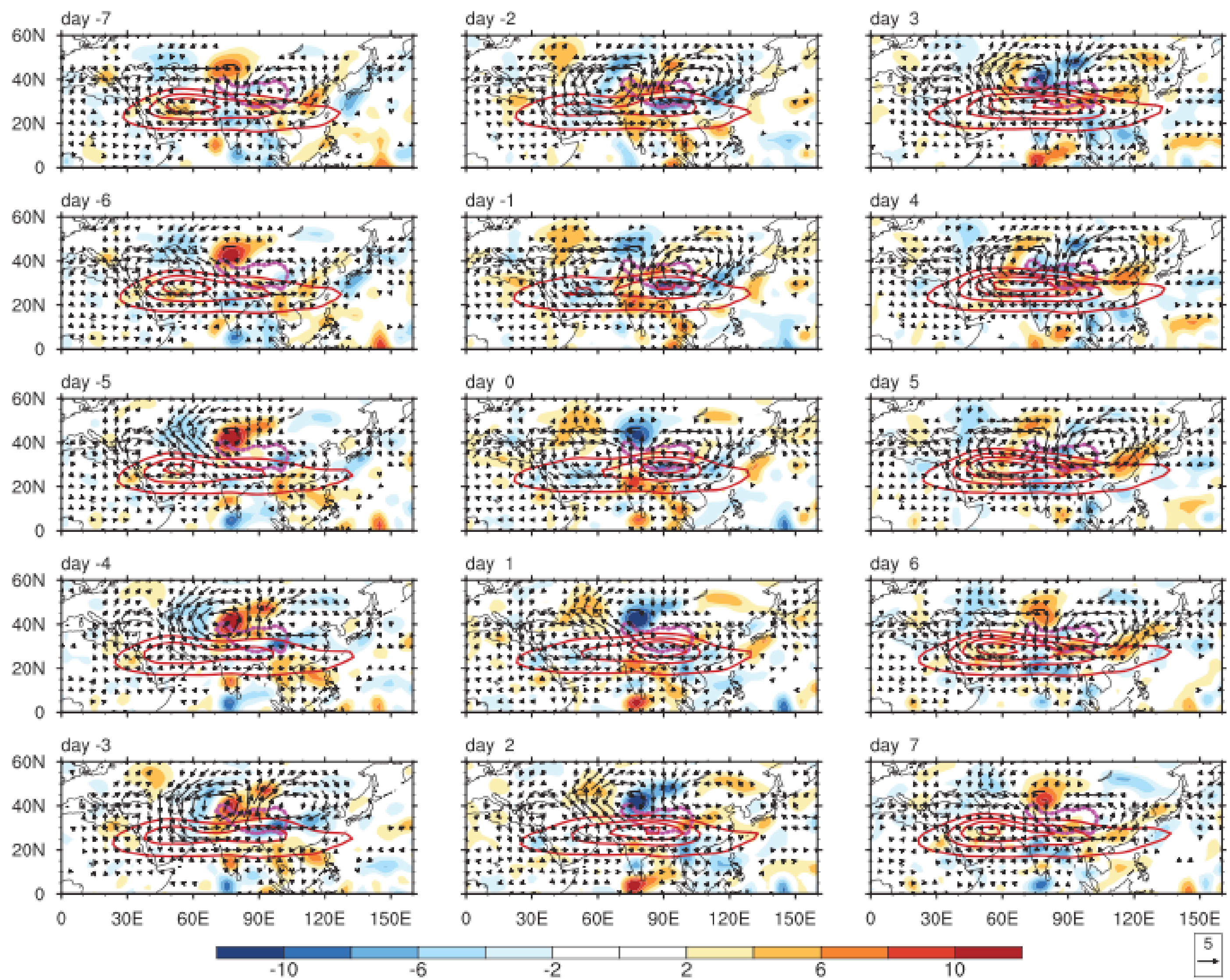

Figure 3. Composite patterns of 10–20 day filtered divergence anomalies (shaded; 10^{-7} s^{-1}), horizontal wind anomalies (vectors; m/s), and the SAH (red contours from outside to inside indicate 12,500, 12,540, 12,560, and 12,575 gpm, respectively) at 200 hPa from Day −7 to Day 7 based on the SAH index from NCEP-DOE 2 data. The contours in magenta indicate the TP region with elevations exceeding 3,000 m.

Wei et al., GRL, 2019

Asian tropopause aerosol layer

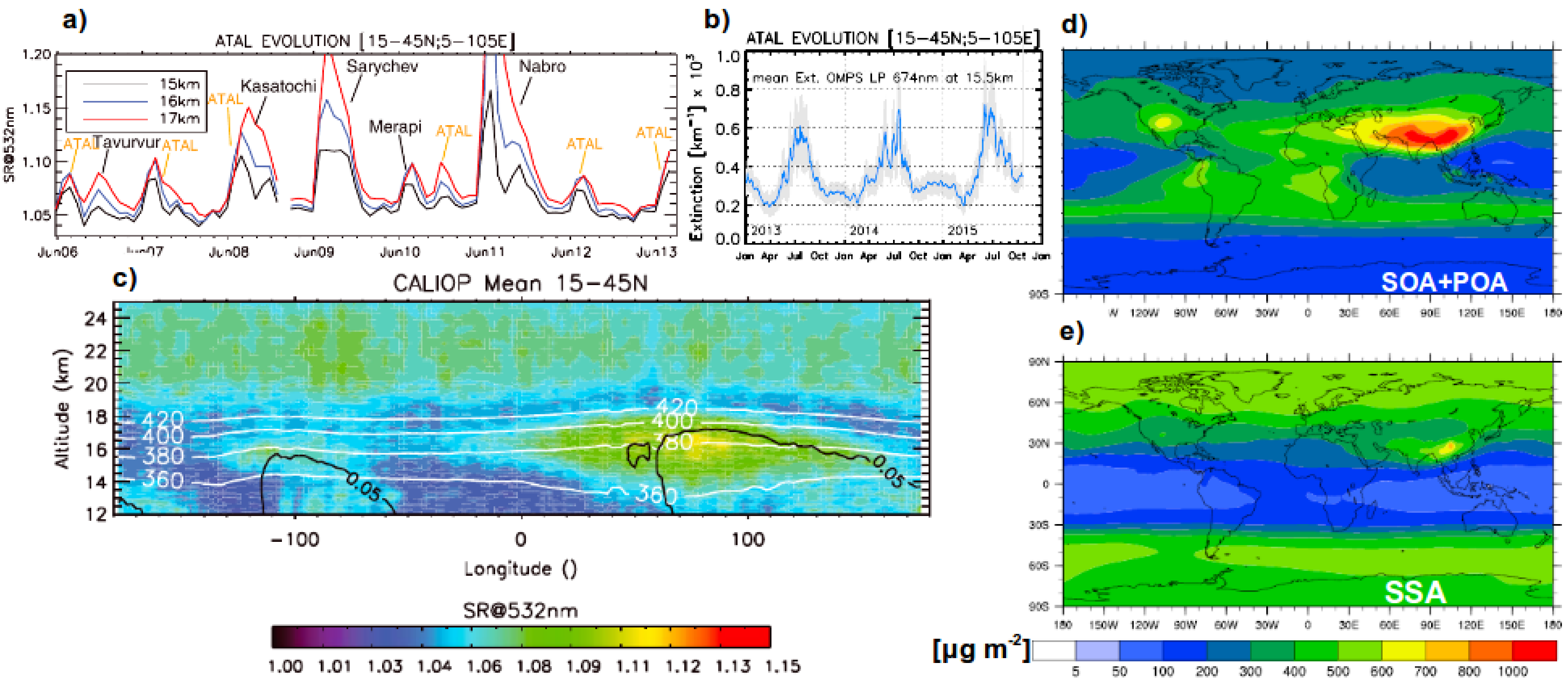

Vernier at al., 2015

I Etat moyen et cycle saisonnier

II La mousson

III ENSO

IV Mode de Madden-Julian

V Ondes tropicales

VI Cyclones tropicaux

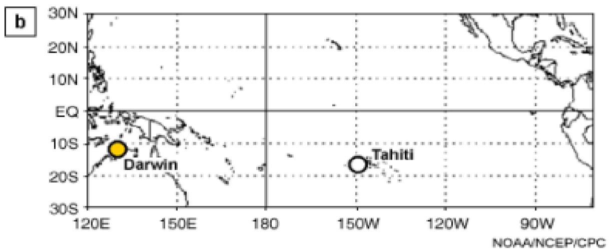

South Oscillation Index

SOI=P(Tahiti) – P (Darwin)

normalized

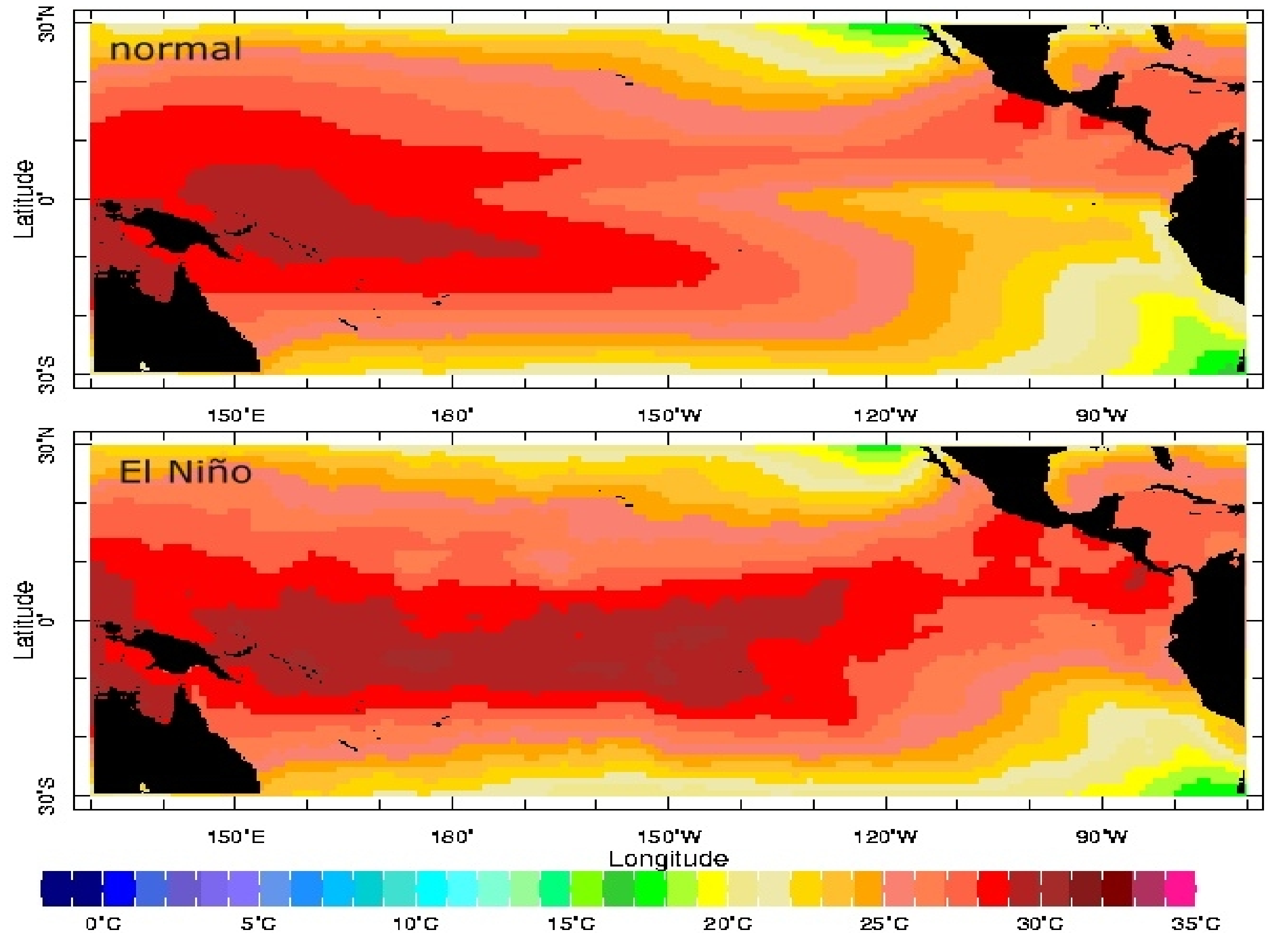

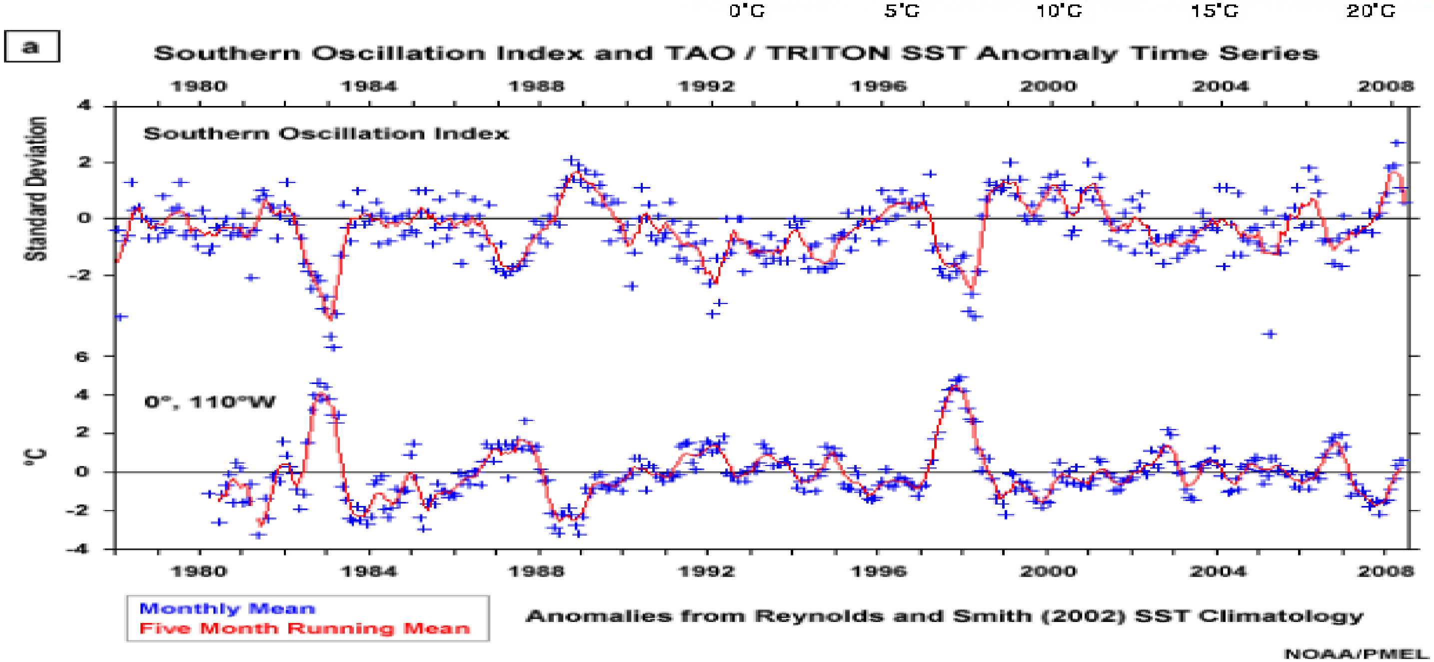

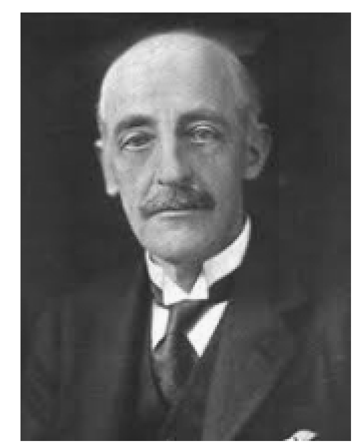

Sir Gilbert Walker

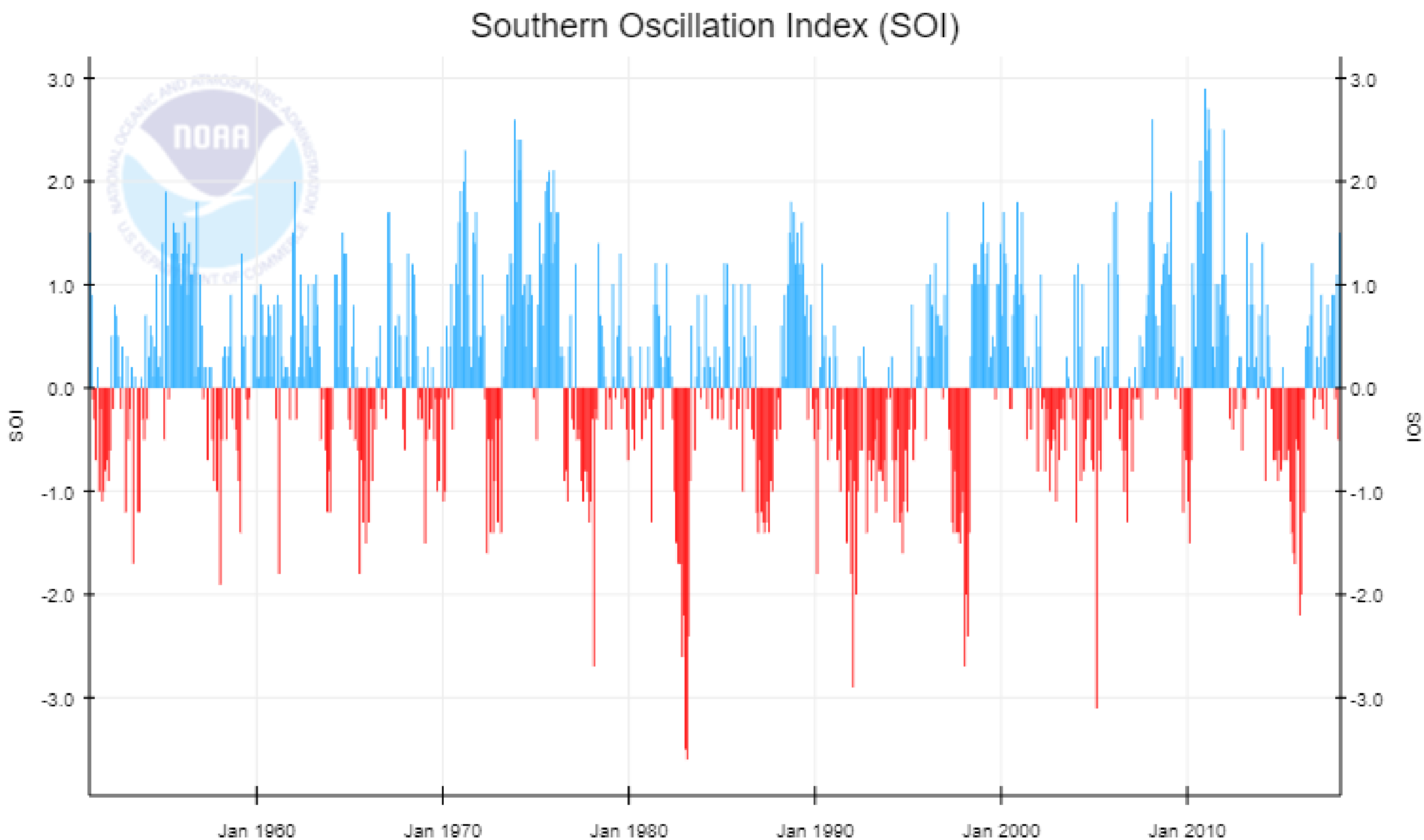

SOI= normalized pressure difference between Tahiti et Darwin (AU)
In red warm episodes (El Nino) , in blue cold episodes

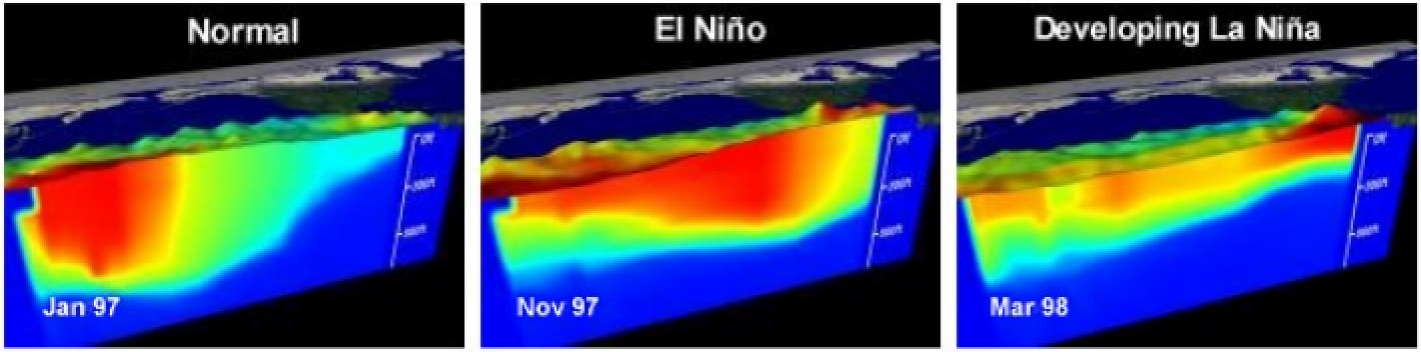

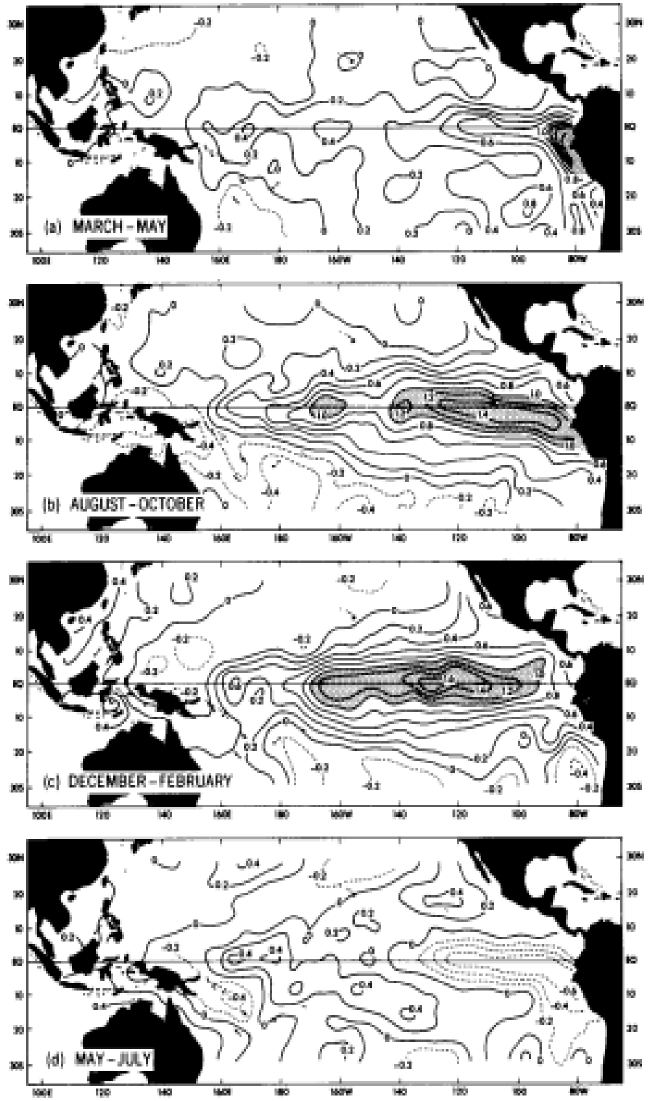

Figure 11.18: Maps of sea surface temperature anomalies during 1982 and 1983. From Philander (1990).

Ocean temperature during a El Nino – La Nina cycle.

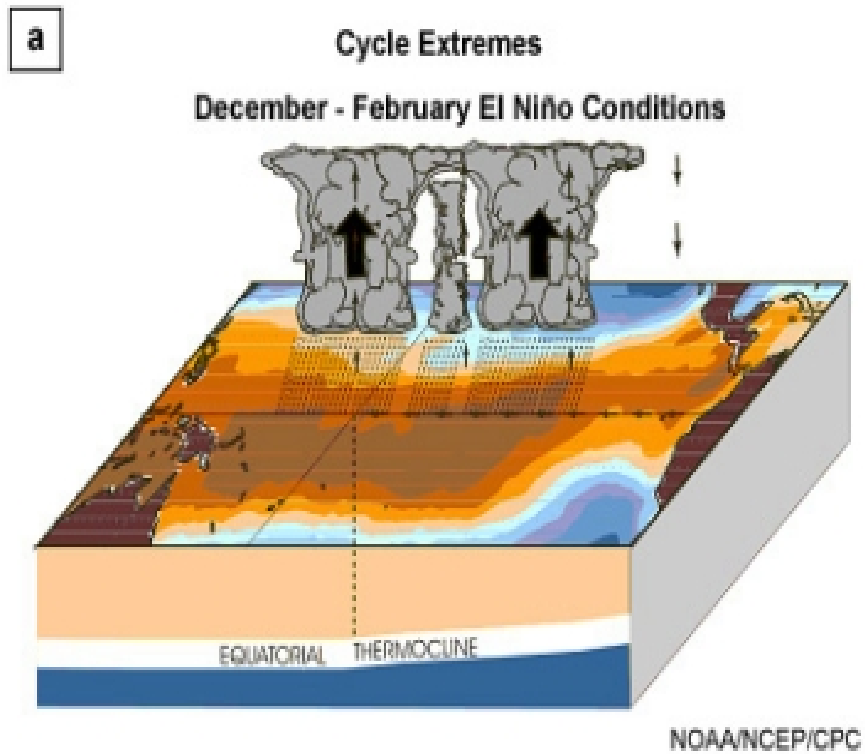
a
Cycle Extremes
December - February El Niño Conditions
EQUATORIAL THERMOCLINE
NOAA/NCEP/CPC

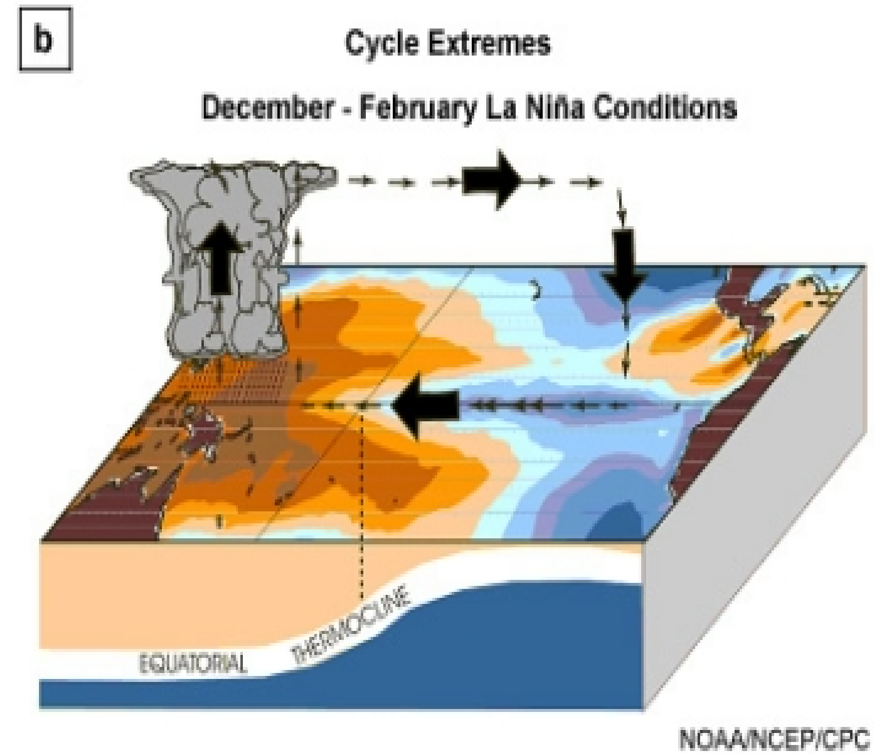
b
Cycle Extremes
December - February La Niña Conditions
EQUATORIAL THERMOCLINE
NOAA/NCEP/CPC

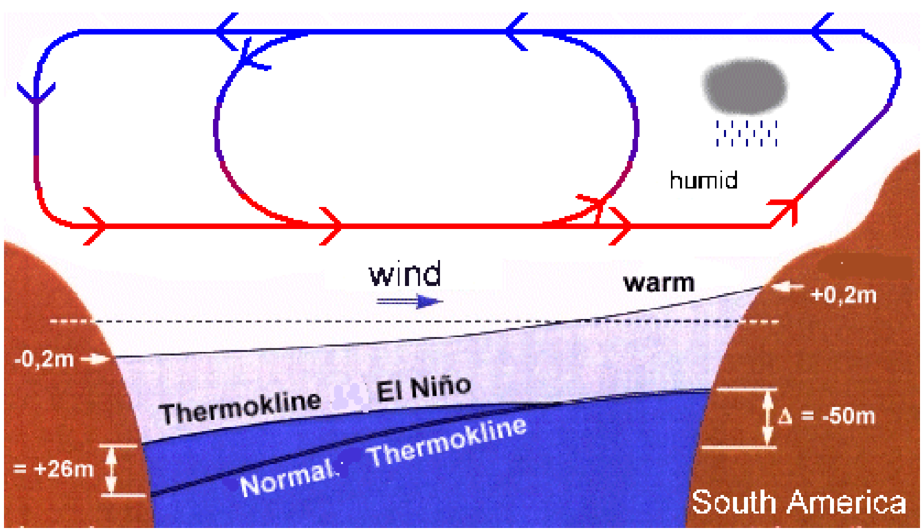
humid
wind
warm
+0,2m
-0,2m
Thermokline
El Niño
Δ = -50m
= +26m
Normal
Thermokline
South America

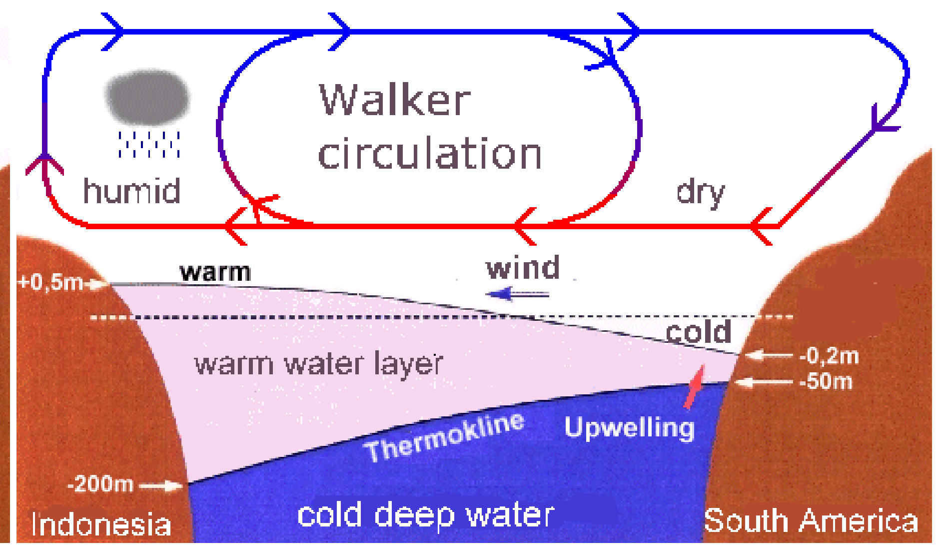
Walker
circulation
humid
dry
warm
wind
+0,5m
cold
warm water layer
-0,2m
-50m
Thermokline
Upwelling
-200m
Indonesia
cold deep water
South America

a

El Niño's Impacts Warm Episode Relationships, December - February

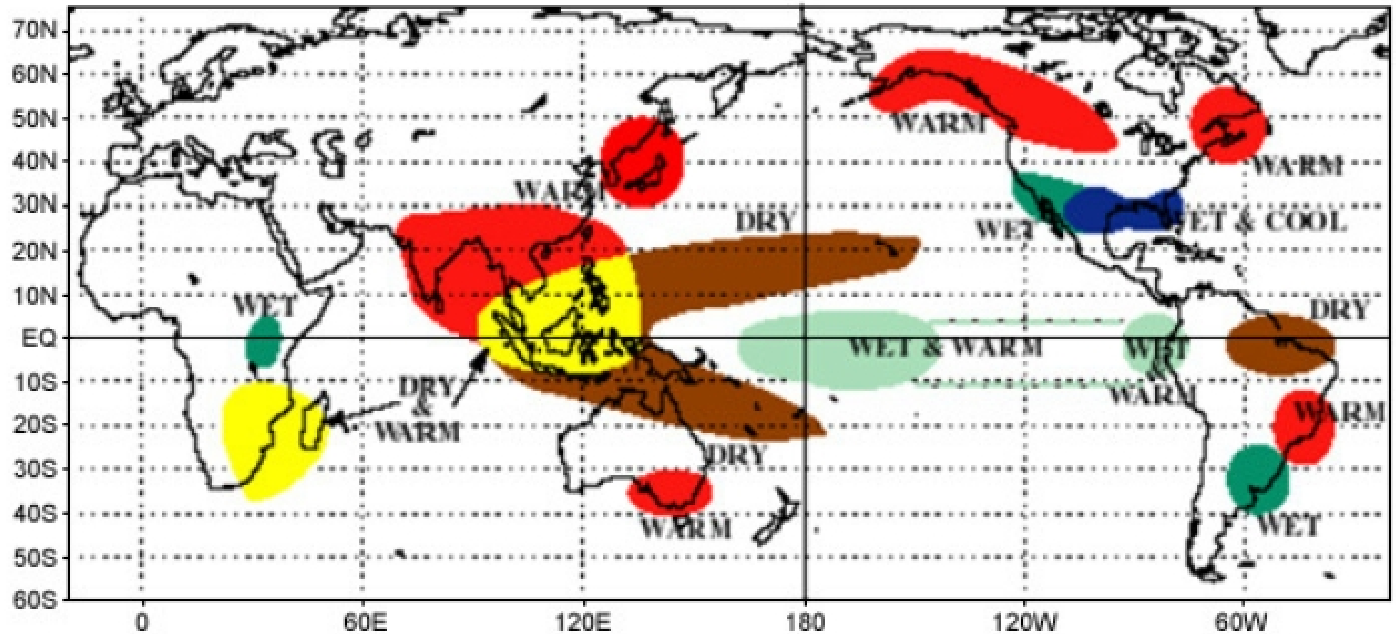

NOAA/NCEP/CPC

c

La Niña's Impacts Cold Episode Relationships, December - February

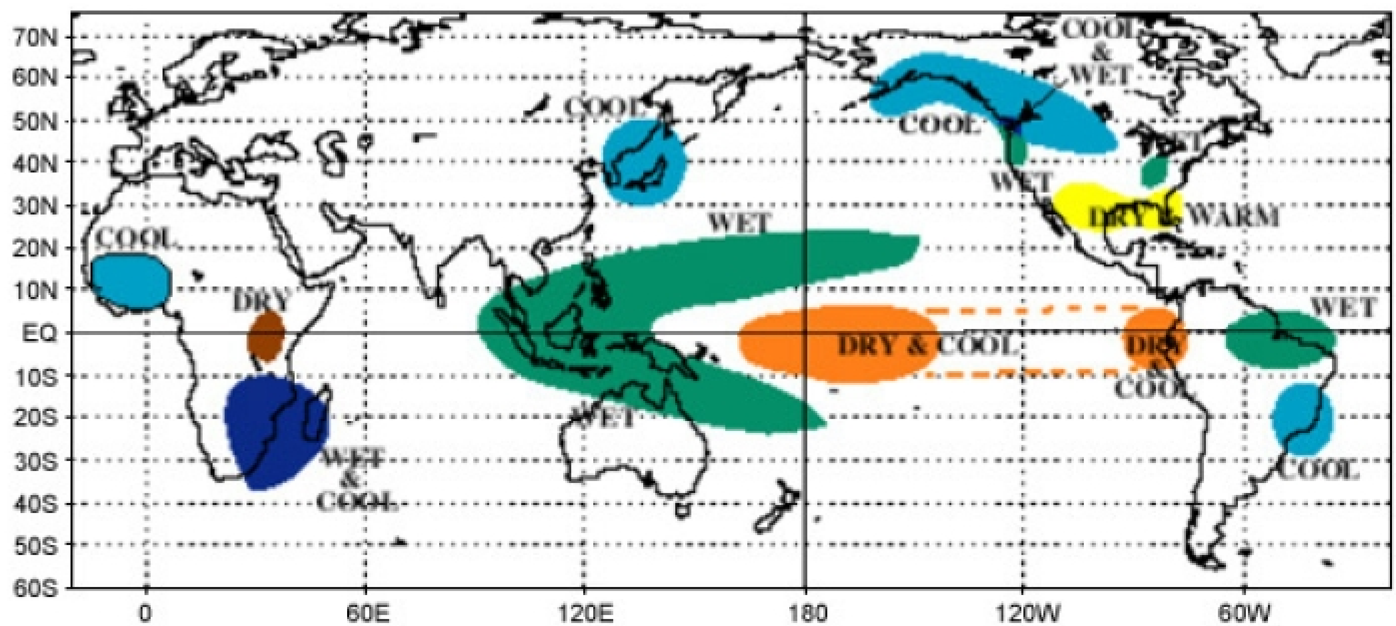

NOAA/NCEP/CPC

The effect of ENSO on the Indian monsoon and food productivity

Gagil, 2005,
DOI : 10.1146/annurev.earth.31.100901.141251

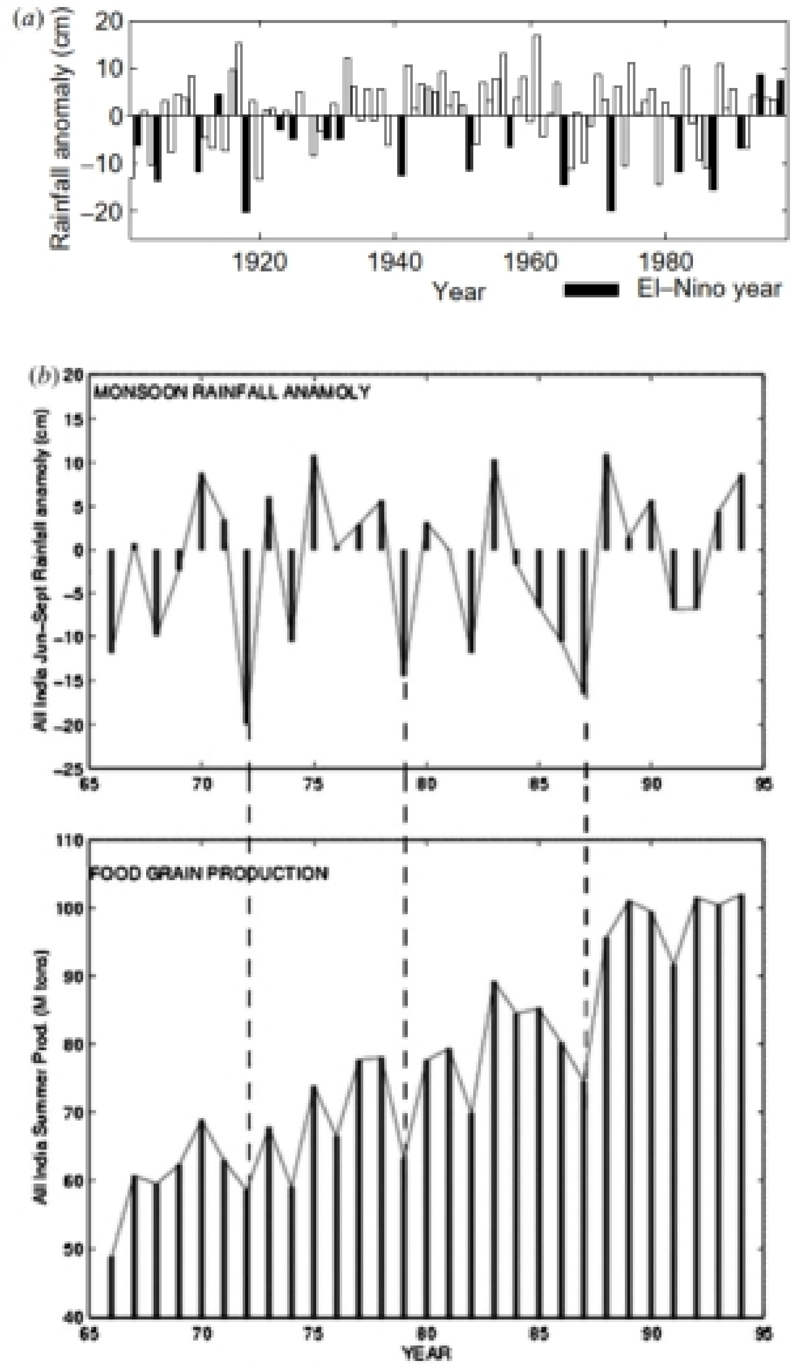

Figure 3 (*a*) Interannual variation of the all-India summer monsoon rainfall (ISMR) during 1901–1998; the El Niño years are shaded. (*b*) Variation of ISMR anomaly (*top*) and the Indian summer foodgrain production.

I Mean state and seasonal cycle

II Monsoon

III ENSO

IV Madden-Julian mode

V Equatorial waves

VI Tropical cyclones

Madden-Julian Oscillation

60_90 days
Towards the east

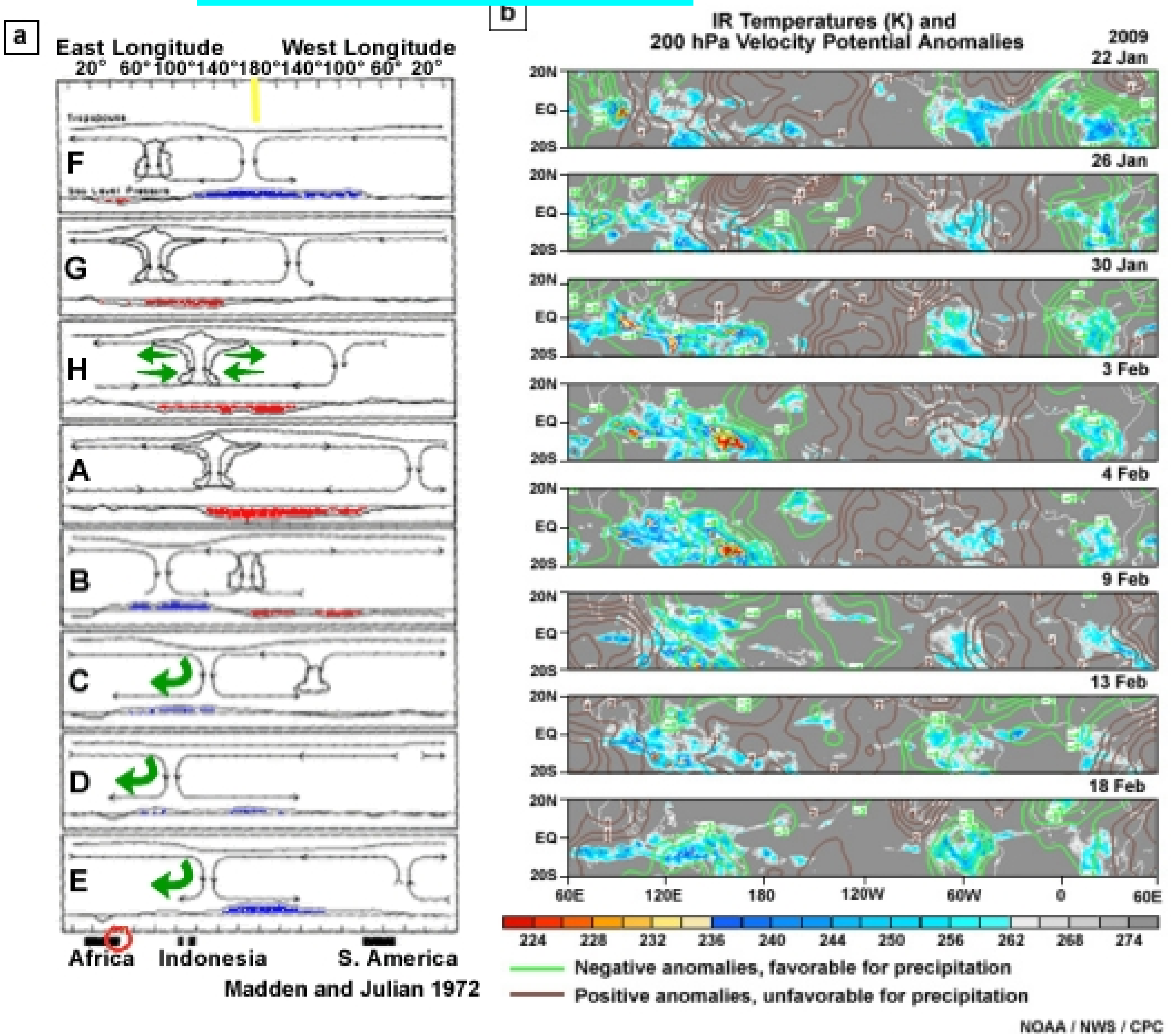

Zhang, 2005

doi:10.1029/2004RG000158

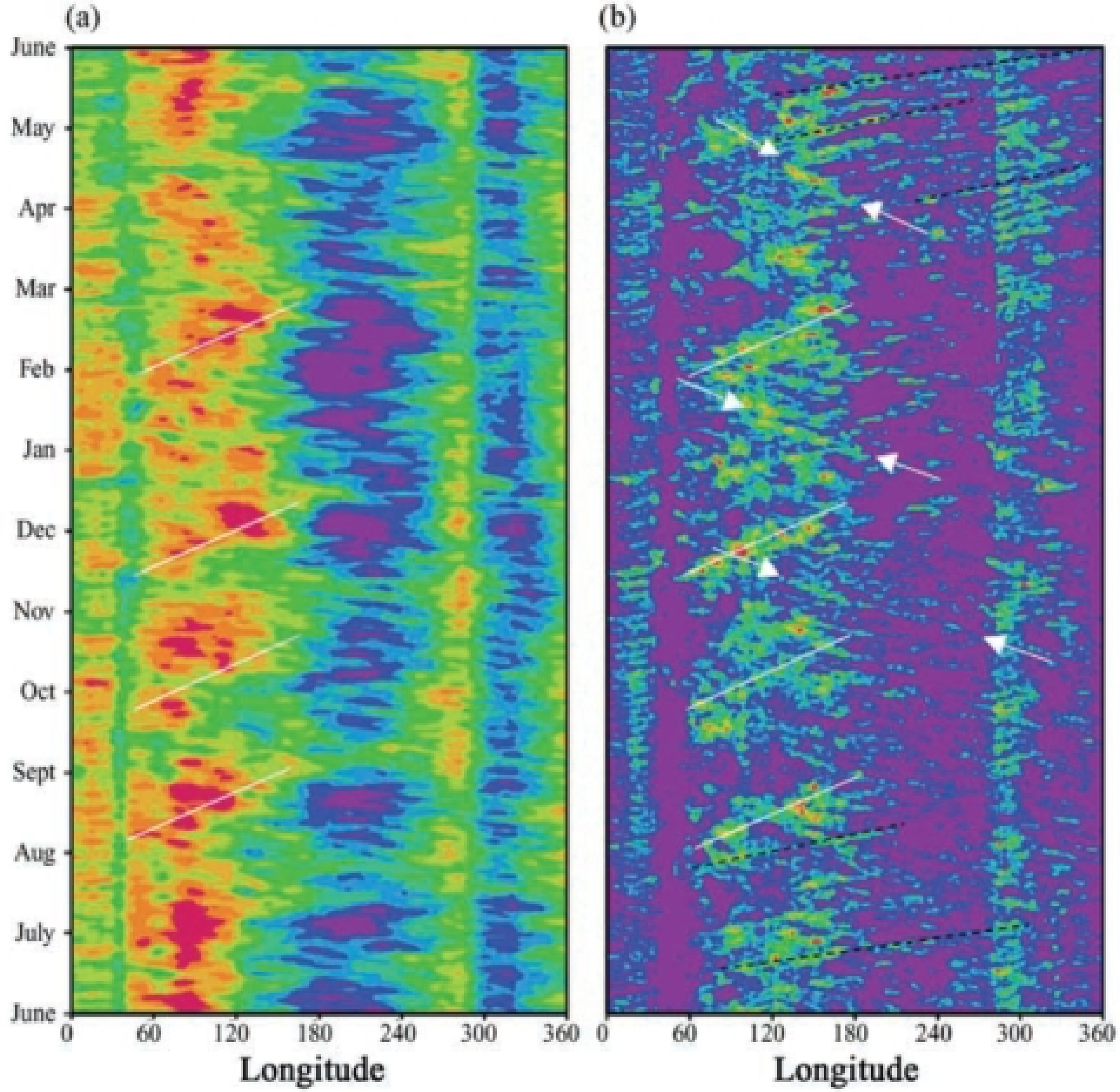

Figure 2. Longitude-time plots of daily (a) zonal wind (2.5° × 2.5°, m s^{-1}) at 850 hPa (roughly 1.5 km above sea level) from the National Centers for Environmental Prediction/National Center for Atmospheric Research (*NCEP/NCAR*) reanalysis [*Kalnay et al.*, 1996] and (b) precipitation (1° × 1°, mm d^{-1}) from the *GPCP* combined data set [*Huffman et al.*, 1997] for June 2000 to May 2001, both averaged over 10°N–10°S. The white straight lines mark identified MJO events, with a slope corresponding to an eastward propagation speed of 5 m s^{-1}. Notice that each MJO event may propagate eastward at a slightly different speed. The faster eastward moving (15 m s^{-1}) signals with shorter periods (5–10 days) (examples marked with black dashed lines) are of convectively coupled Kelvin waves and should not be mistaken for the MJO [e.g., *Takayabu et al.*, 1999]. The westward moving synoptic signals (examples marked with white arrows) are likely of Rossby or mixed Rossby-gravity waves.

Structure of the MJO

Schematic Depiction of the Large-scale Wind Structure of the MJO

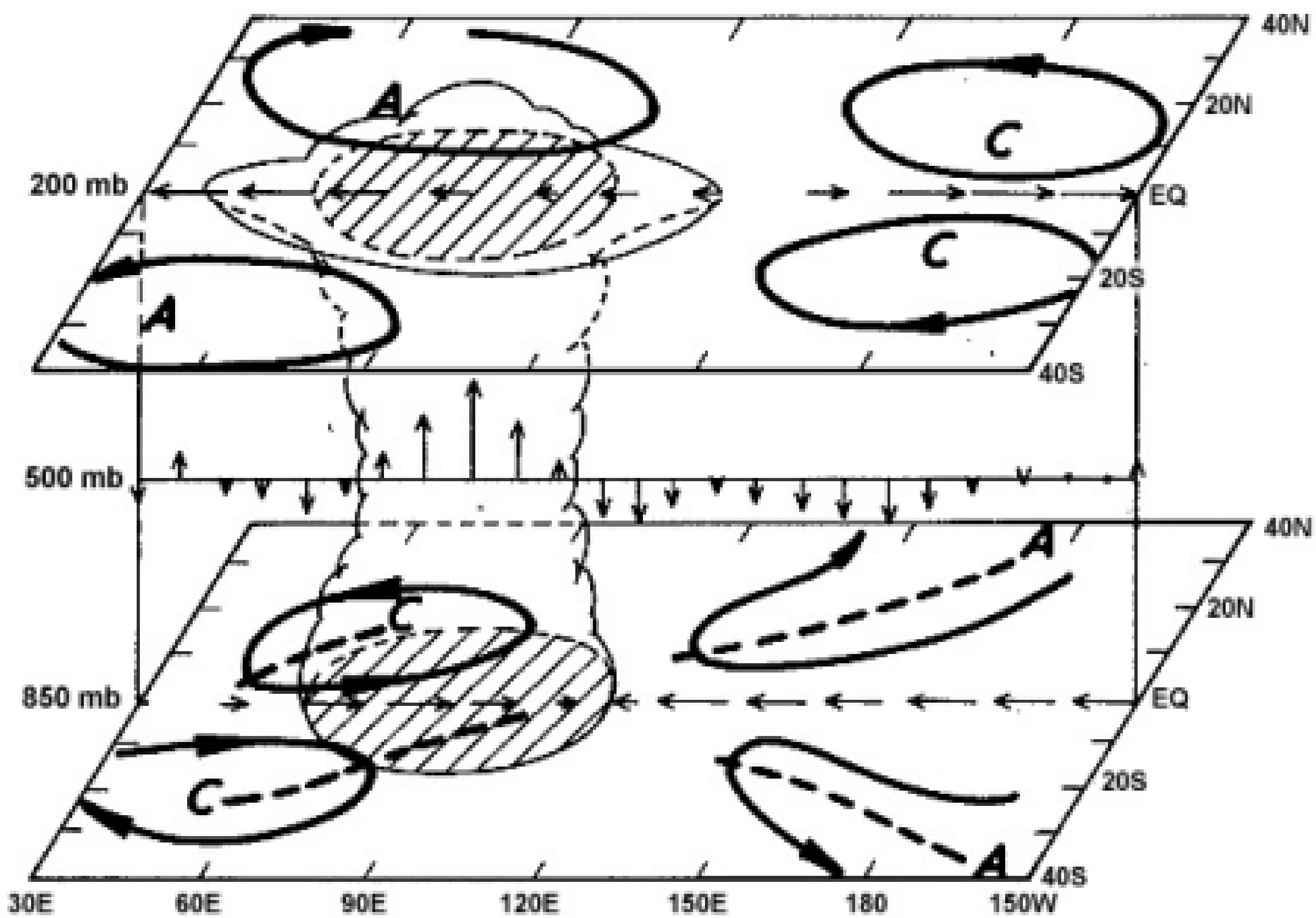

Rui and Wang 1990

Composite of the MJO during winter

Anomaly : OLR / wind
grey : - / -
hatched : + / +

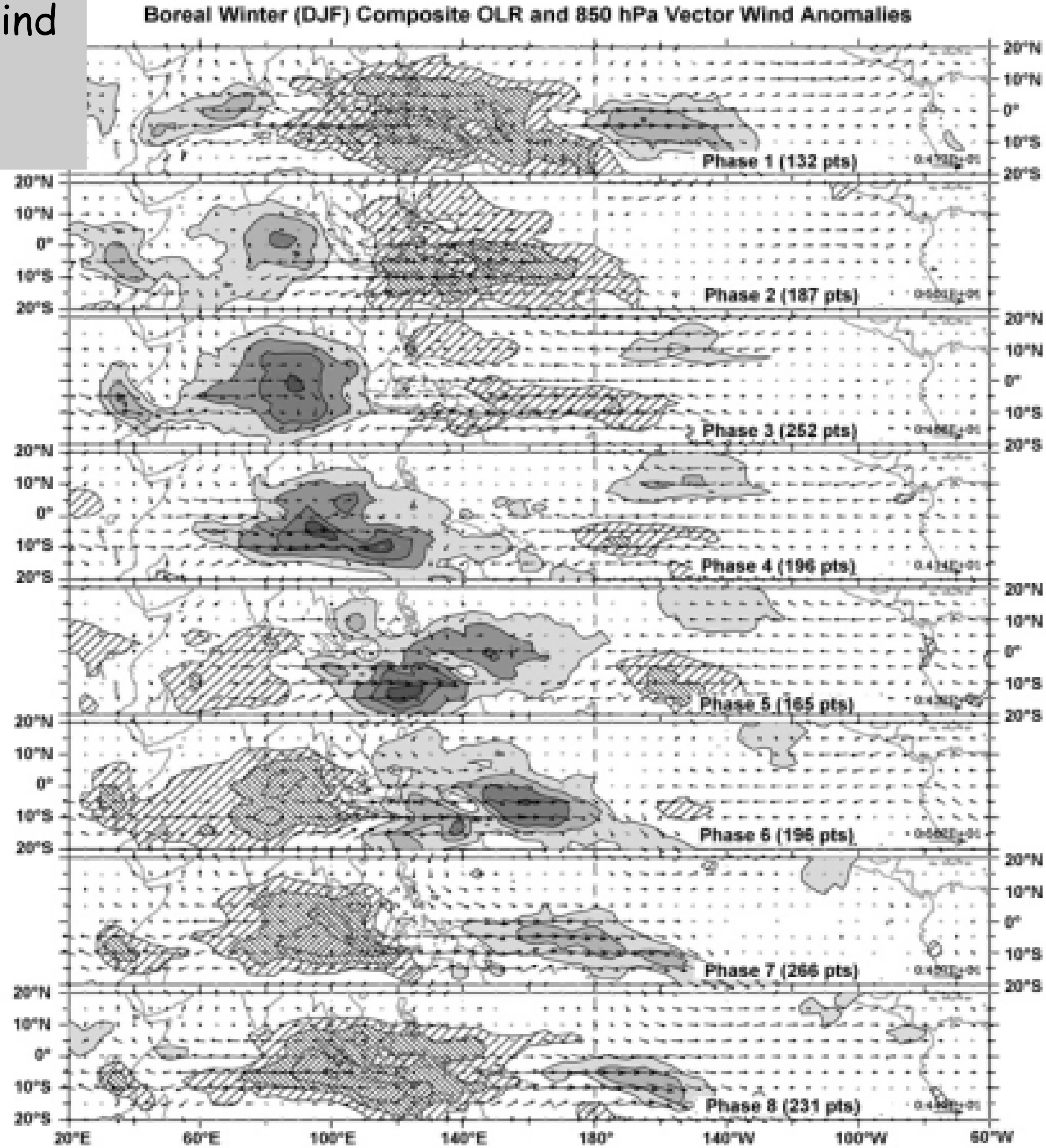

Wheeler and Hendon 2004

Reviews of Geophysics

REVIEW ARTICLE
10.1029/2019RG000685

Four Theories of the Madden-Julian Oscillation

C. Zhang[1], Á. F. Adames[2], B. Khouider[3], B. Wang[4], and D. Yang[5,6]

[1]NOAA Pacific Marine Environmental Laboratory, Seattle, WA, USA, [2]Department of Climate and Space Sciences and Engineering, University of Michigan, Ann Arbor, MI, USA, [3]Department of Mathematics and Statistics, University of Victoria, Victoria, British Columbia, Canada, [4]Department of Atmospheric Sciences, University of Hawaii, Honolulu, HI, USA, [5]Department of Land, Air and Water Resources, University of California, Davis, CA, USA, [6]Lawrence Berkeley National Laboratory, Berkeley, CA, USA

Key Points:
- A theory for the Madden-Julian Oscillation (MJO) must explain its most fundamental features of temporal-spatial scales and eastward propagation
- Four theories provide contrasting explanations for the MJO based on different assumptions and treatment of physical processes
- These MJO theories represent a general progress toward understanding the MJO and also the need to further advance such understanding

Correspondence to:
C. Zhang,
chiding.zhang@noaa.gov

Citation:
Zhang, C., Adames, Á. F., Khouider, B., Wang, B., & Yang, D. (2020). Four theories of the Madden-Julian Oscillation. *Reviews of Geophysics*, *58*, e2019RG000685. https://doi.org/10.1029/2019RG000685

Received 1 OCT 2019
Accepted 9 APR 2020
Accepted article online 29 APR 2020

Abstract Studies of the Madden-Julian Oscillation (MJO) have progressed considerably during the past decades in observations, numerical modeling, and theoretical understanding. Many theoretical attempts have been made to identify the most essential processes responsible for the existence of the MJO. Criteria are proposed to separate a hypothesis from a theory (based on the first principles with quantitative and testable assumptions, able to predict quantitatively the fundamental scales and eastward propagation of the MJO). Four MJO theories are selected to be summarized and compared in this article: the skeleton theory, moisture-mode theory, gravity-wave theory, and trio-interaction theory of the MJO. These four MJO theories are distinct from each other in their key assumptions, parameterized processes, and, particularly, selection mechanisms for the zonal spatial scale, time scale, and eastward propagation of the MJO. The comparison of the four theories and more recent development in MJO dynamical approaches lead to a realization that theoretical thinking of the MJO is diverse and understanding of MJO dynamics needs to be further advanced.

Plain Language Summary The Madden-Julian Oscillation (MJO) is a tropical phenomenon that includes heavy rainfall and stiff wind over an area of roughly 1,500 km in latitude and 4,500 km in longitude. It starts over the Indian Ocean and moves eastward to the Pacific Ocean in about a month. As it moves eastward, it influences weather and climate phenomena in many parts of the world. Understanding the fundamental physics of the MJO forms the base for forecasting it and its global influences. This article reviews four theories of the MJO and compares their similarities and differences. Future studies needed to further our understanding of the MJO are recommended.

I Mean state and seasonal cycle

II Monsoon

III ENSO

IV Mode de Madden-Julian

V Tropical waves

VI Tropical cyclones

Wave propagation in the tropics

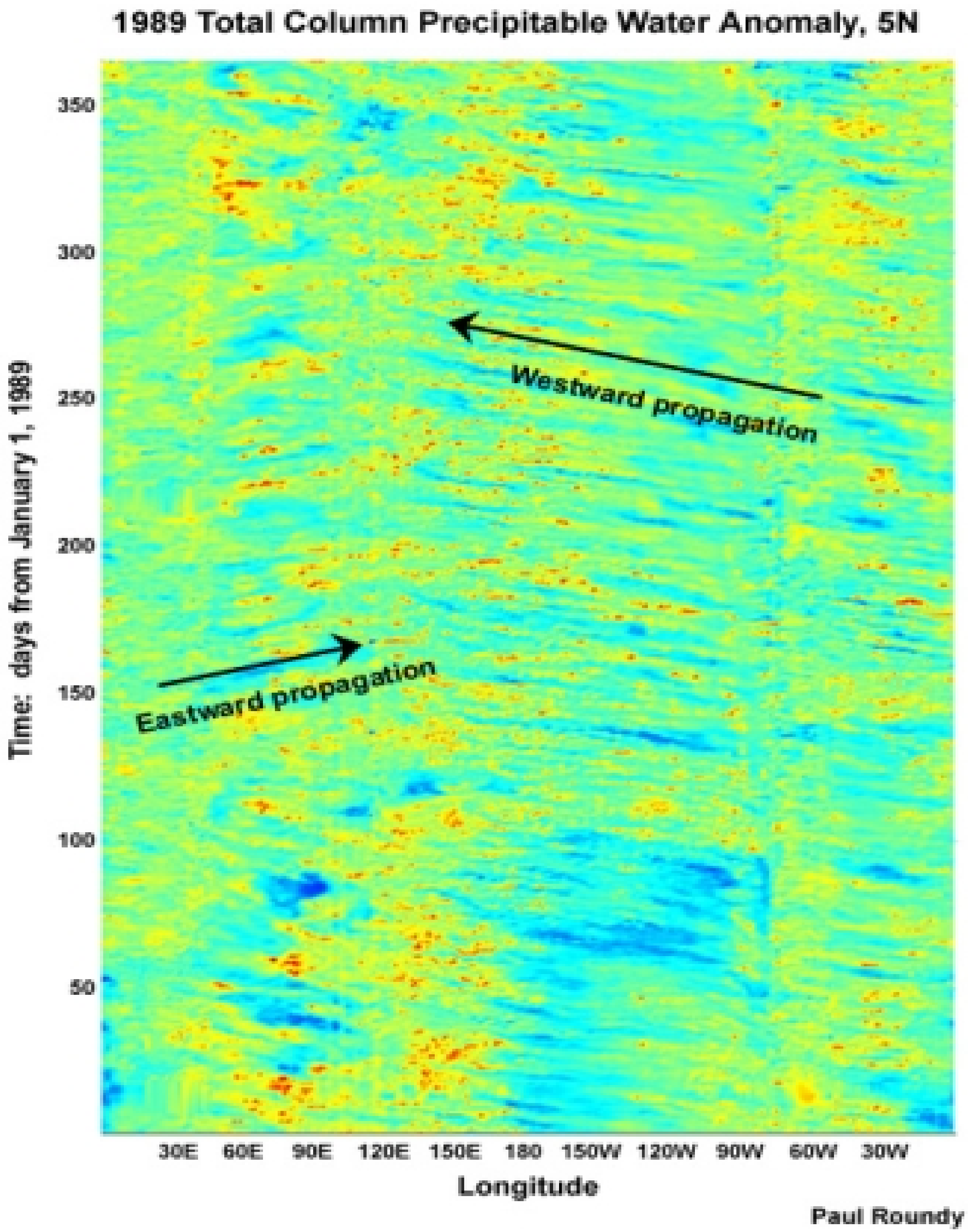

Ondes tropicales dans les observations satellitates (à 20 km)

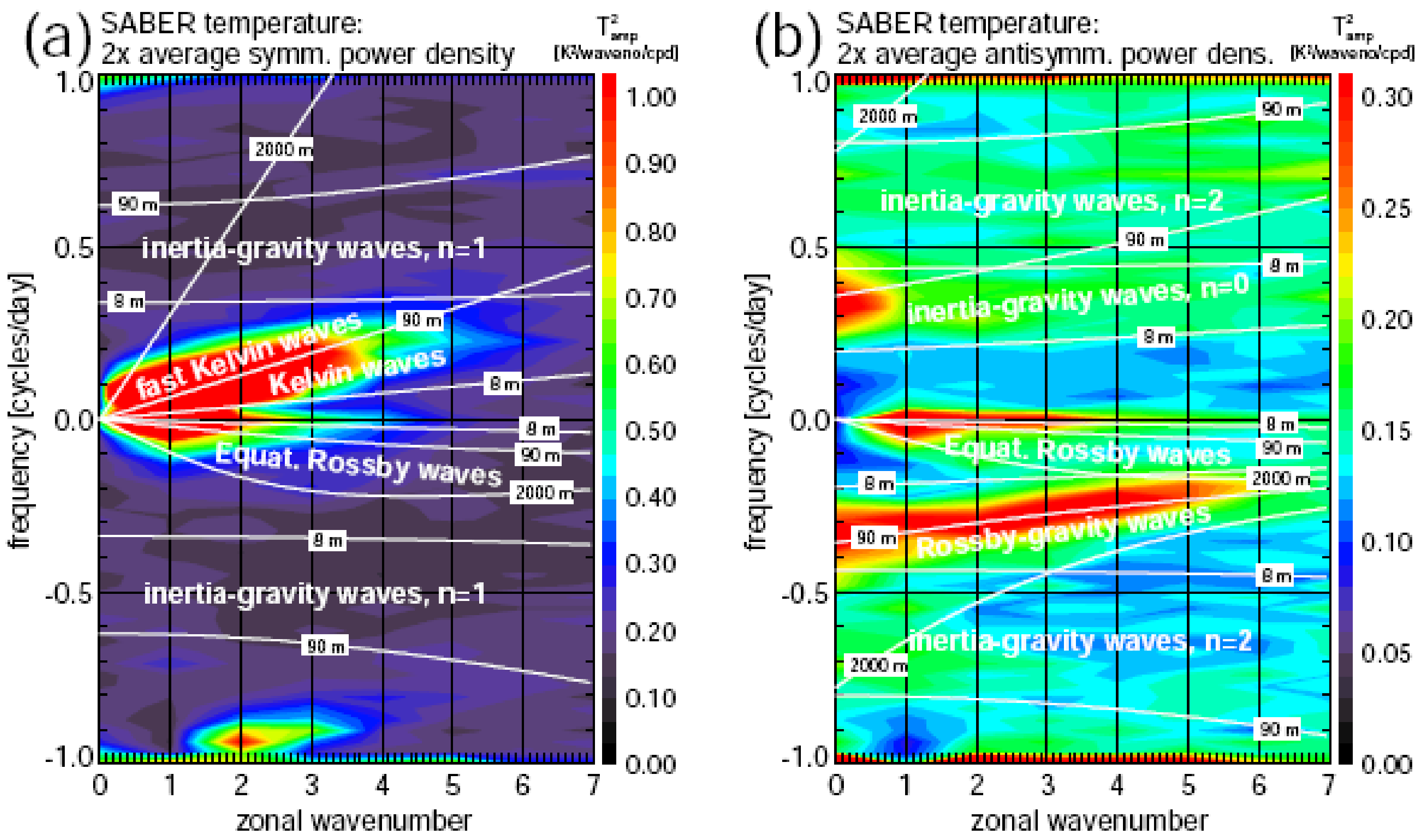

Ern et al, ACP, 2008

The special conditions of the tropical region (15S-15N) (1)

- Small horizontal temperature variations
- Geopotential fluctuations and vertical velocities (excluding convective systems) are an order of magnitude lower than at temperate latitudes
- Strong interaction convection / mesoscale / large scale circulation
- In the convective zones, precipitation of the order of 2 cm/day, i.e. 20 kg per m^2, or (with L=2.5 10^6 J kg^{-1}), heating of the column for 5 10^7 J m^{-2} day $^{-1}$. Assuming this heat is uniformly distributed in the column with mass p0/g ≈ 104 kg m^{-2}, the heating per unit mass of air is J/cp ≈ 5 K day^{-1}. In practice, this unequally distributed heating is 2 to 4 times greater, resulting in average speeds of the order of 3 to 5 cm s^{-1}, much stronger than outside convective systems. At th ecore of the convective towers, vertical speed of several m s^{-1} are recorded.
- Convergence of humidity in the convection zone (precipitation greatly exceeds local evaporation)

The special conditions of the tropical region (15S-15N) (2)

- $f \leq 10^{-5}\ s^{-1}$
- Vertical scale of motion = atmospheric thickness (H)
- Moisture is an essential ingredient of the energetics

The equations of motion (in log-pressure)

$$(\partial_t + \vec{v}\cdot\vec{\nabla}_h + \tilde{w}\,\partial_{\tilde{z}})\vec{v} + f\,\vec{k}\times\vec{v} = -\vec{\nabla}_h \Phi$$

$$\partial_{\tilde{z}}\Phi = RT/H$$

$$\vec{\nabla}_h\cdot\vec{V} + \partial_{\tilde{z}}\tilde{w} - \tilde{w}/H = 0$$

$$c_p(\partial_t + \vec{v}\cdot\nabla_h)T + \frac{\tilde{w}\,N^2 H}{\kappa} = J$$

where J is the total heating (radiative + condensation)

The fluctuations of the geopotential $\delta\Phi$ are of the same order as the advection term

$$\delta\Phi \approx U^2 \approx 100\, m^2 s^{-2}$$

Following the hydrostatic relation, the temperature fluctuations are $\approx \delta\Phi/R \approx U^2/R \approx 0{,}3\, K$

The heating term, which can be of the order of $J/c_p \approx 1\, K/day$, is balanced by the vertical transport and determines $\tilde{w}$, hence $W \approx 0{,}3\, cm\, s^{-1}$ for $N^2 H/R \approx 3\, K\, km^{-1}$

Scales of motion

vertical motion	$D \approx H \approx 10^4\, m$
horizontal motion	$L \approx 1000\, km$
horizontal speed	$U \approx 10\, ms^{-1}$
vertical speed	$W \leqslant DU/L$
Rossby number	$Ro \geq 1$
deformation radius	$H\dfrac{N}{f} \geq 10000\, km$

The modes of the tropical variability
(shallow water version, no vertical dependency)

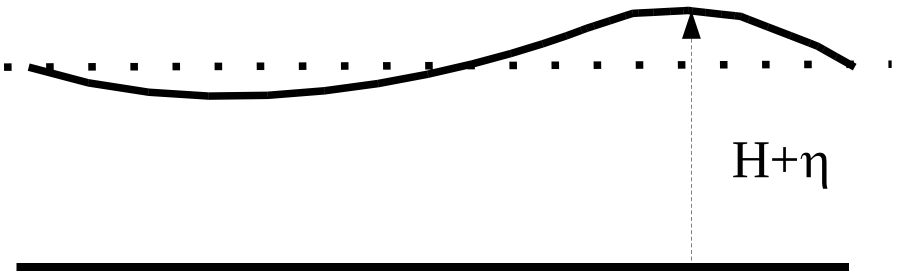

The linearized basic equations

Approximation of the equatorial β *plane* $(f=\beta y)$

$$\partial_t u - \beta y v = -g \partial_x \eta$$

$$\partial_t v + \beta y u = -g \partial_y \eta$$

$$\partial_t \eta + H(\partial_x u + \partial_y v) = 0$$

Free modes: case of the Kelvin wave (no meridian velocity: v=0)

In the case of the Kelvin wave, the equations are reduced to

$$\partial_t u = -g\,\partial_x \eta$$
$$\partial_t \eta + H\,\partial_x u = 0$$
$$\beta\, y u = -g\,\partial_y \eta$$

Assuming $u = \hat{u}(y)\exp i(kx - \omega t)$ et

$$\eta = \hat{\eta}(y)\exp i(kx - \omega t)$$

We obtain $\omega \hat{u} = g k \hat{\eta}$ et $-\omega\hat{\eta} + kH\hat{u} = 0$

hence $\omega^2 = c^2 k^2$ with $c^2 = gH$

The sign of ω/k is fixed by the third relation

$$\partial_y \hat{\eta} = \frac{-\beta y k}{\omega}\hat{\eta}$$

ω/k must be positive for the wave to be confined

under the shape $\hat{\eta} = \eta_0 \exp\left(\frac{-\beta k}{2\omega} y^2\right) = \eta_0 \exp\left(\frac{-\beta y^2}{2c}\right)$

The Kelvin wave propagates eastward

For $c \approx 30\,m\,s^{-1}$, the width of the wave is given by $|2c/\beta|^{1/2} \approx 1600\,km$

In the ocean, c is much smaller, $c \approx 0{,}5 - 3\,m\,s^{-1}$, hence a width of 100-250 km

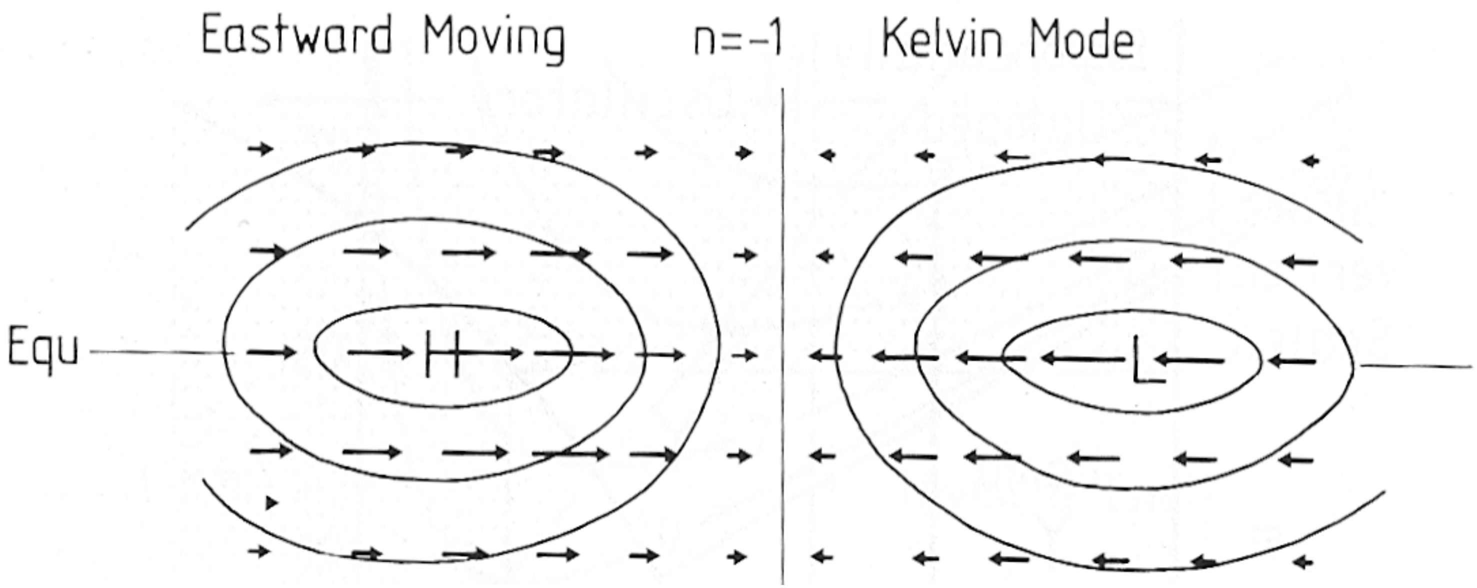
Eastward Moving n=-1 Kelvin Mode
Equ
H
L

Kelvin mode

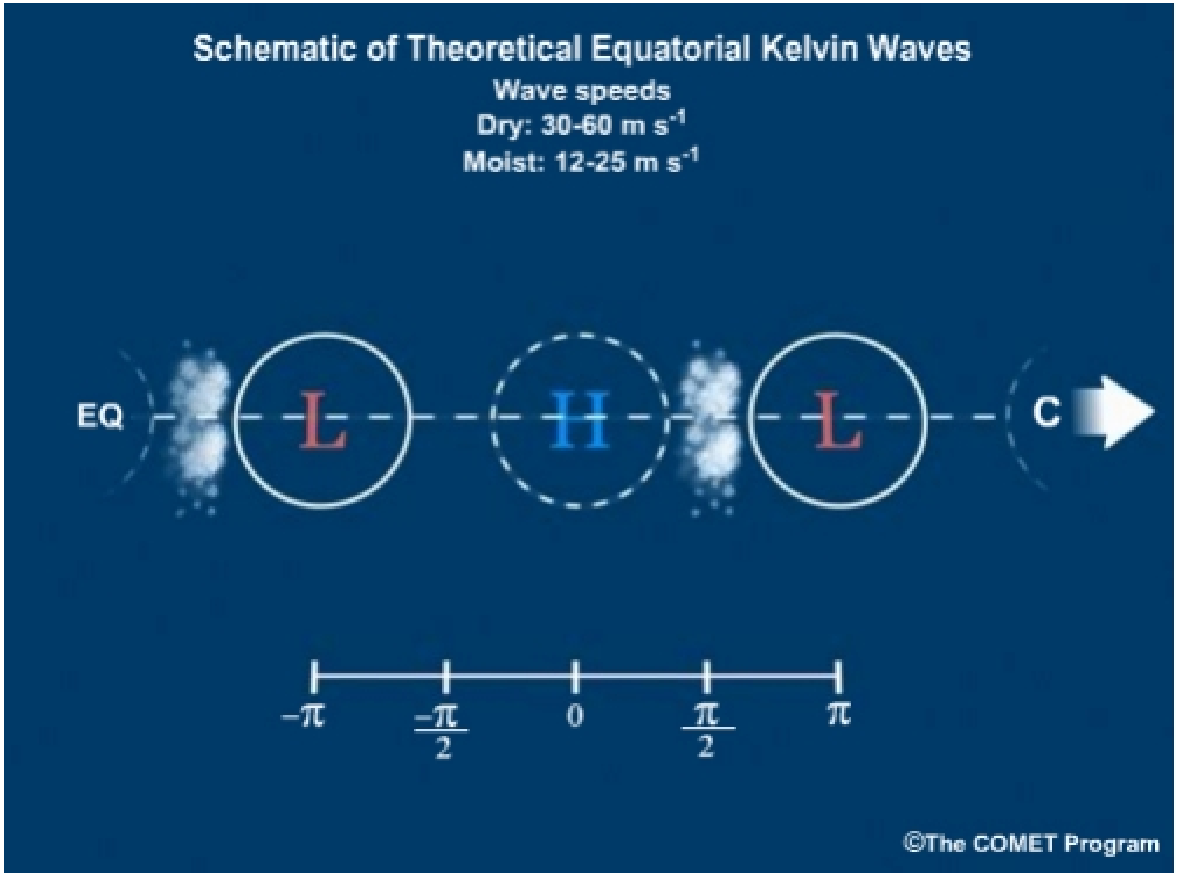
Schematic of Theoretical Equatorial Kelvin Waves
Wave speeds
Dry: 30-60 m s-1
Moist: 12-25 m s-1
EQ
L
H
L
C
-π
-π/2
0
π/2
π
©The COMET Program

Example of atmopsheric kelvin mode

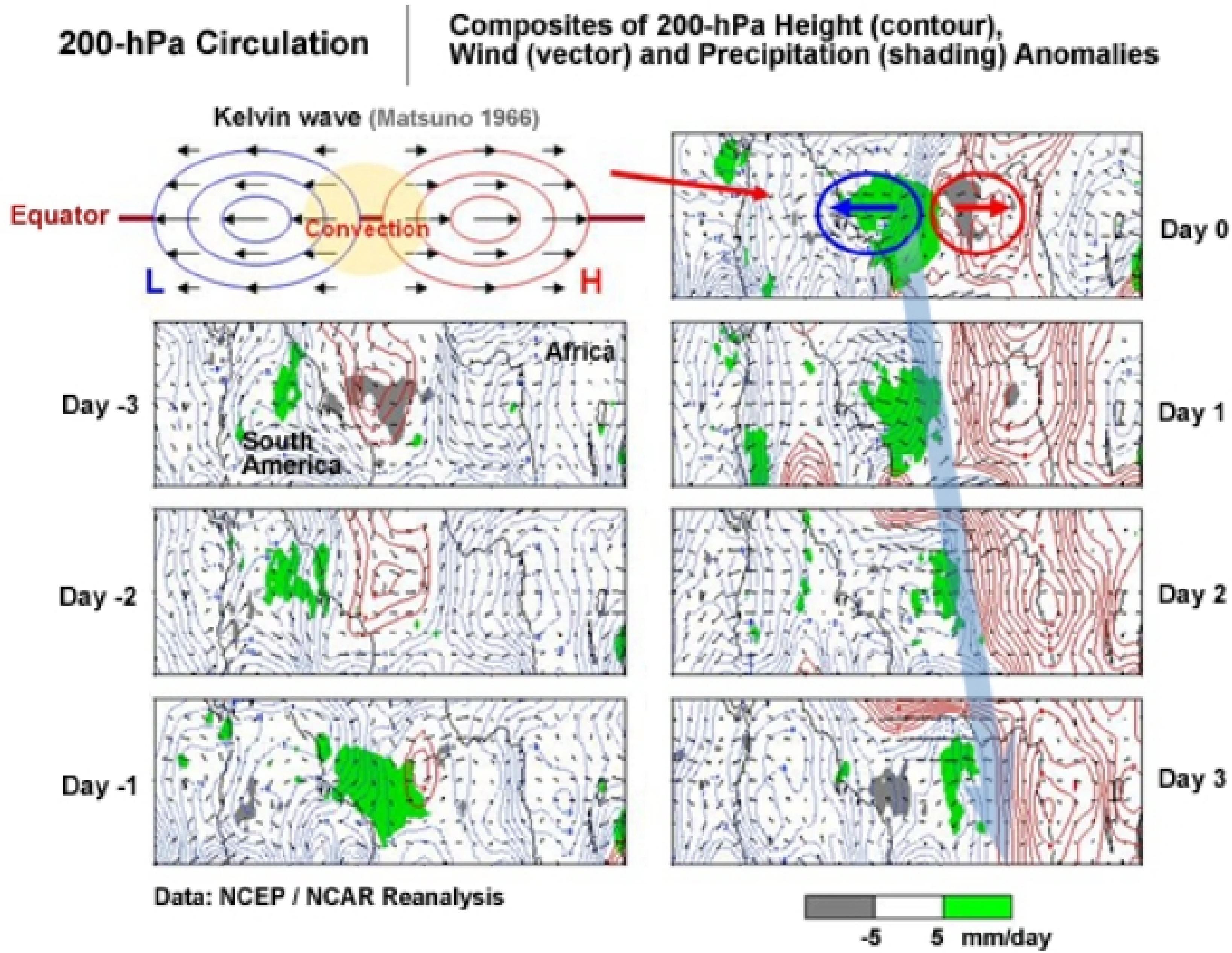

Hui Wang and Rong Fu

Free modes: general case

After a few manipulations, one gets an equation for the sole variable v

$$\partial_t\{\frac{1}{c^2}(\partial_{t^2}v+\beta^2 y^2 v)-(\partial_{x^2}v+\partial_{y^2}v)\}-\beta\partial_x v=0$$

Assuming now $v=\hat{v}(y)\exp(i(k\,x-\omega\,t))$, we obtain

$$d_y^2\hat{v}+(\frac{\omega^2}{c^2}-k^2-\frac{\beta k}{\omega}-\frac{\beta^2 y^2}{c}{}^2)\hat{v}=0$$

The solutions of this equation are kown under the form

$$\hat{v}=H_n((\frac{\beta}{c})^{1/2}y)\exp(\frac{-\beta y^2}{2c})$$

where H_n is a Hermite poynomial and the dispersion relation is

$$\frac{\omega^2}{c^2}-k^2-\frac{\beta k}{\omega}=(2n+1)\frac{\beta}{c}$$

Dispersion relation for the free equatorial waves

n=-1 : Kelvin mode

n= 0: Rossby-gravity mode

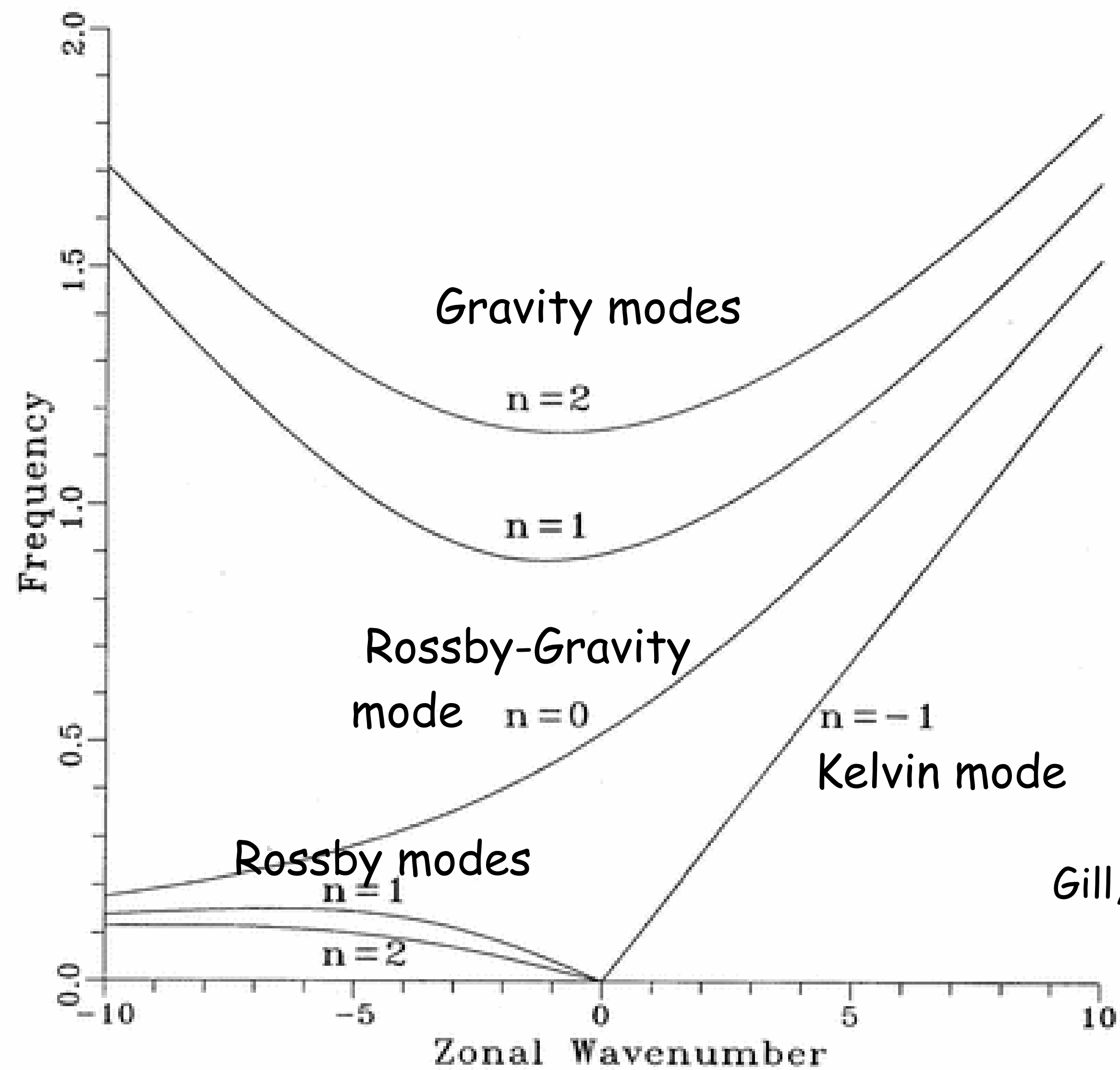

Gill, 1980

Kelvin mode

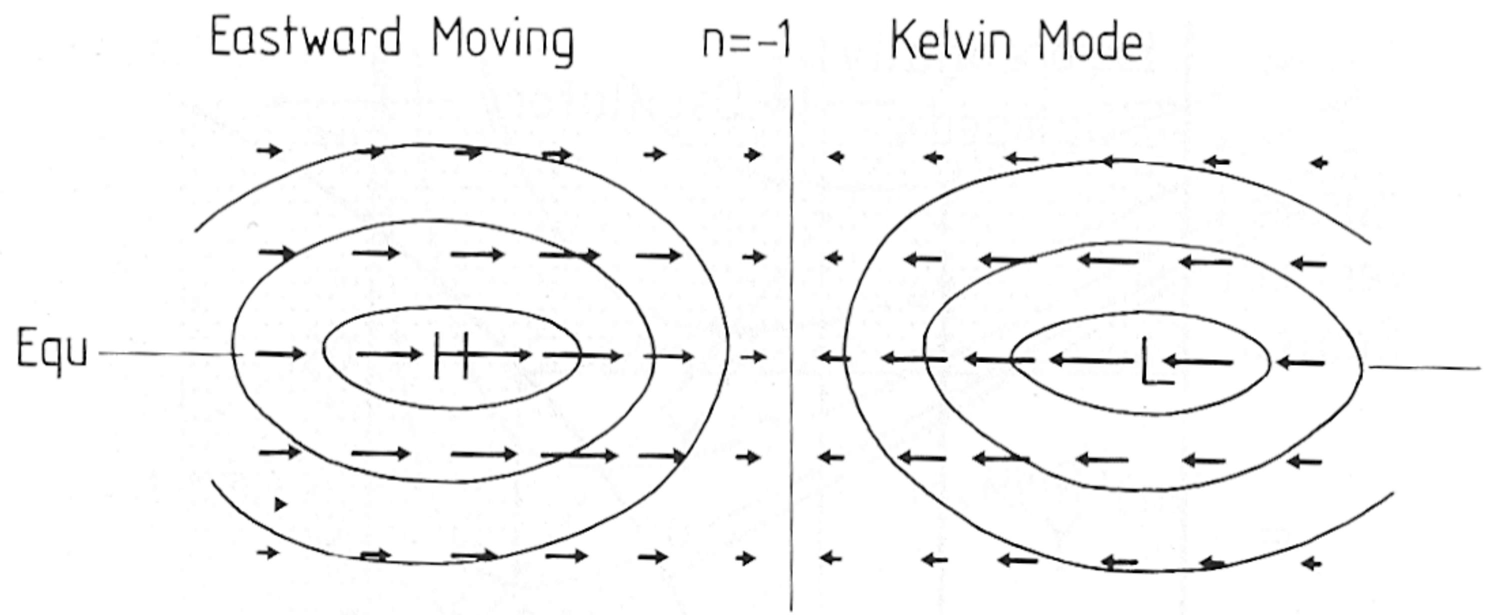

Rossby-gravity mode

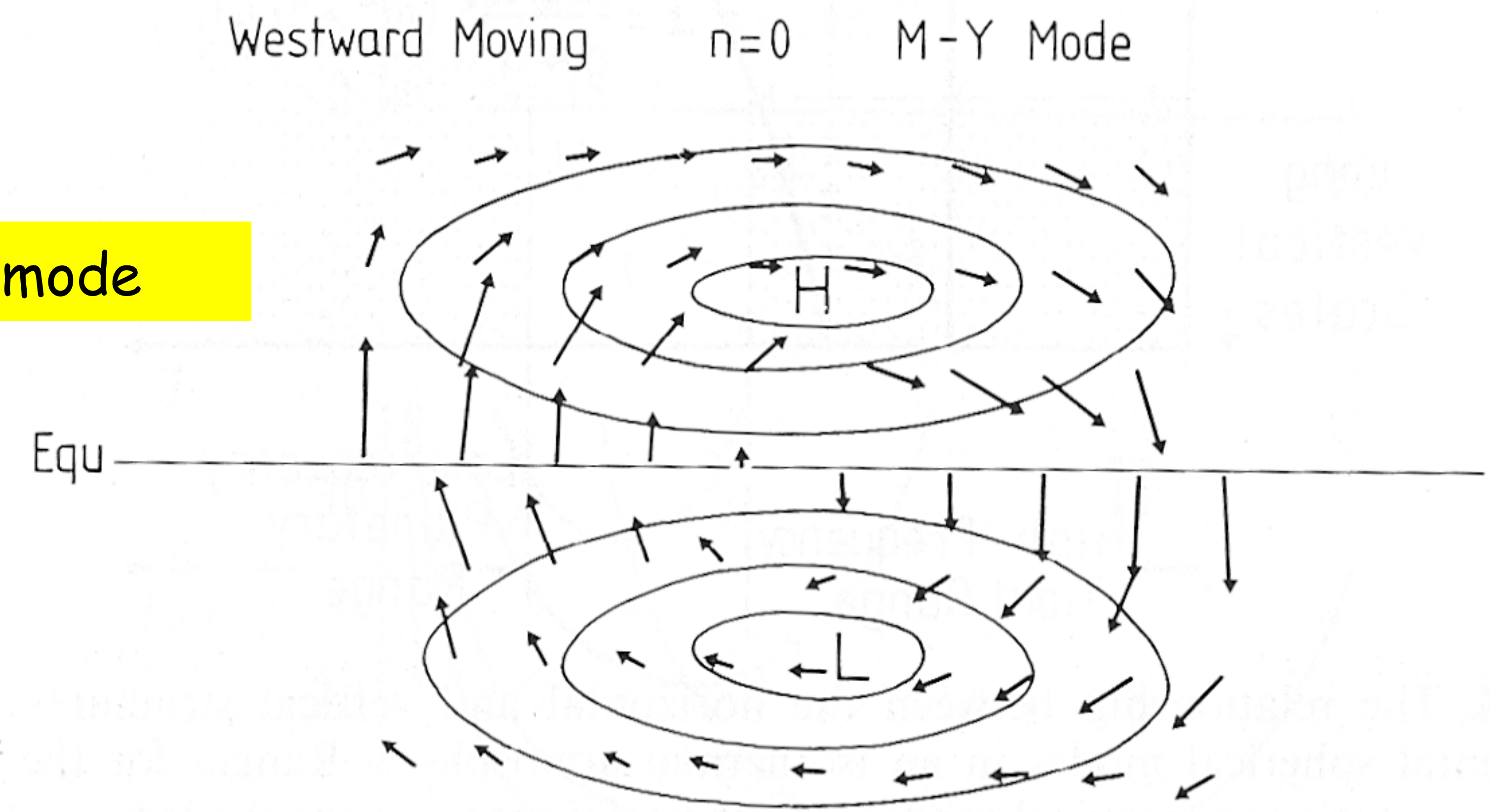

Rossby mode

Symétrique with respect to the equator, propagating westward

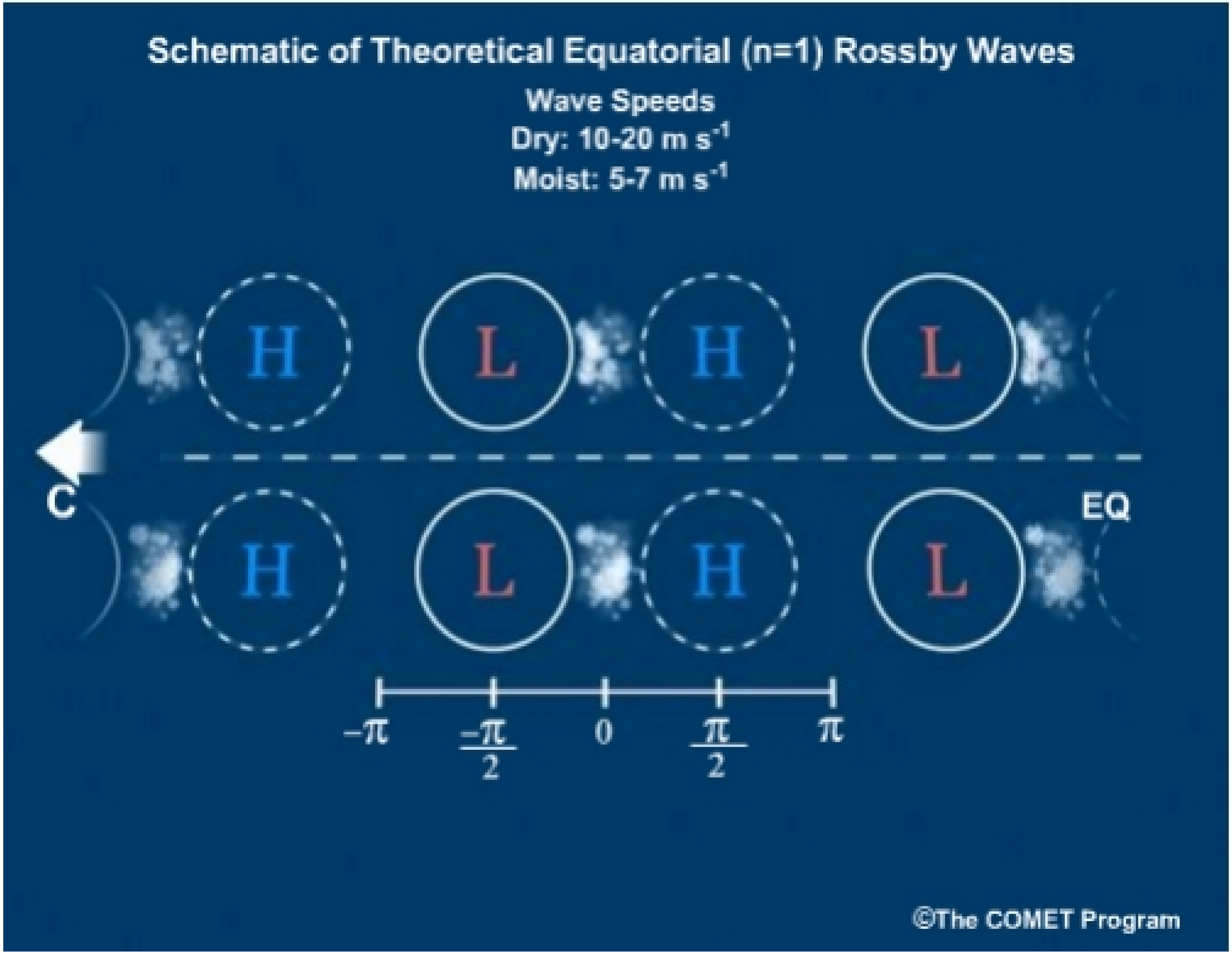

The continuity equation is replaced by

$$\frac{\partial u}{\partial x}+\frac{\partial v}{\partial y}+\frac{1}{\rho_0}\frac{\partial \rho_0 w}{\partial z}=0$$

and the temperature equation

$$\frac{\partial}{\partial t}\frac{\partial \phi}{\partial z}+w N^2=0$$

where $\rho_0(z)=\rho_S \exp(-z/H)$ and N is the Brünt-Vaissala frequency, assumed to be constant. Combining the two equations to eliminate w leads to $\frac{\partial}{\partial t}L[\phi]-N^2(\frac{\partial u}{\partial x}+\frac{\partial v}{\partial y})=0$ with $L=\frac{1}{\rho_0}\frac{\partial}{\partial z}\rho_0\frac{\partial}{\partial z}$.

We then assume that ϕ has a vertical structure which is an eigenfunction of L, that is $L[\phi]=-\lambda\phi$. Then the equation for ϕ is $\frac{\partial \phi}{\partial t}+\frac{N^2}{\lambda}(\frac{\partial u}{\partial x}+\frac{\partial v}{\partial y})=0$

Hence the shallow-water theory applies by replacing H by $\frac{N^2}{g\lambda}$.

(because in the shallow-water model $\phi=g\eta$)

Now the effect of moisture can be accounted by adding a heating in the temperature equation: $\frac{\partial}{\partial t}\frac{\partial \phi}{\partial z}+w N^2=Q$. If $Q=\alpha w N^2$, then the effect is to replace N^2 by $(1-\alpha)N^2$, that is to reduce the effective stability.

SPECTRAL TIME-SPACE ANALYSIS OF OLR IN THE TROPICAL REGION

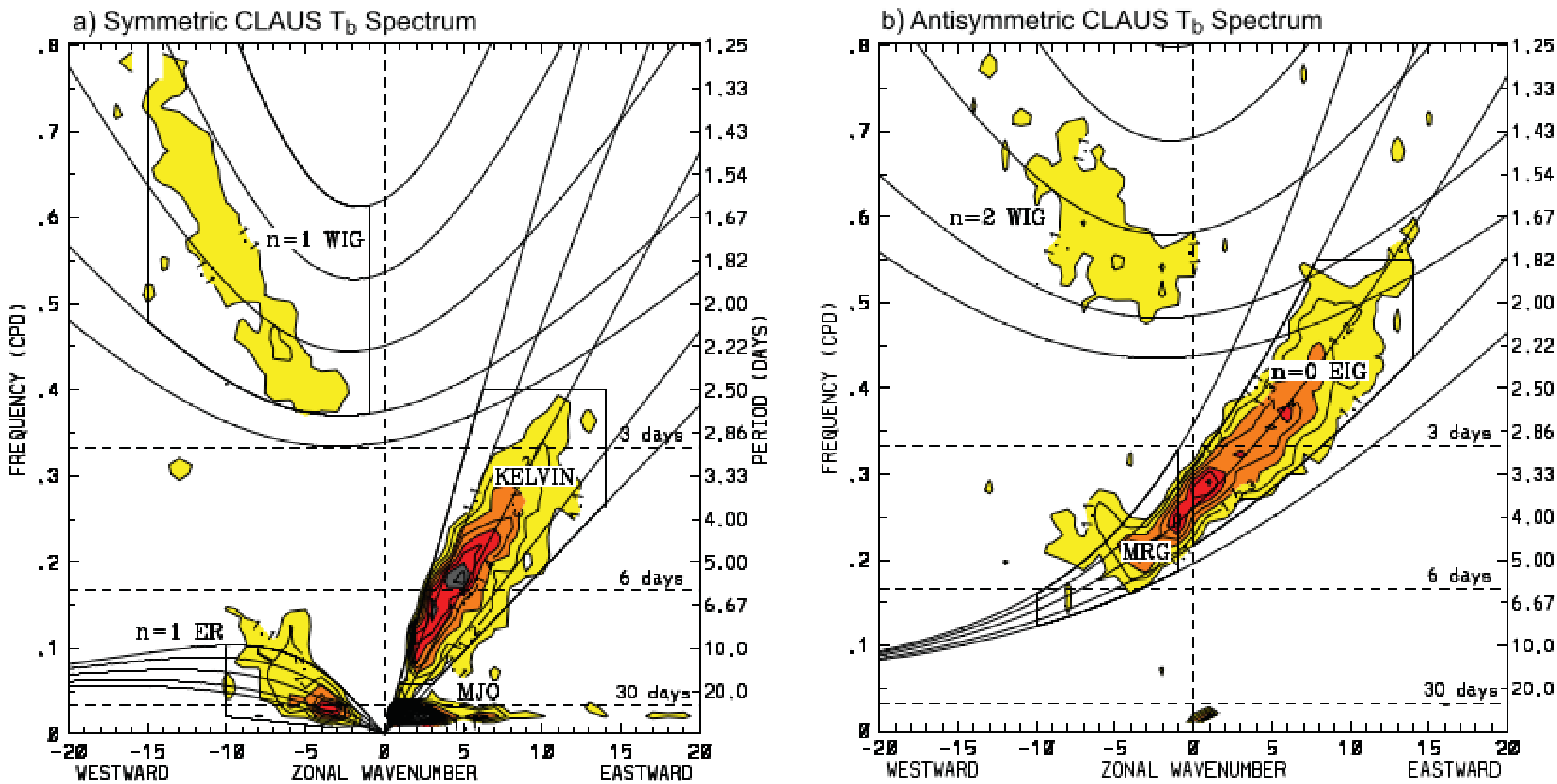

This analysis used the CLAUS dataset of brightness temperature at 10.8 μm produced from the belt of geostationary satellites. The two panels show modes symmetric to equator on the left and antisymmetric on the right.

The theoretical curves are plotted for several values of the equivalent depth H.

Kiladis et al., Rev. Geophysics, 2009.

Notice that the MJO propagation is much too slow to be explained by dry waves.

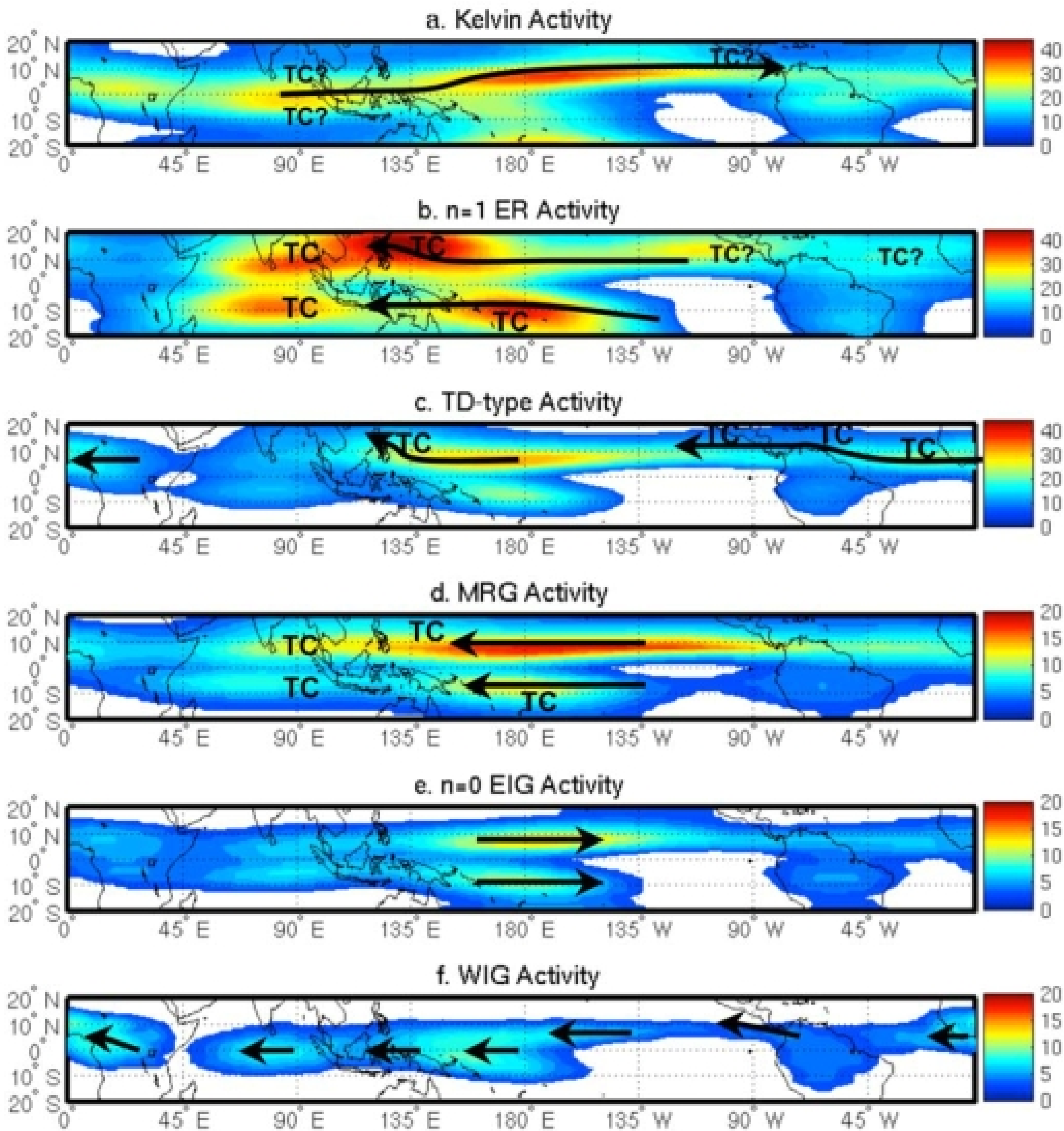

a. Kelvin Activity
TC?
TC?
TC?
b. n=1 ER Activity
TC
TC
TC
TC
TC?
TC?
c. TD-type Activity
TC
TC
TC
TC
d. MRG Activity
TC
TC
TC
TC
e. n=0 EIG Activity
f. WIG Activity
20° N
10° N
0°
10° S
20° S
0
45° E
90° E
135° E
180° E
135° W
90° W
45° W
40
30
20
10
0
20
15
10
5
0

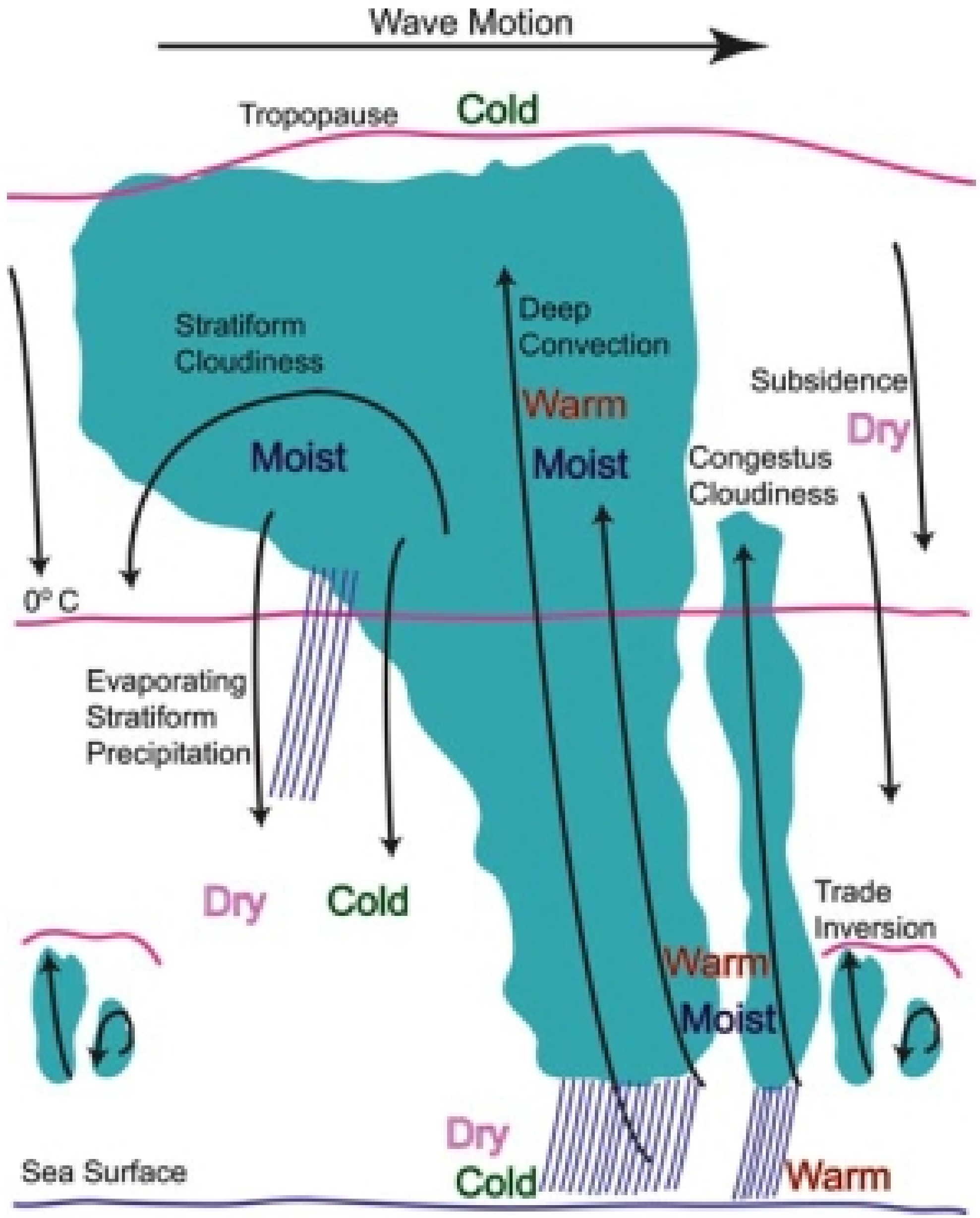

Figure 19. The hierarchy of cloudiness, temperature, and humidity within CCEWs, valid from MCS to MJO scales. Wave movement is from left to right (adapted from *Johnson et al.* [1999], *Straub and Kiladis* [2003c], and *Khouider and Majda* [2008]).

Forced waves, stationary response

We add a forcing and a damping. The forcing can be interpretated as convective heating. The damping can be interpreted as a friction or a thermal damping. Same coefficient for a matter of simplicity.

The equations are reduced to

$$\frac{\partial}{\partial t}=-\alpha$$

$$-\alpha u-\beta y v=-g\partial_x \eta$$

$$-\alpha \eta+H(\partial_x u+\partial_y v)=\frac{-Q}{N^2}$$

with $w=\dfrac{Q}{N^2}$ at mid-troposphere

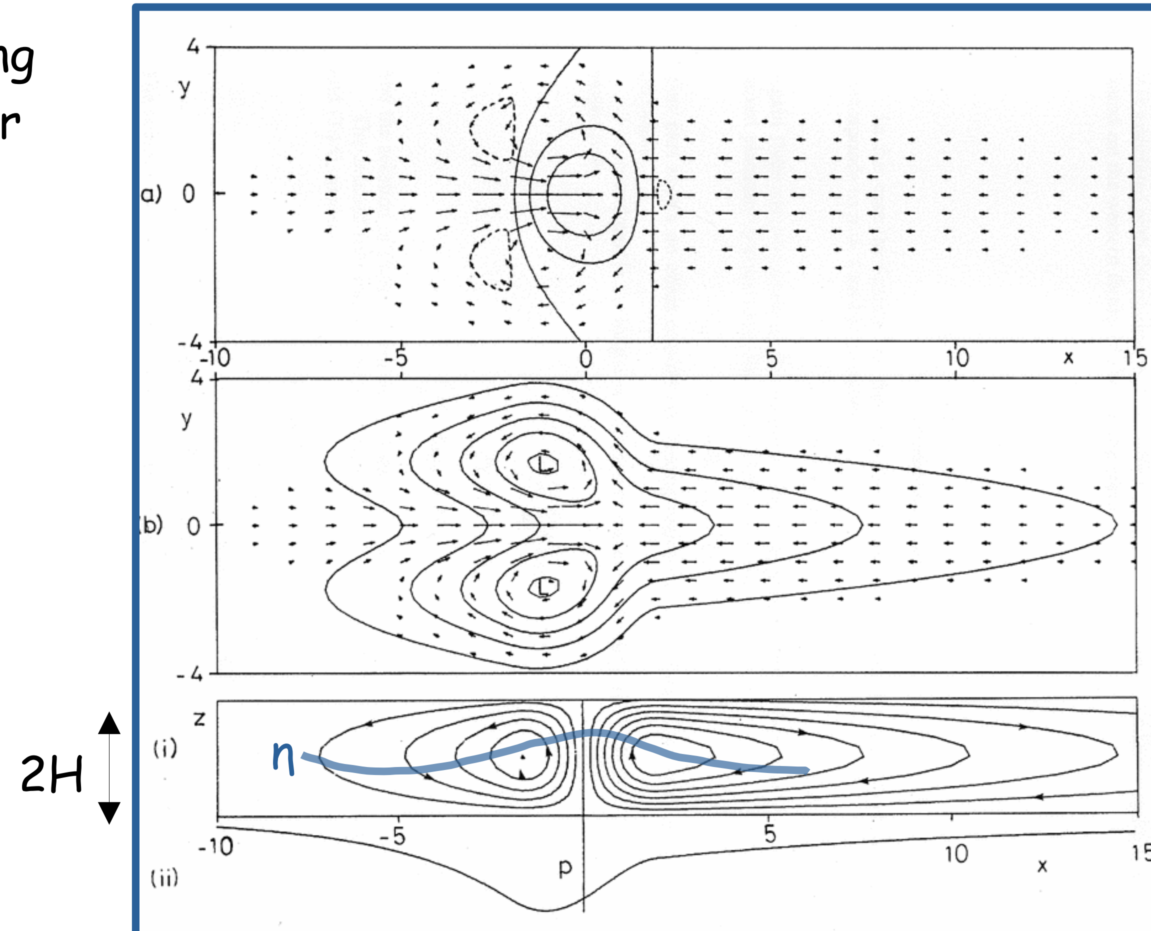

Gill, 1980, fig.1

Solution for a forcing centered on the equator.

The monsoon anticyclone as a response to heating

geopotentiel and wind à 100 hPa

anticyclones

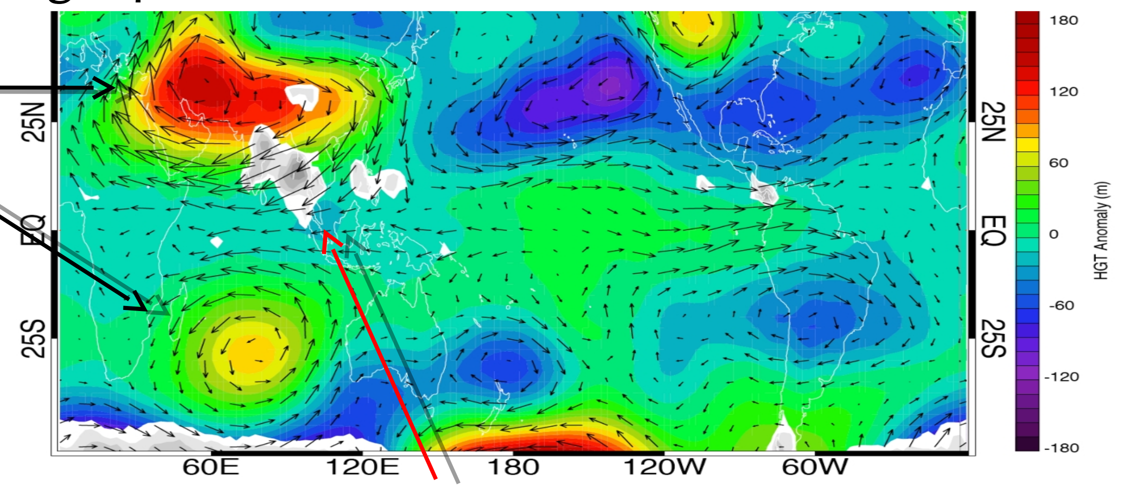

Convection (heating)

observations

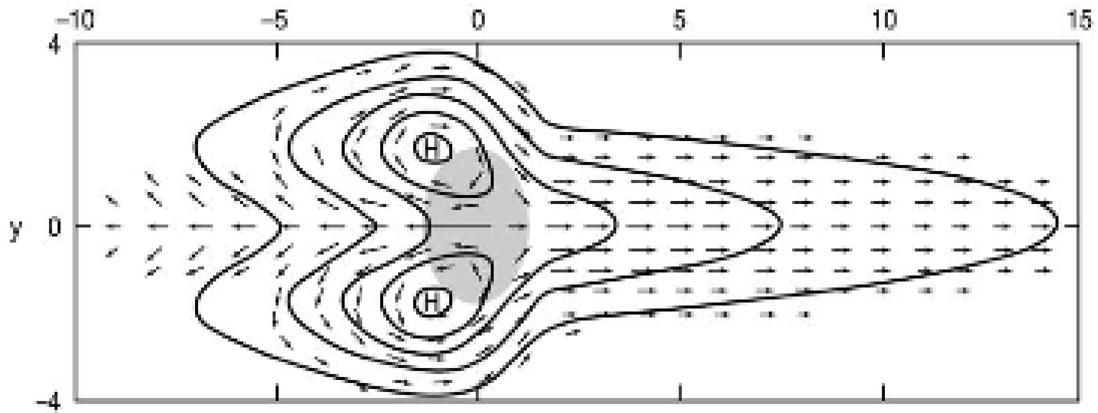

theory

Two-Layer Model of Equatorial Heating

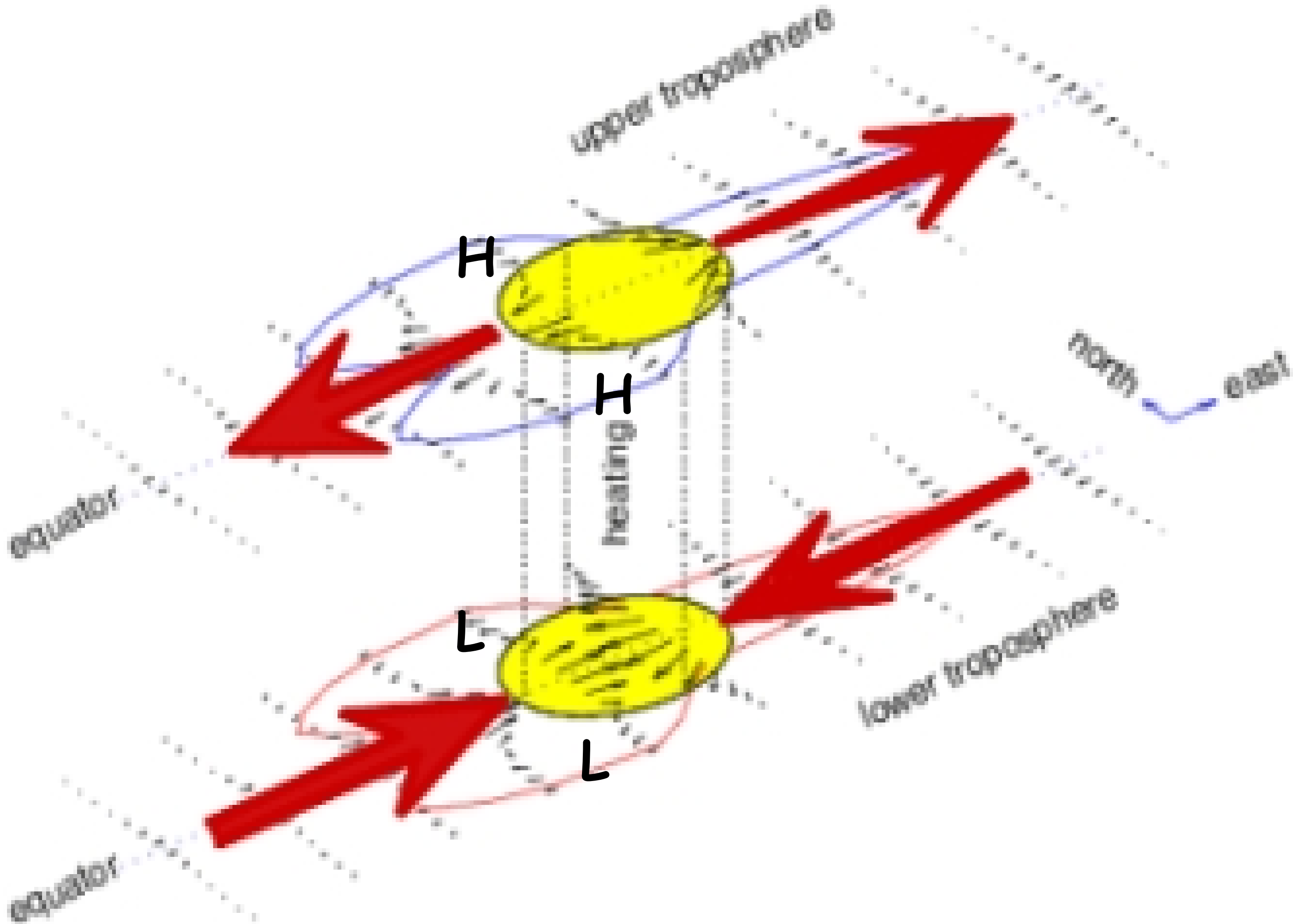

Gill, 1980: QJRMS

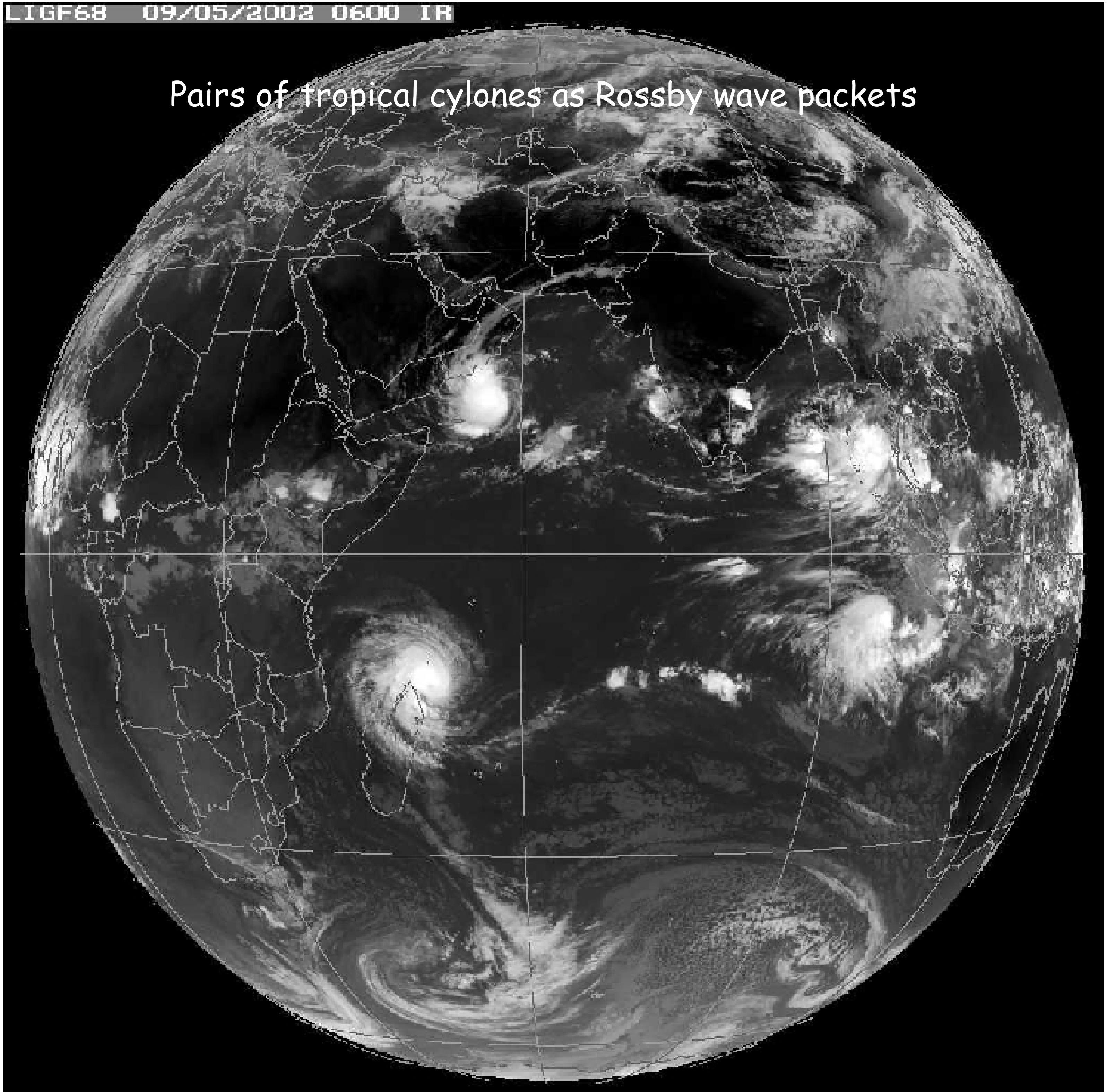
LIGF68 09/05/2002 0600 IR
Pairs of tropical cylones as Rossby wave packets

Westerly burst

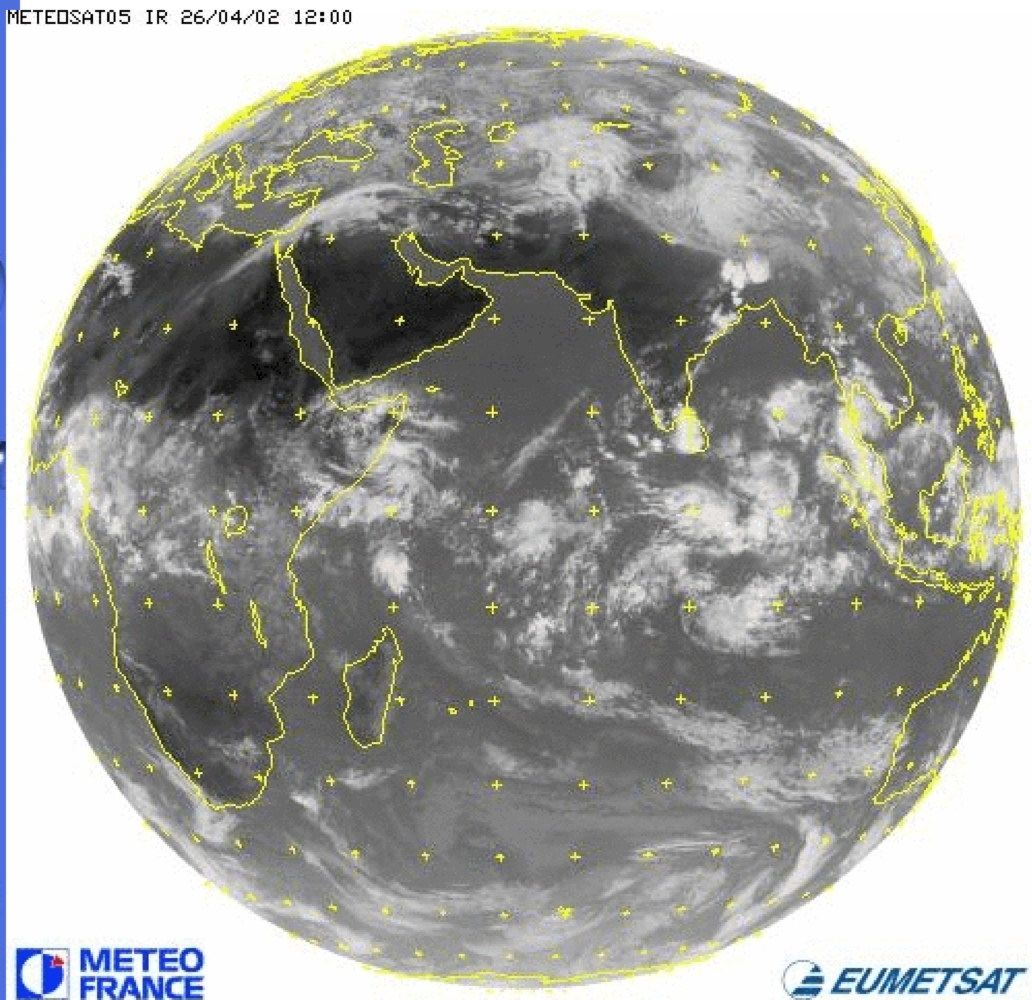

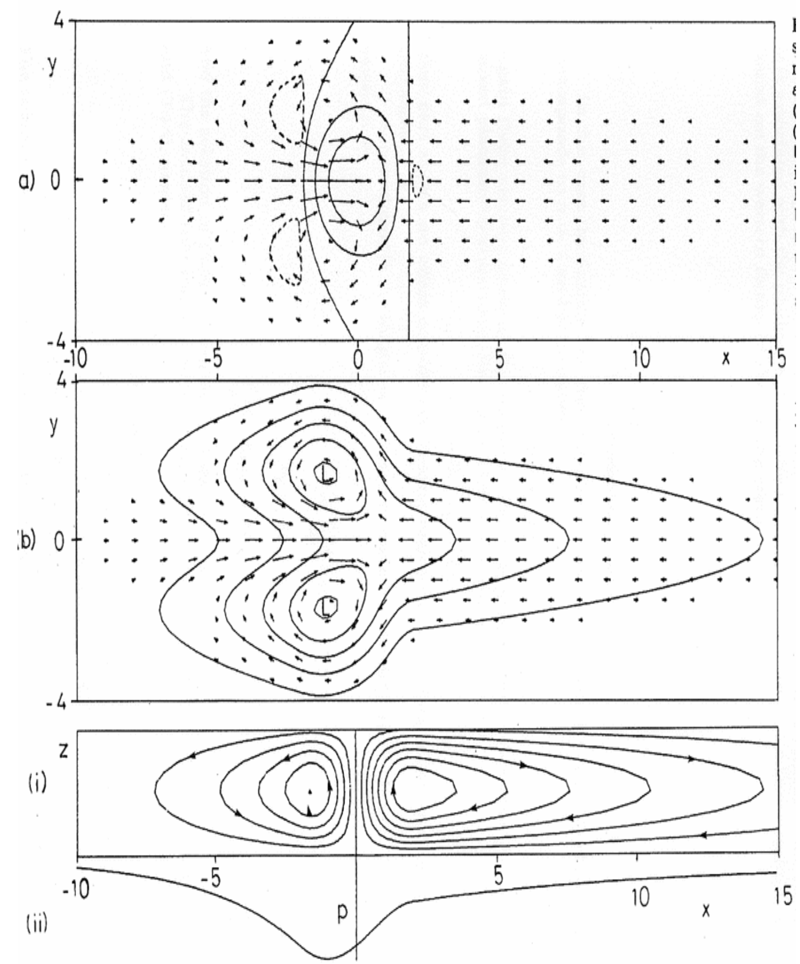

Quasi-biennal oscillation

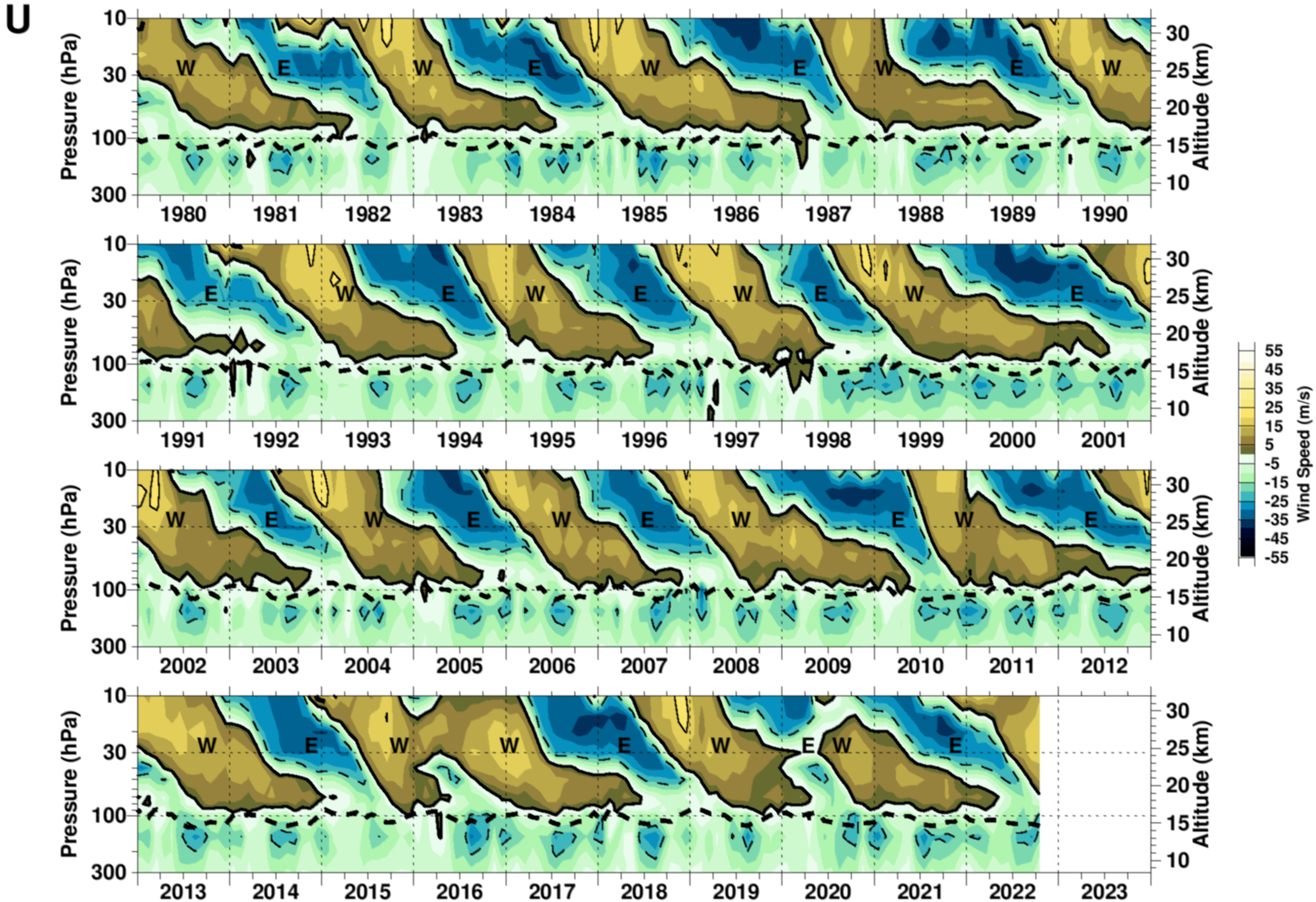

Paul A. Newman, Larry Coy, Leslie R. Lait, Eric R. Nash (NASA/GSFC) Wed Nov 2 16:21:50 2022

Méchanism of the quasi-biennal oscillation

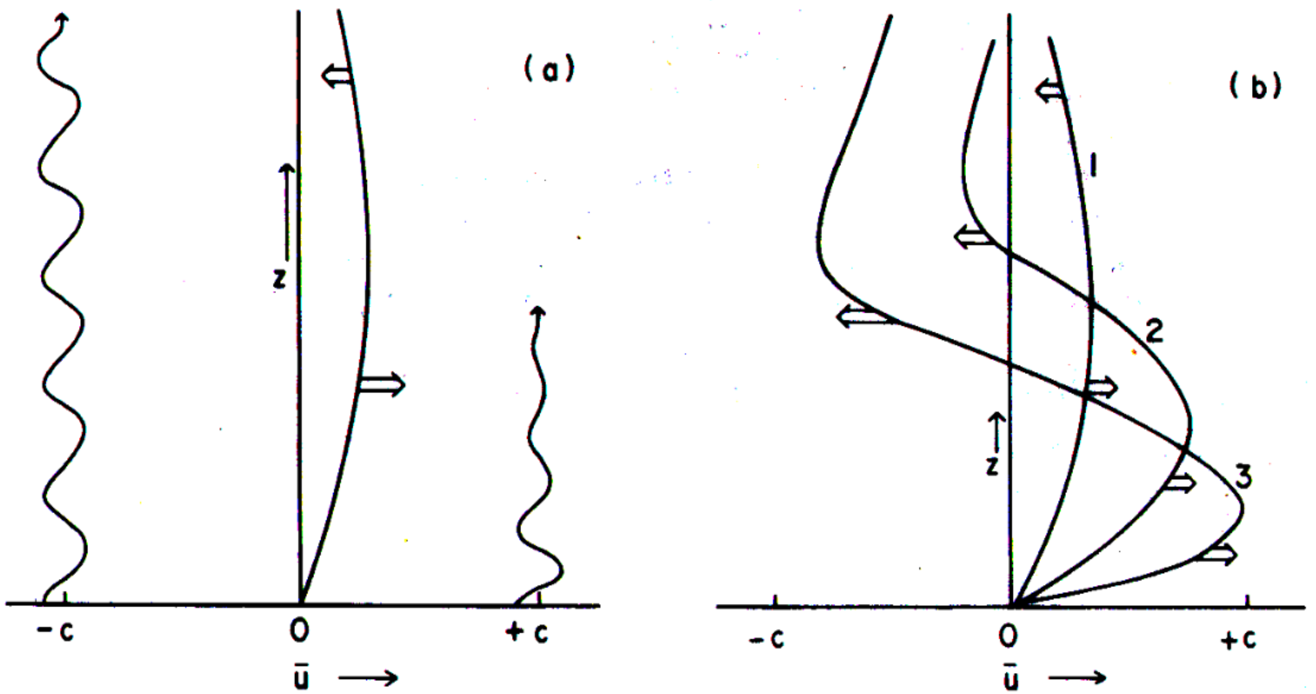

Fig. 8.6. Schematic representation of the instability of zonal flow in a stratified fluid with standing-wave forcing at a lower boundary. (a) Onset of instability from a small zonal flow perturbation. (b) Early stages of the subsequent mean-flow evolution. Broad arrows show locations and direction of maxima in mean wind acceleration. Wavy lines indicate relative penetration of wave components of positive and negative phase speeds *c*. [From Plumb (1982), with permission.]

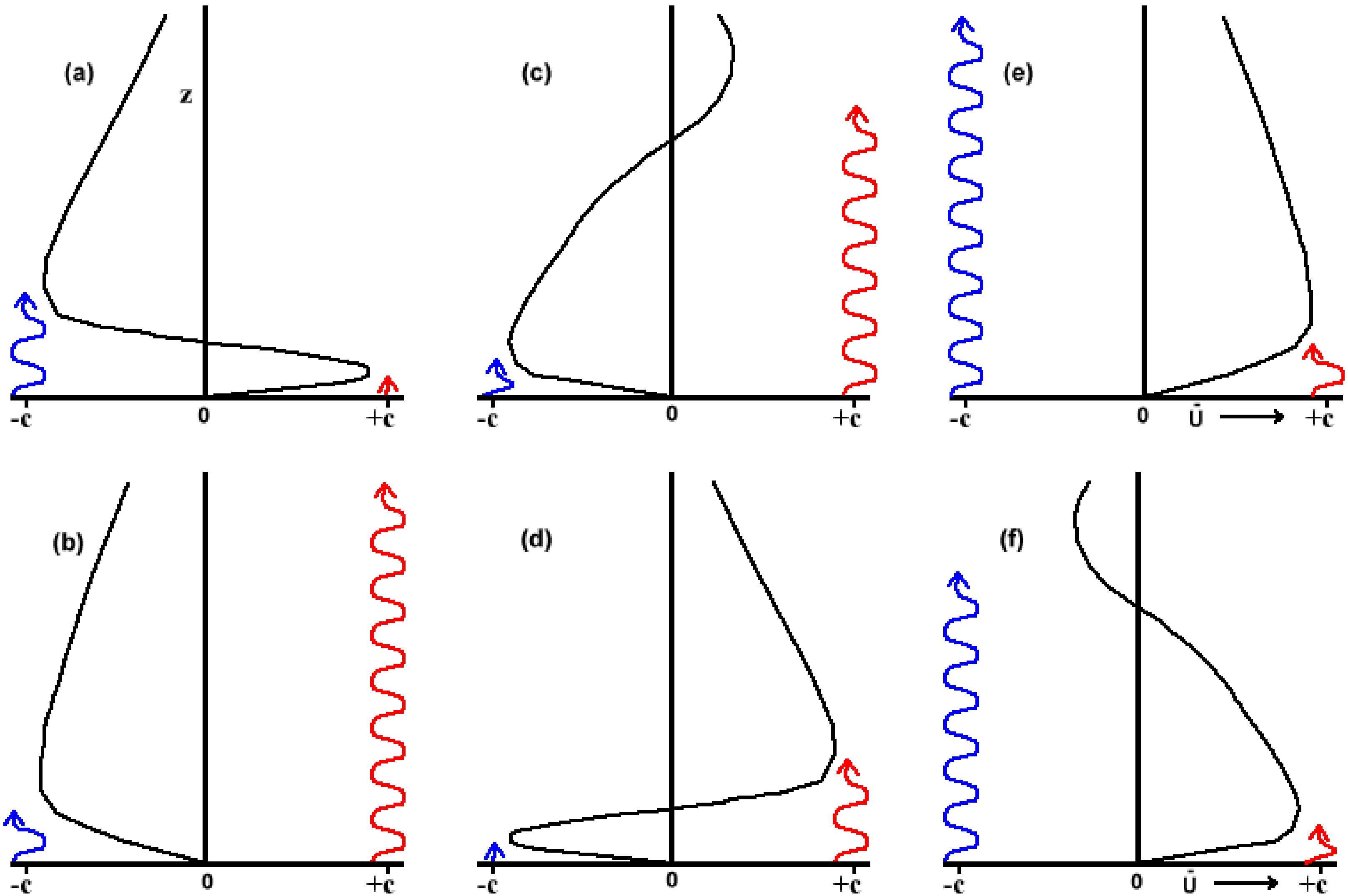

Mechanism of the QBO

Eastward propagated waves are provided by the Kelvin mode, westward propagating waves are provided by the Rossby-garvity mode. Gravity waves provide both directions.

I Mean state and seasonal cycle

II Monsoon

III ENSO

IV Madden-Julian mode

V Equatorial waves

VI Tropical cyclones

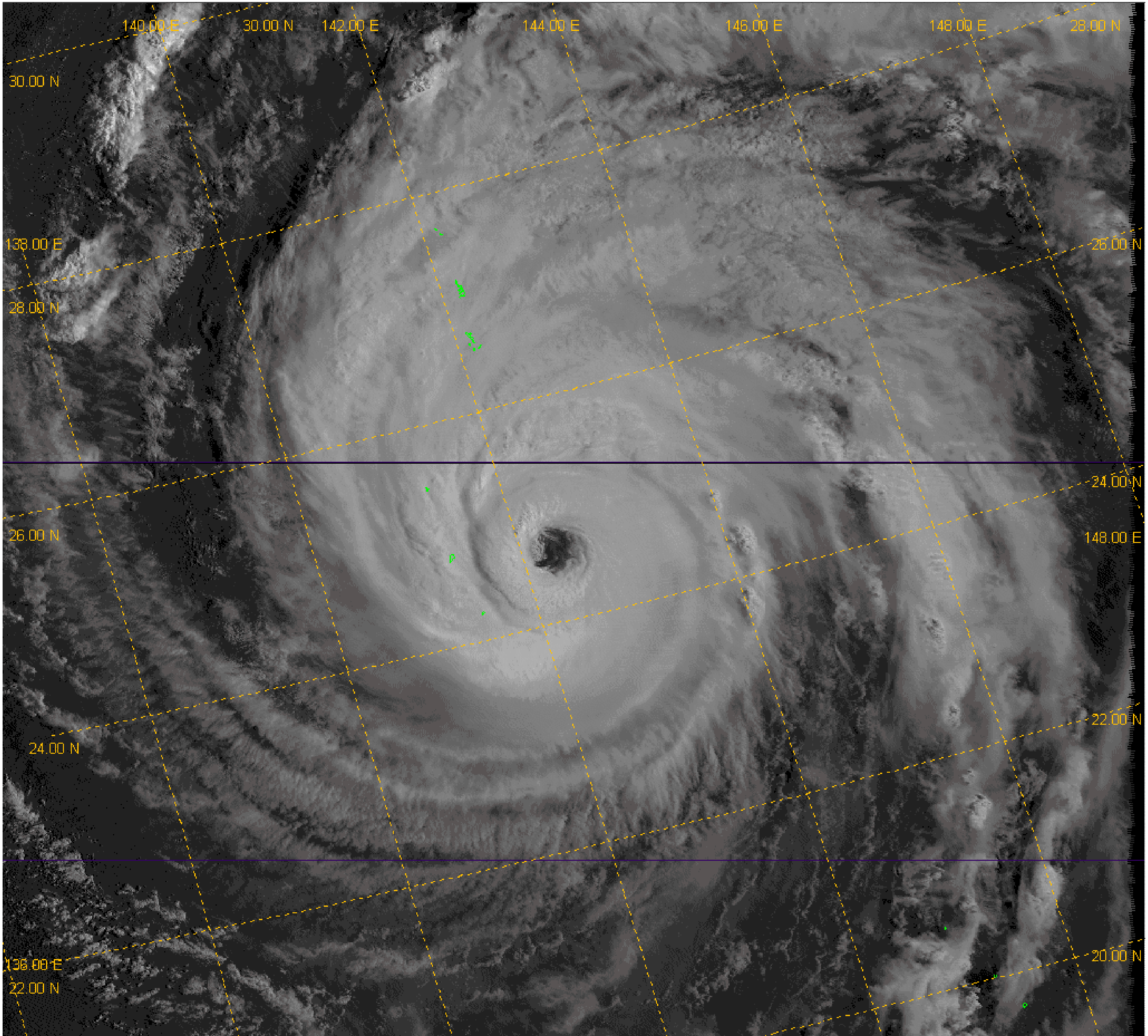
140.00 E
30.00 N
142.00 E
144.00 E
146.00 E
148.00 E
28.00 N
30.00 N
138.00 E
26.00 N
28.00 N
24.00 N
26.00 N
148.00 E
22.00 N
24.00 N
20.00 N
136.00 E
22.00 N

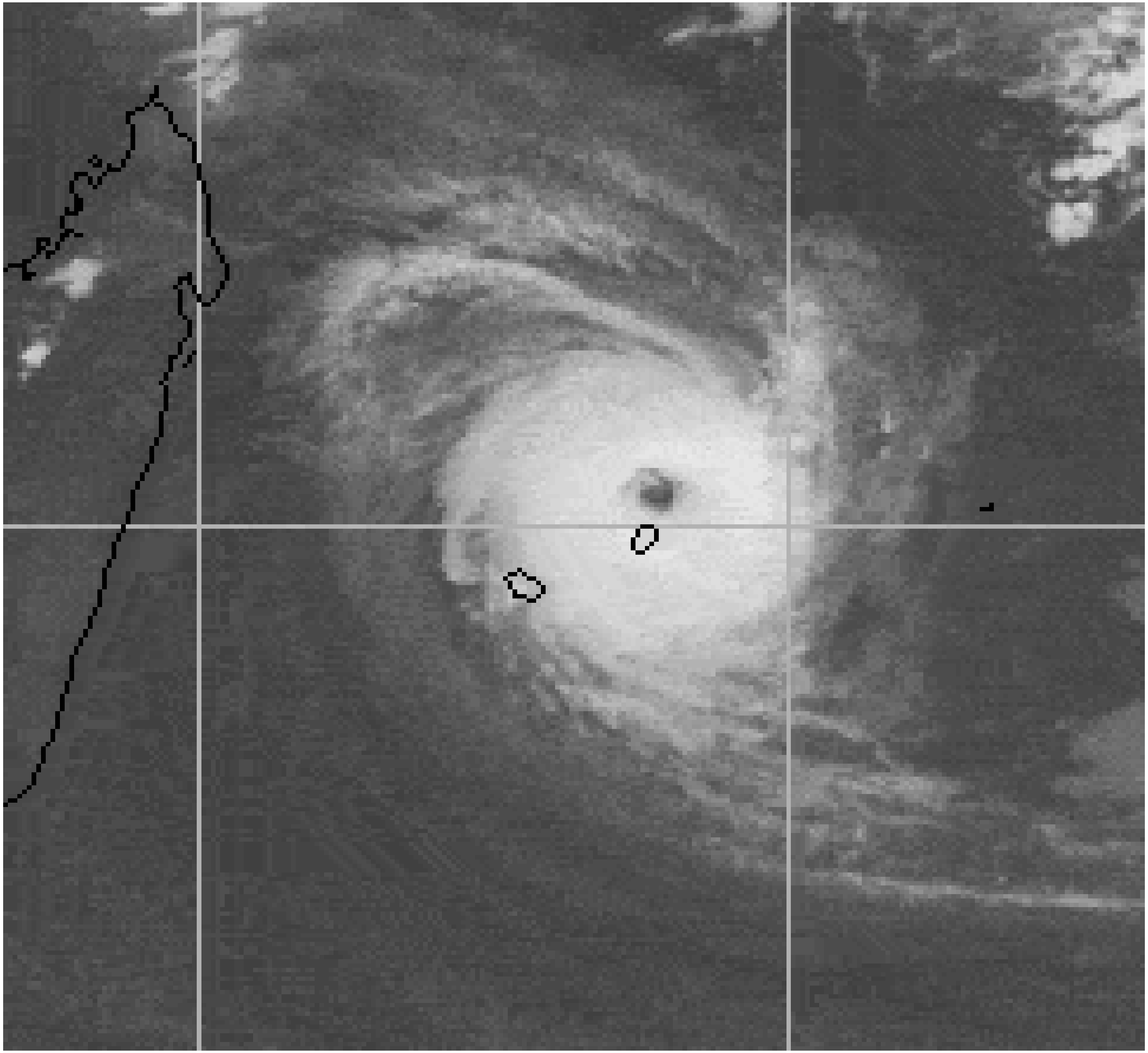

DINA - 22 January 2002

Tracks and Intensity of Tropical Cyclones, 1851-2006

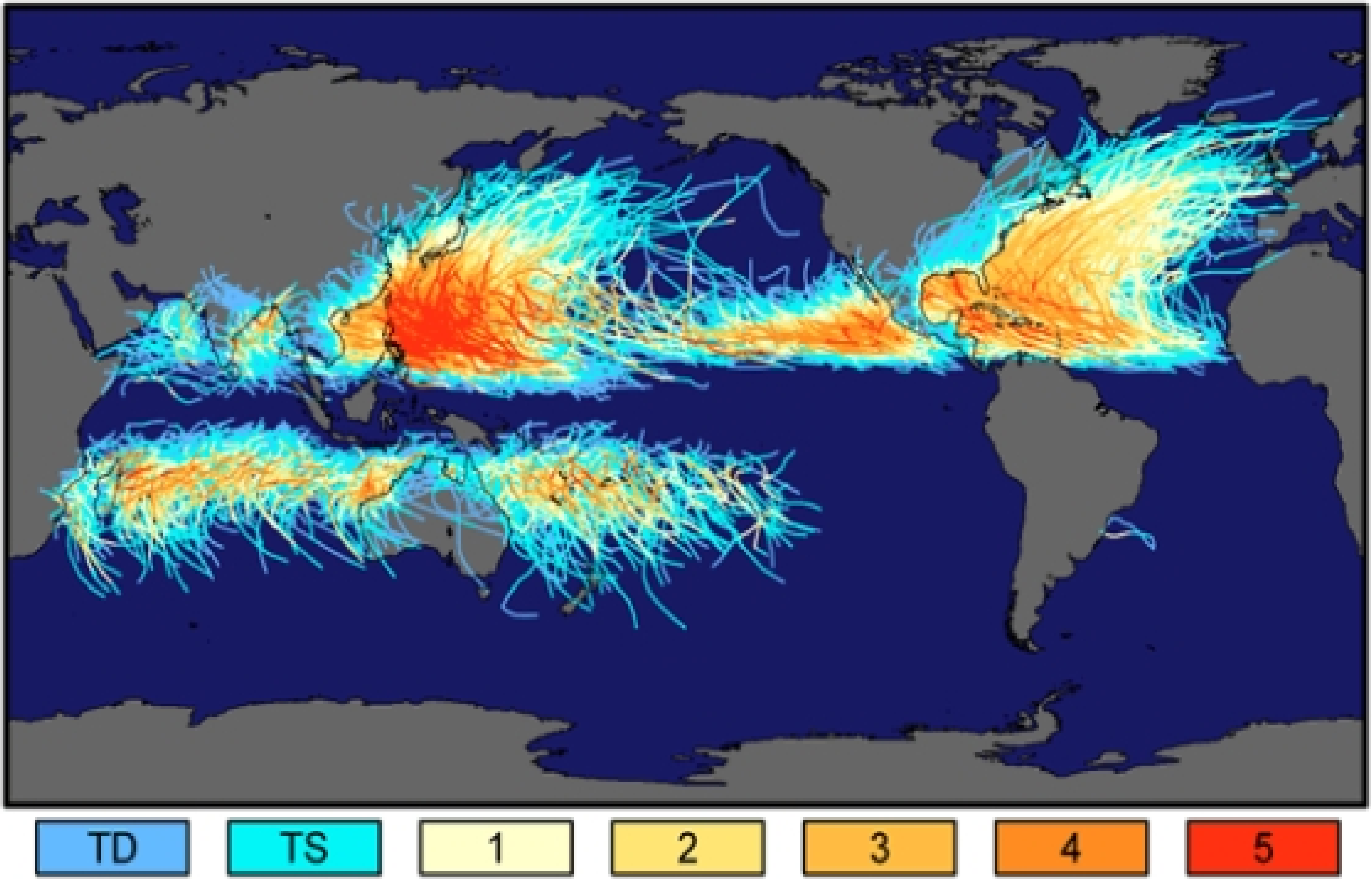

Saffir-Simpson Hurricane Intensity Scale

NASA

Typical life-cycle of an atlantic cyclone

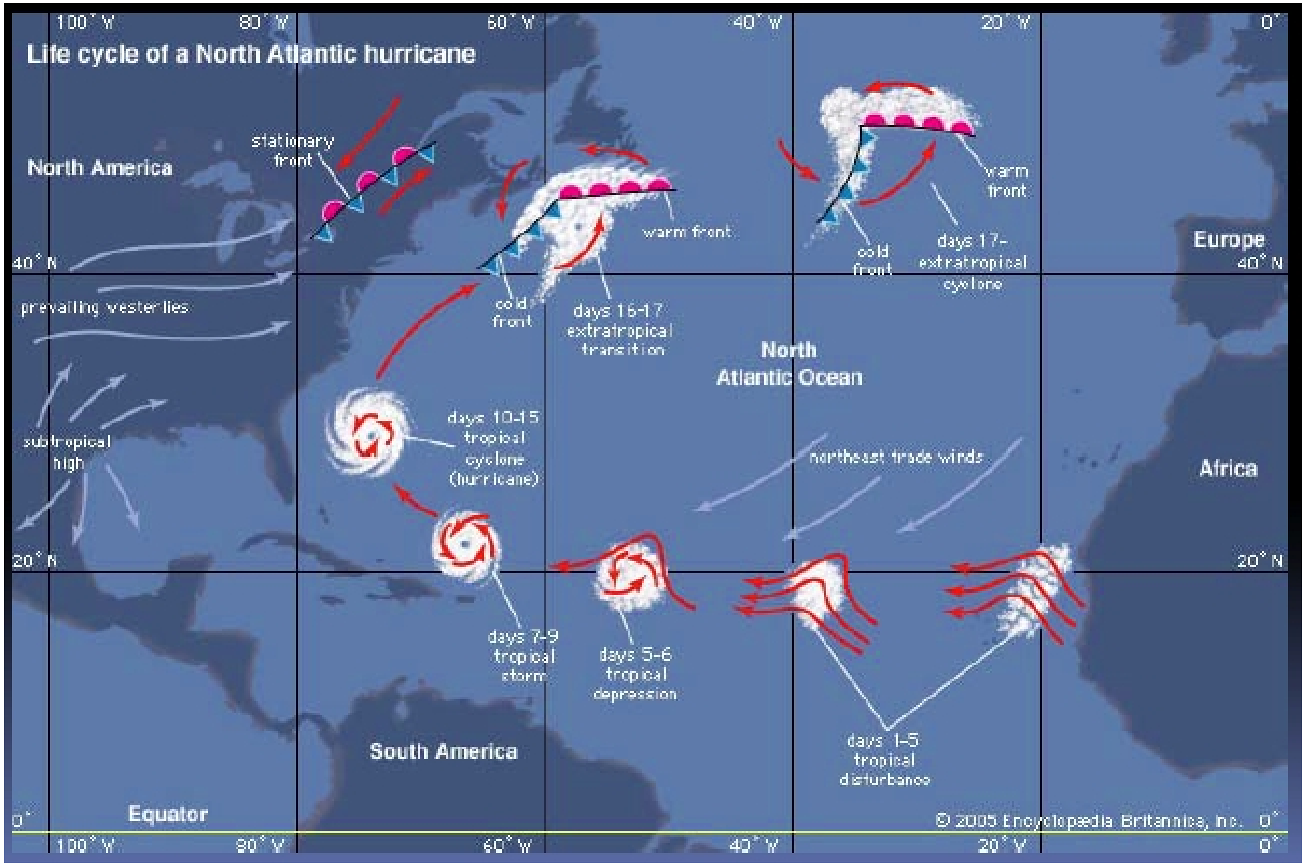

NOAA

<table>
<tr><th>Vitesse vents (kt)</th><th>Vitesse vents (m.s^{-1})</th><th>Atlantique Nord Pacifique Nord-Est</th><th>Echelle Saffir-Simpson</th><th>Pacifique Nord-Ouest</th><th>Echelle Typhon</th><th>Sud-Ouest Océan Indien</th></tr>
<tr><td>< 28</td><td>< 14</td><td rowspan="2">Tropical depression (TD)</td><td rowspan="2">-</td><td rowspan="2">TD</td><td rowspan="2">2</td><td>Perturbation Tropicale (PT)</td></tr>
<tr><td>$28 - 33$</td><td>$14 - 16$</td><td>Dépression Tropicale (DT)</td></tr>
<tr><td>$34 - 47$</td><td>$17 - 24$</td><td>Tropical storm (TS)</td><td>-</td><td>TS</td><td>3</td><td>Tempête tropicale (TT) modérée</td></tr>
<tr><td>$48 - 63$</td><td>$25 - 33$</td><td>Severe TS</td><td>-</td><td>Severe TS</td><td>4</td><td>Forte TT</td></tr>
<tr><td>$64 - 83$</td><td>$34 - 42$</td><td>Hurricane (H)</td><td>1</td><td rowspan="6">Typhoon (T)</td><td rowspan="6">5</td><td rowspan="2">Cyclone tropical (CT)</td></tr>
<tr><td>$84 - 89$</td><td>$43 - 45$</td><td rowspan="2">Severe H</td><td rowspan="2">$2 - 3$</td></tr>
<tr><td>$90 - 114$</td><td>$46 - 59$</td><td>CT intense</td></tr>
<tr><td>$115 - 129$</td><td>$60 - 66$</td><td rowspan="3">Very severe or major H</td><td rowspan="2">4</td><td rowspan="3">CT très intense</td></tr>
<tr><td>$130 - 136$</td><td>$67 - 70$</td></tr>
<tr><td>> 136</td><td>> 71</td><td>5</td></tr>
</table>

M.D. Leroux, Météo France

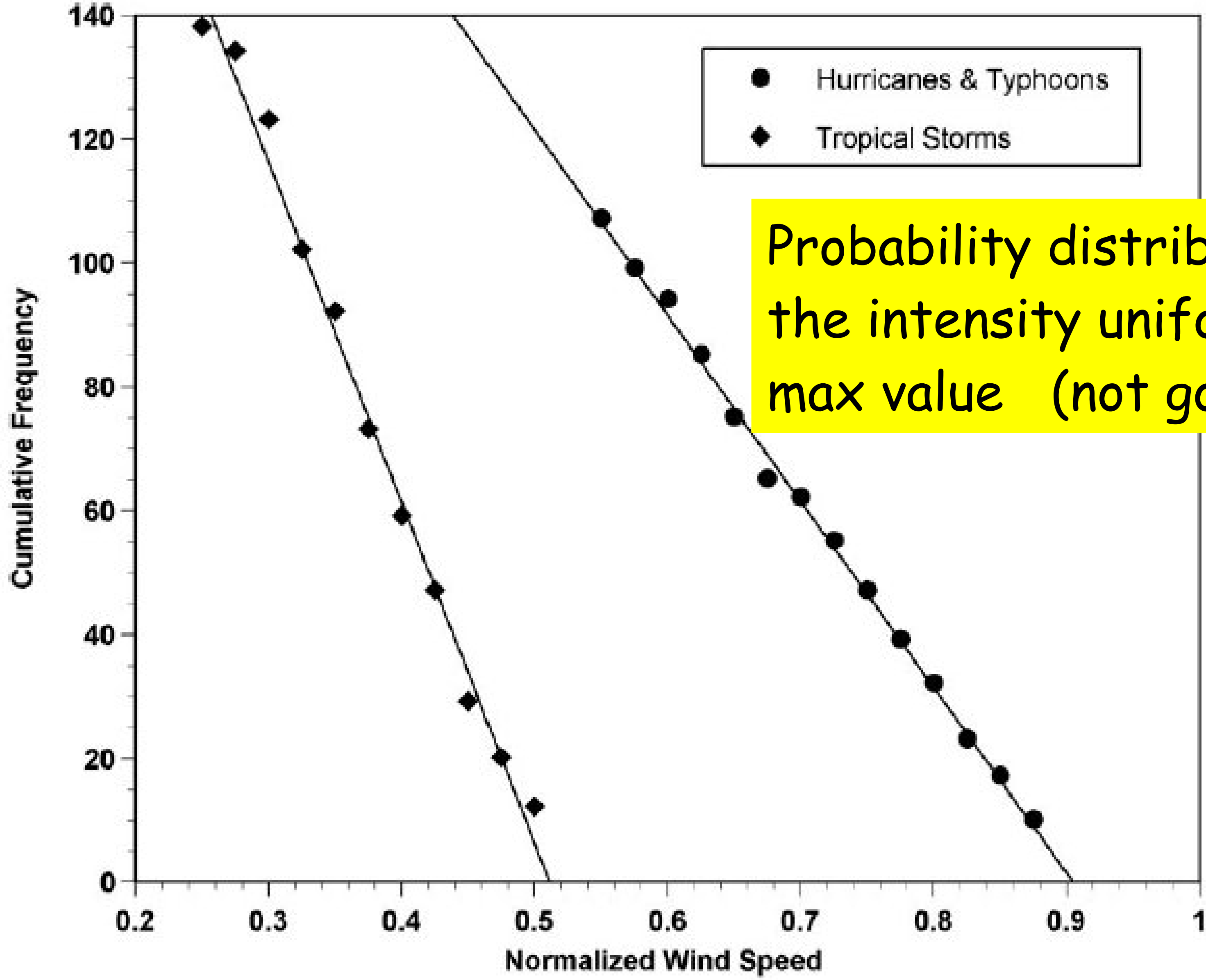

Probability distribution of the intensity uniform until max value (not good)

Figure 2 Total number of tropical cyclones with normalized wind speeds exceeding the value on the abscissa, from 1957 to 1999 in the North Atlantic and from 1970 to 1999 in the western North Pacific. The wind speeds have been normalized by the theoretical maximum wind speed calculated from climatological data using Equation 8. From Emanuel (2000).

Category1

Category 5

Category 3

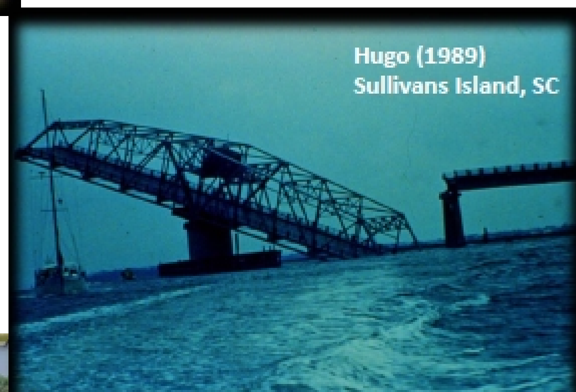

Category 2

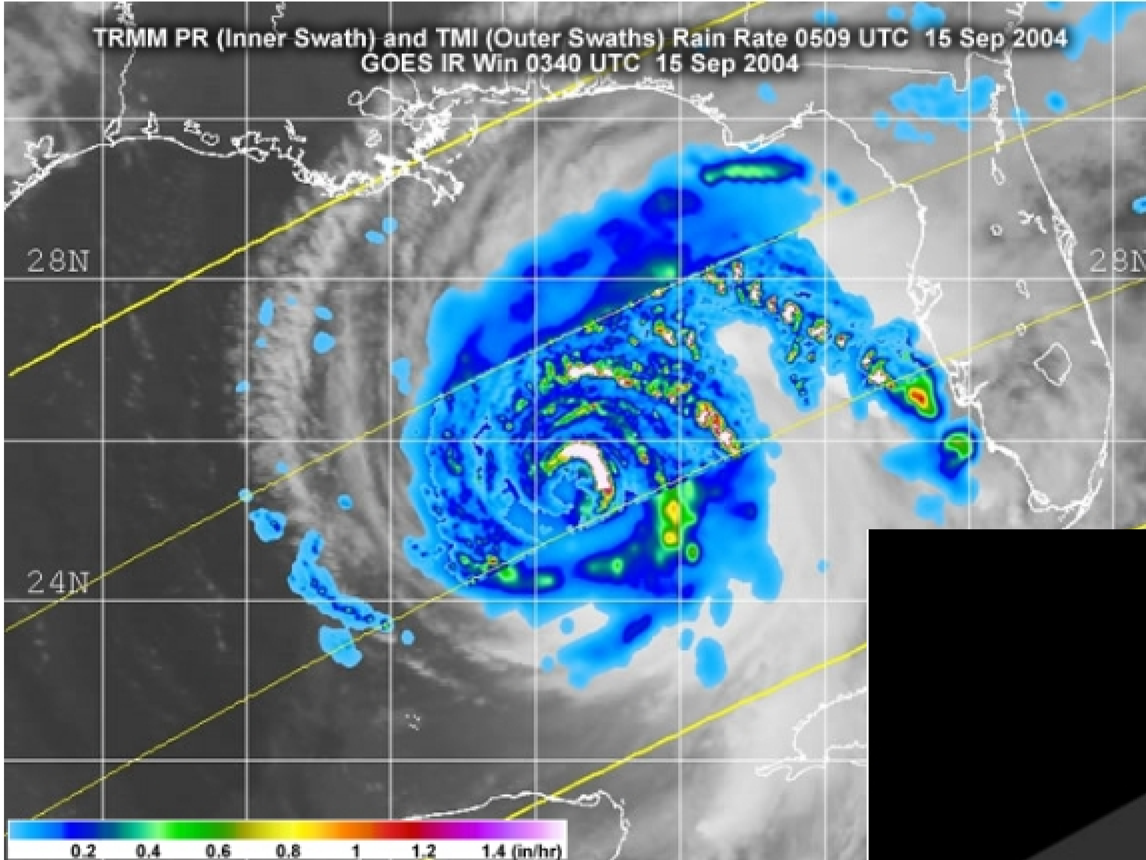

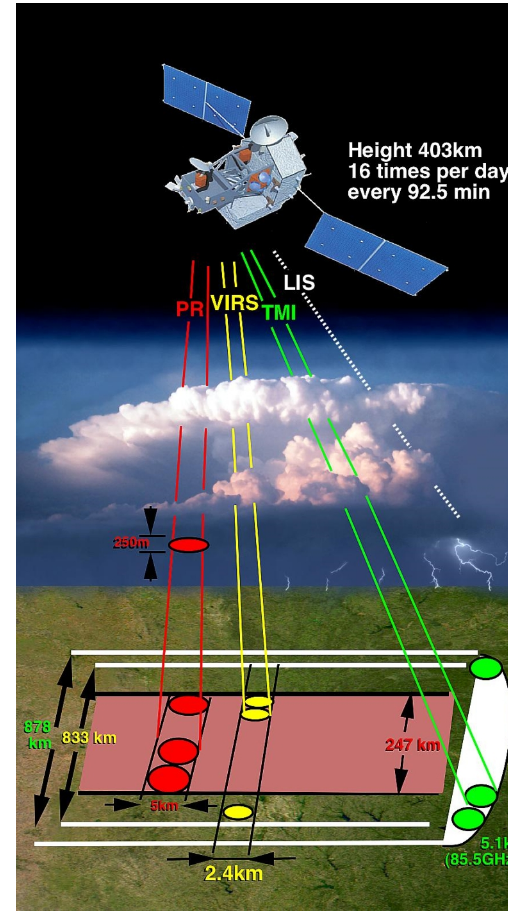

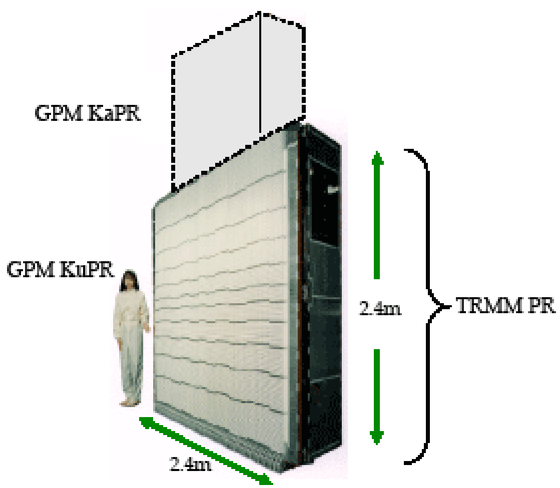

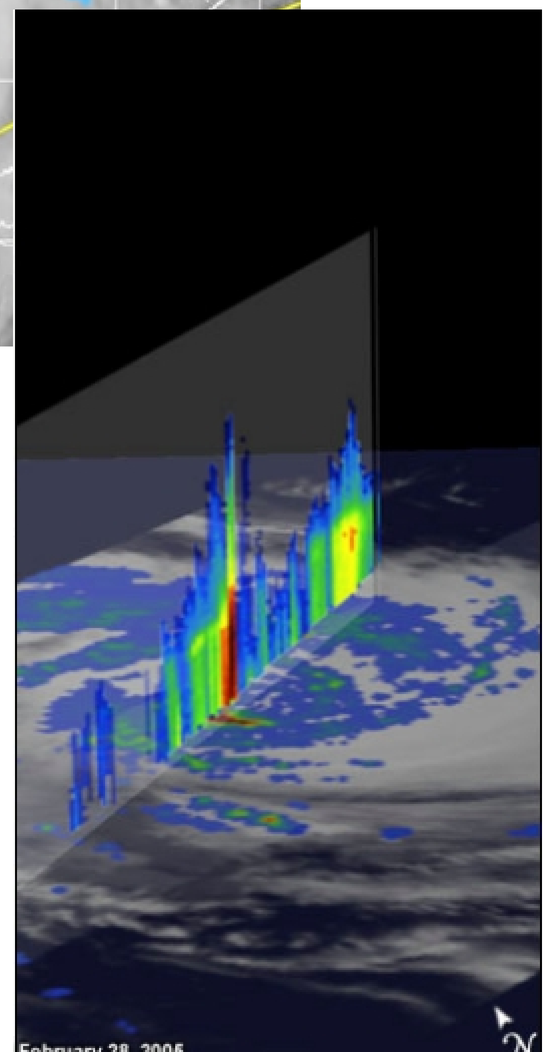

Précipitations obtained from the 13 Ghz radar of TRMM.

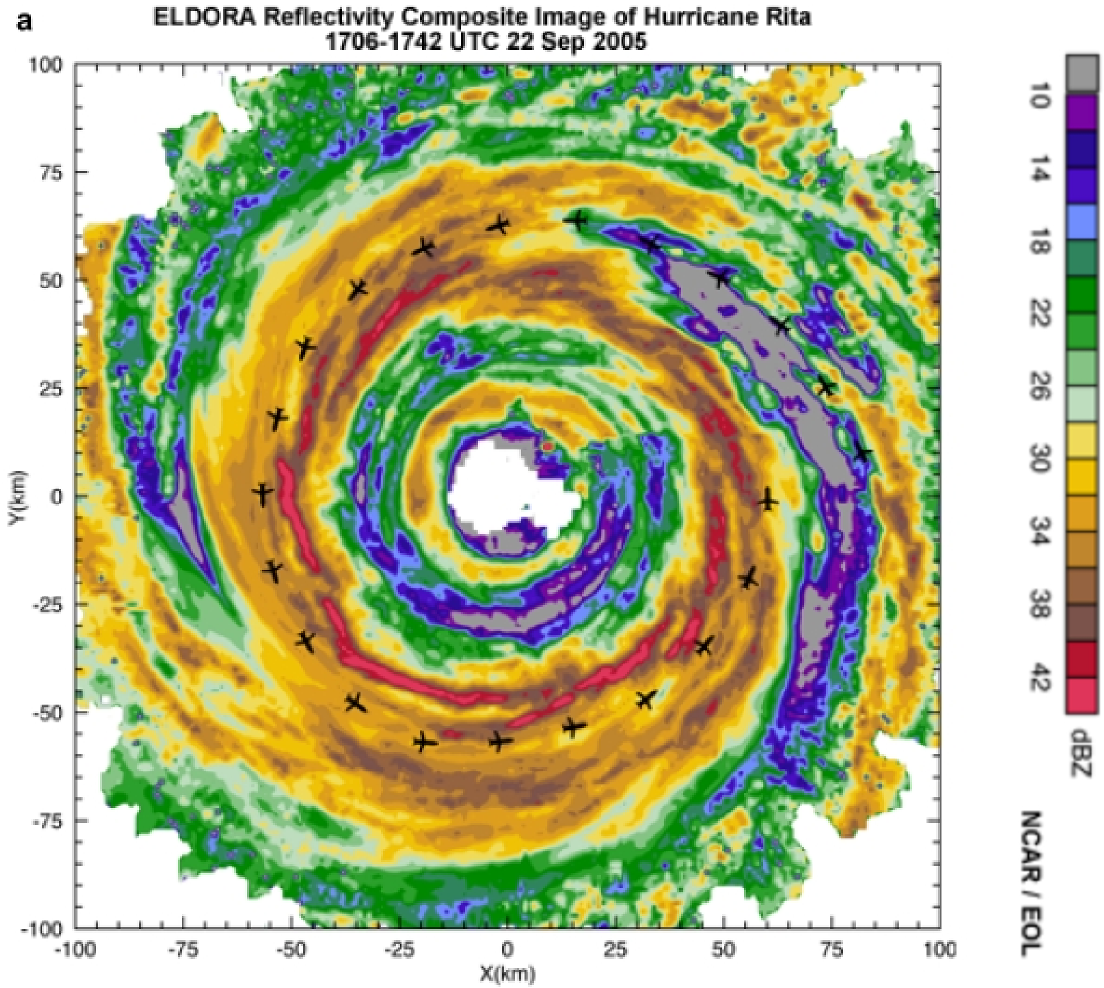

Composite images of the cyclone Rita measured by the airborne radar ELDORA.

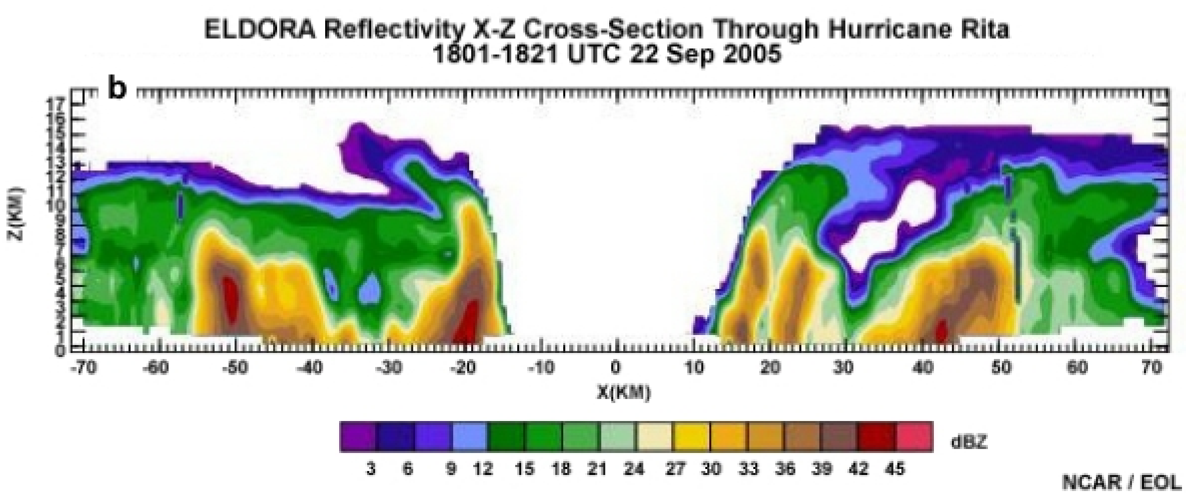

IMAGE DU 22/01/2002 14:51 UTC

METEO-FRANCE - CMRS DE LA REUNION

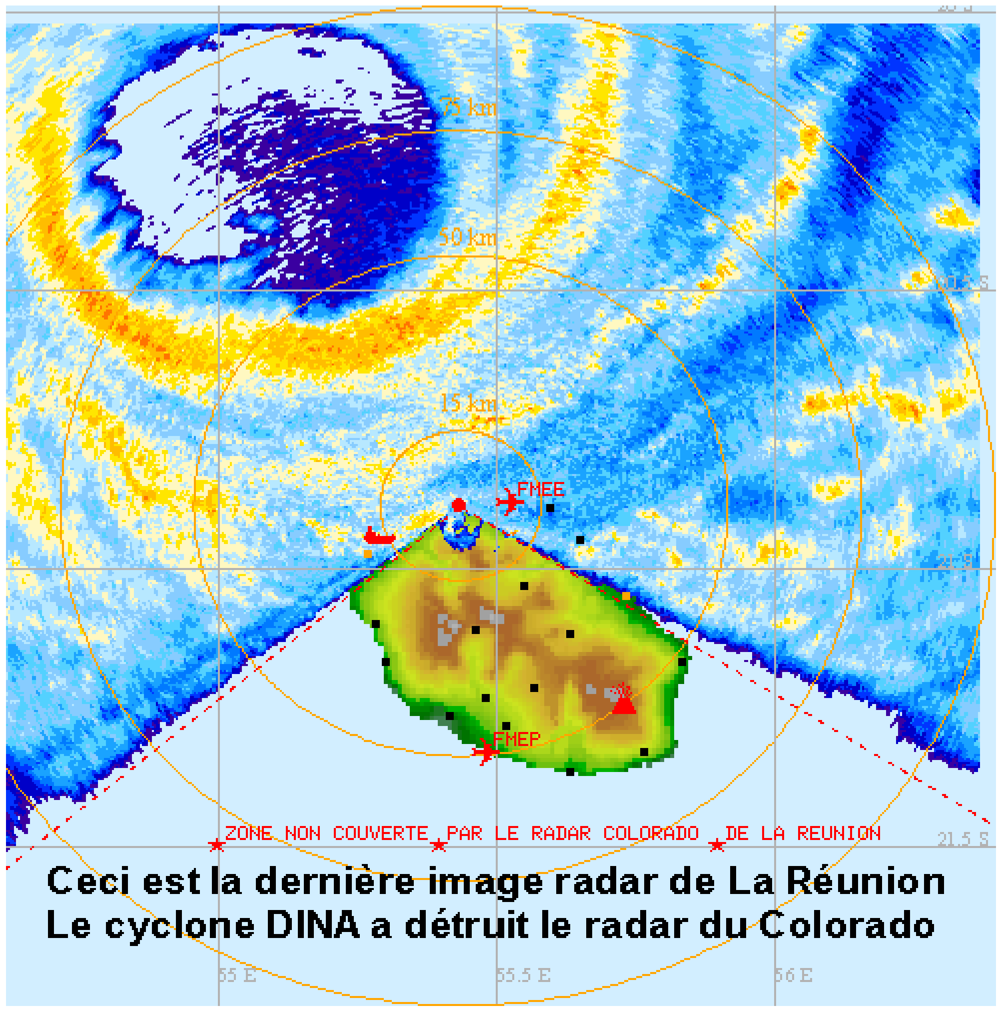

Motion of a cyclone

The low and high perturbations are generated by advection of planetary potential vorticity.

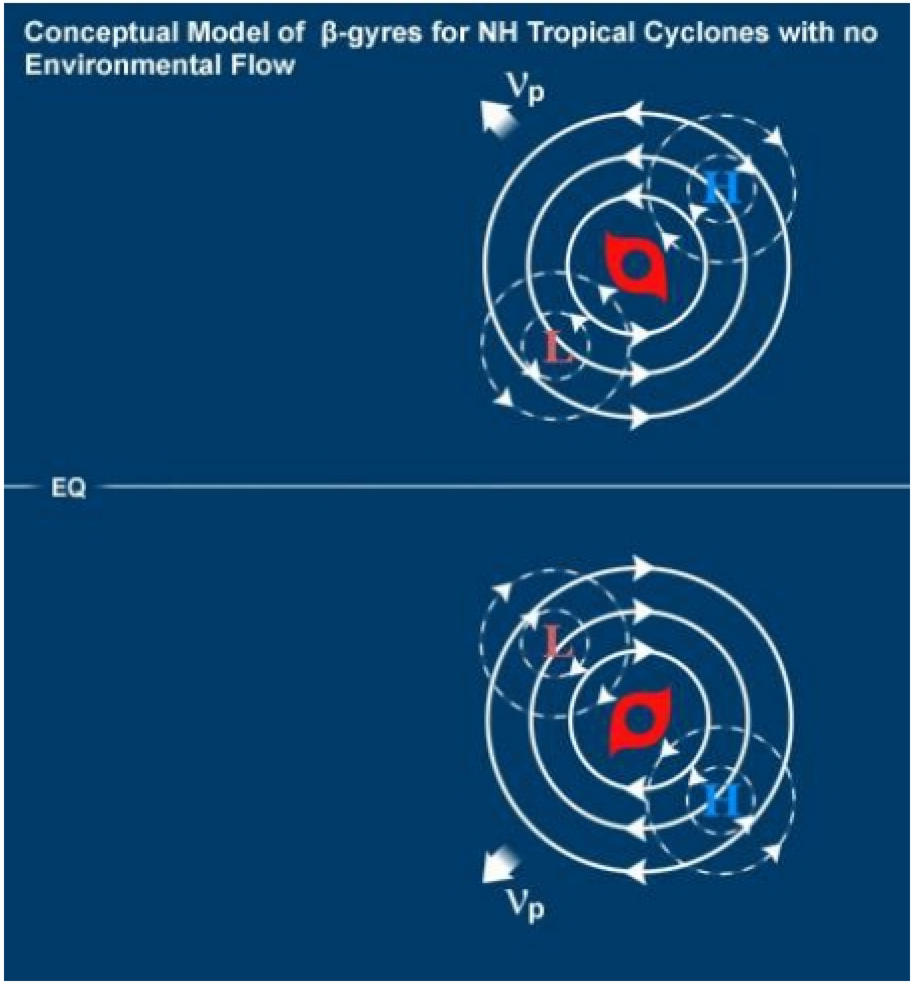

COMETS

Cloud wall inside the eye of the cyclone (photo from a « huricane hunter » plane)

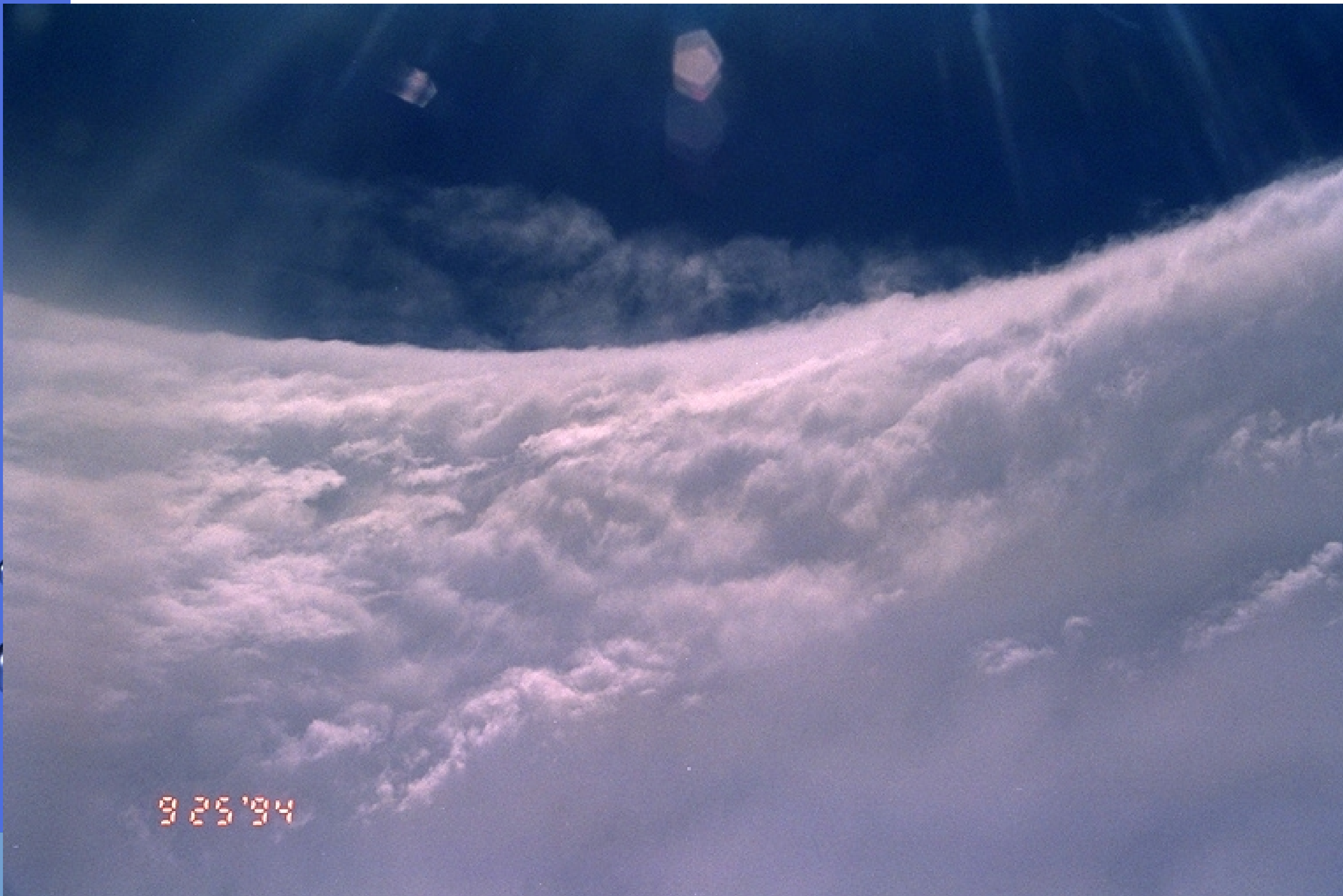

The cyclone eye does not stay always symmetric

Cyclone Isabel
12/09/2003

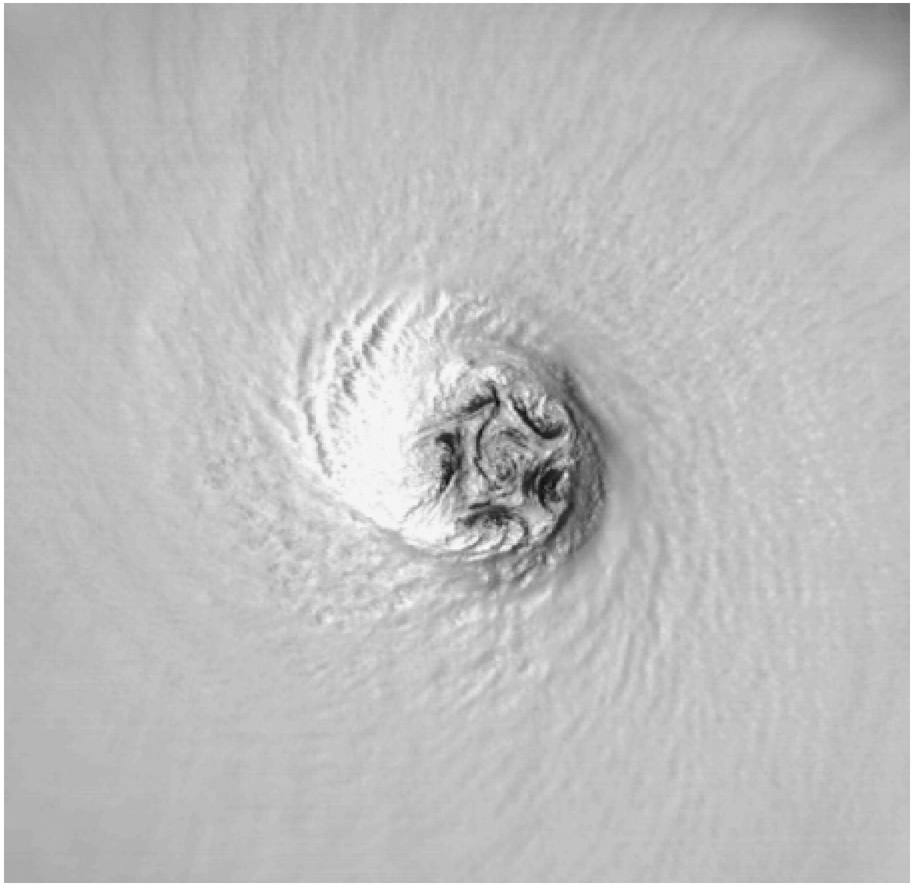

200 km

Rozoff et al., 2006

Regeneration of the cyclone wall and intensification

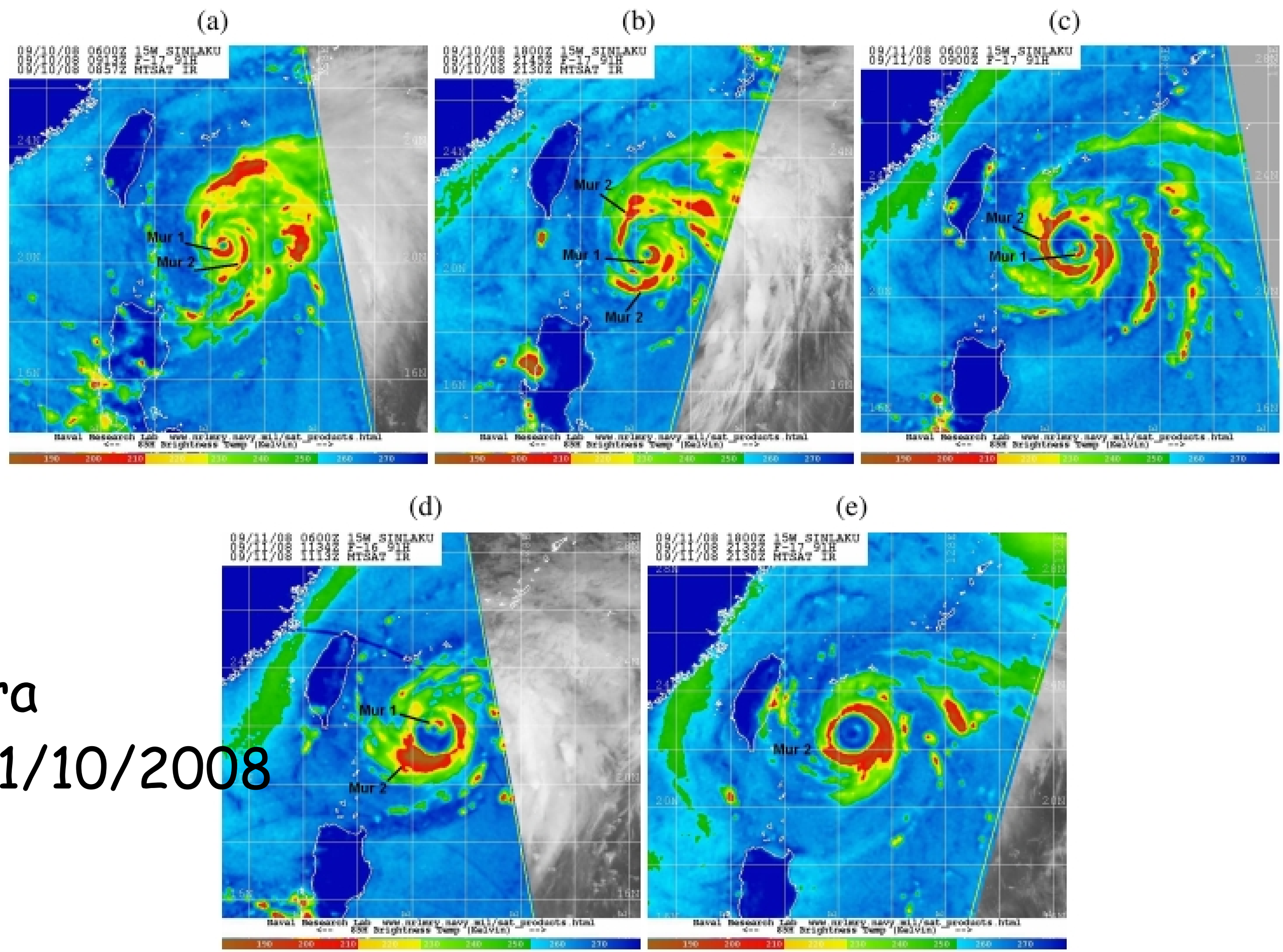

Dora
9-11/10/2008

M.D. Leroux

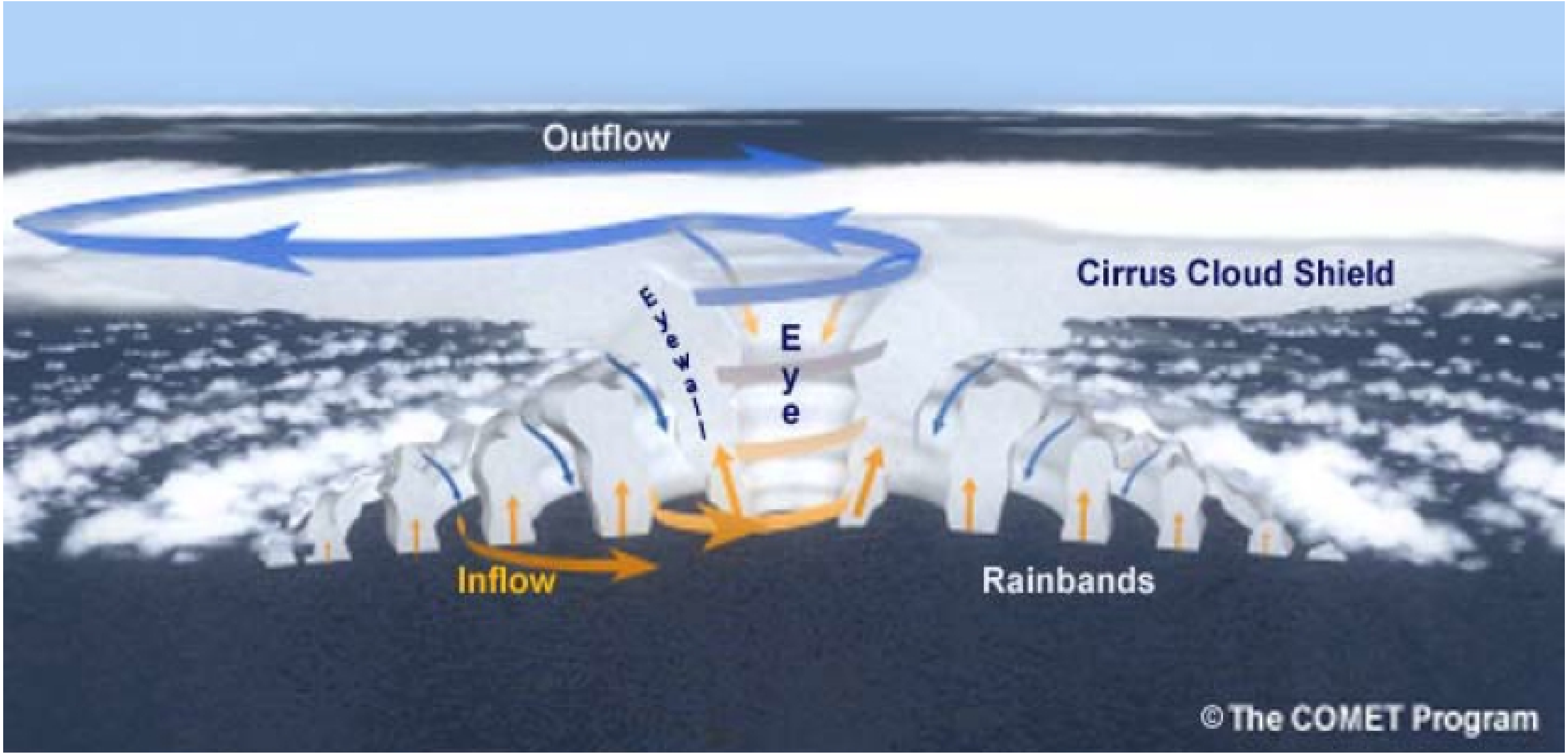
Outflow
Cirrus Cloud Shield
Eyewall
Eye
Inflow
Rainbands
© The COMET Program

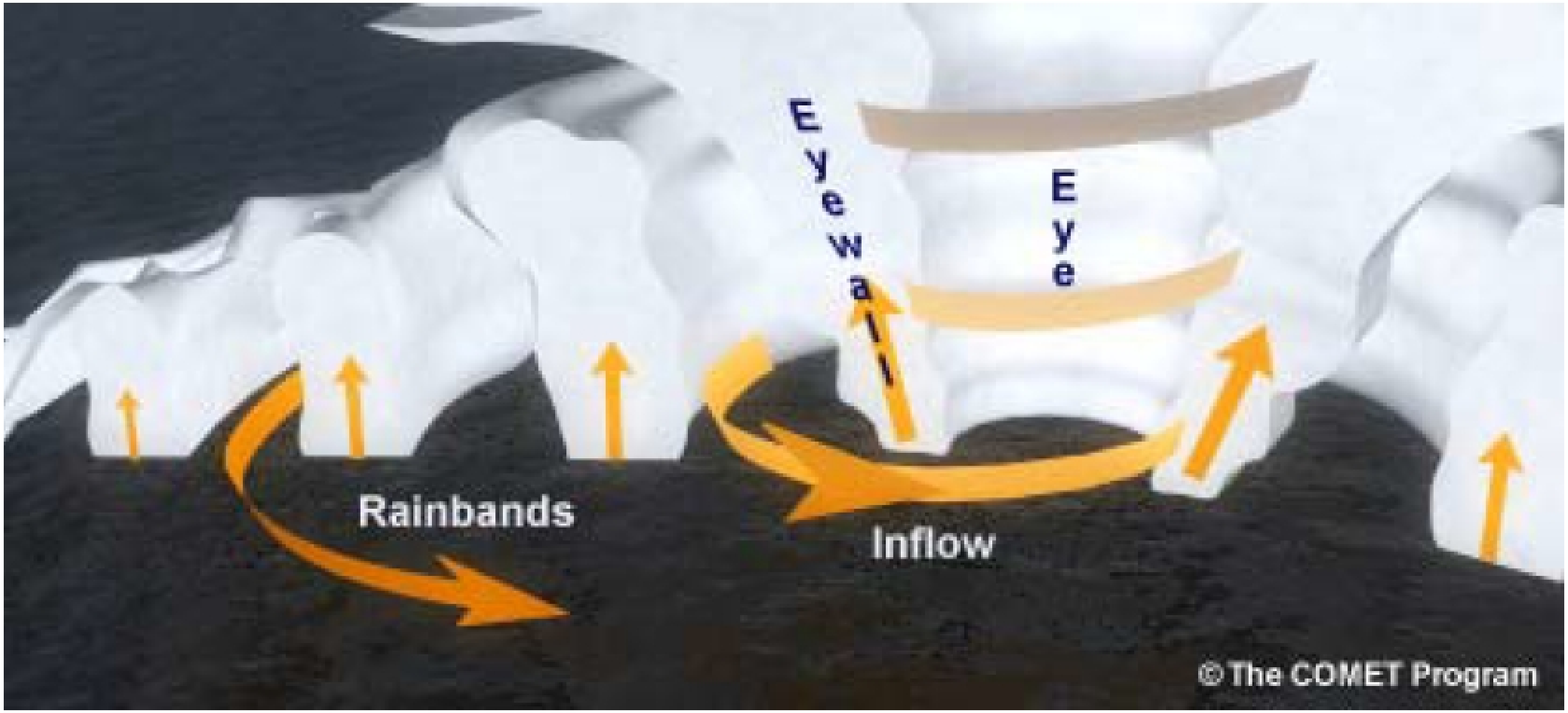
Eyewall
Eye
Rainbands
Inflow
© The COMET Program

Vertical motion in a tropical cyclone

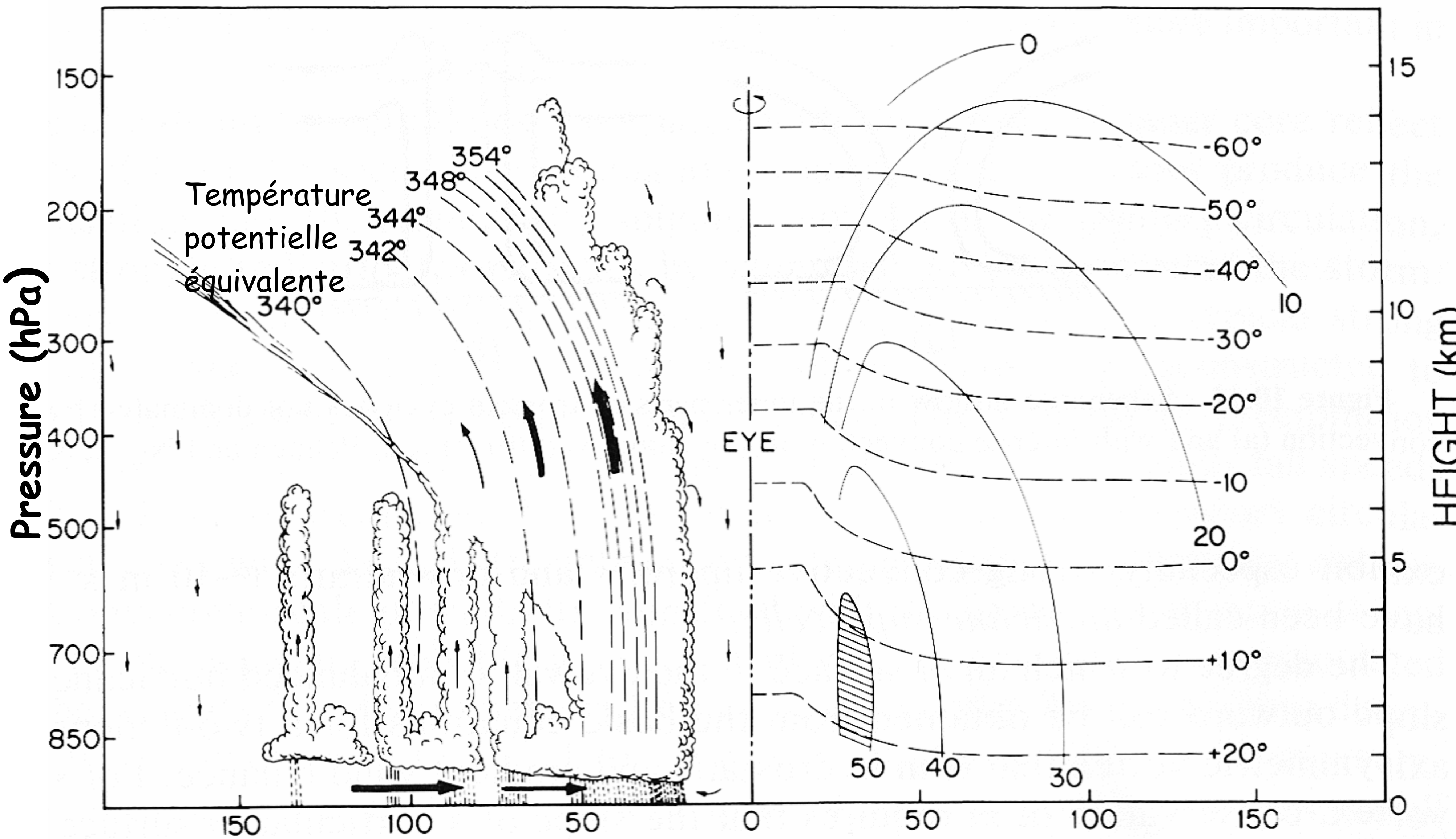

Ascending motion Radial distance (km) **Tangential speed**

The cyclone as a Carnot machine

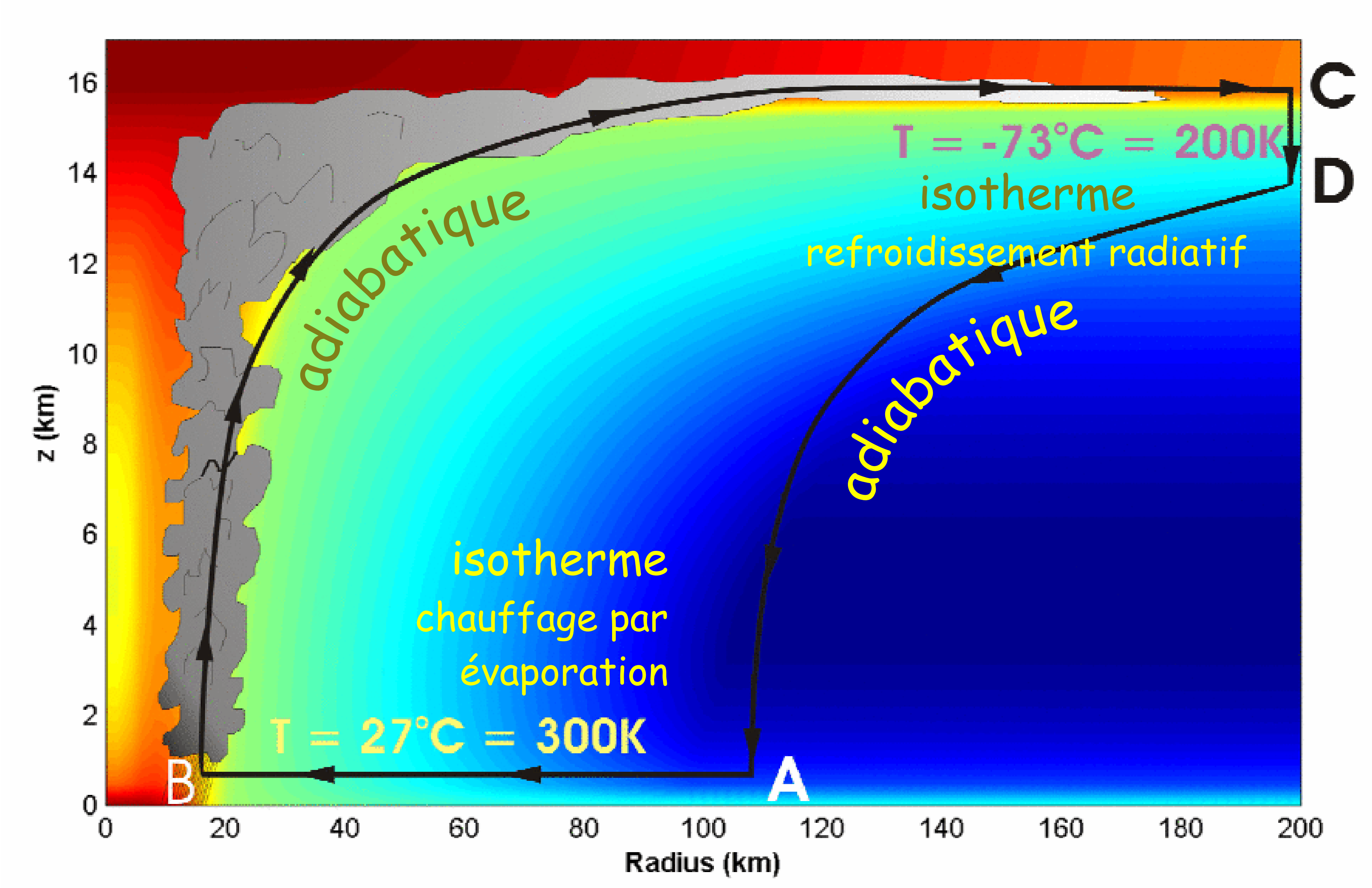

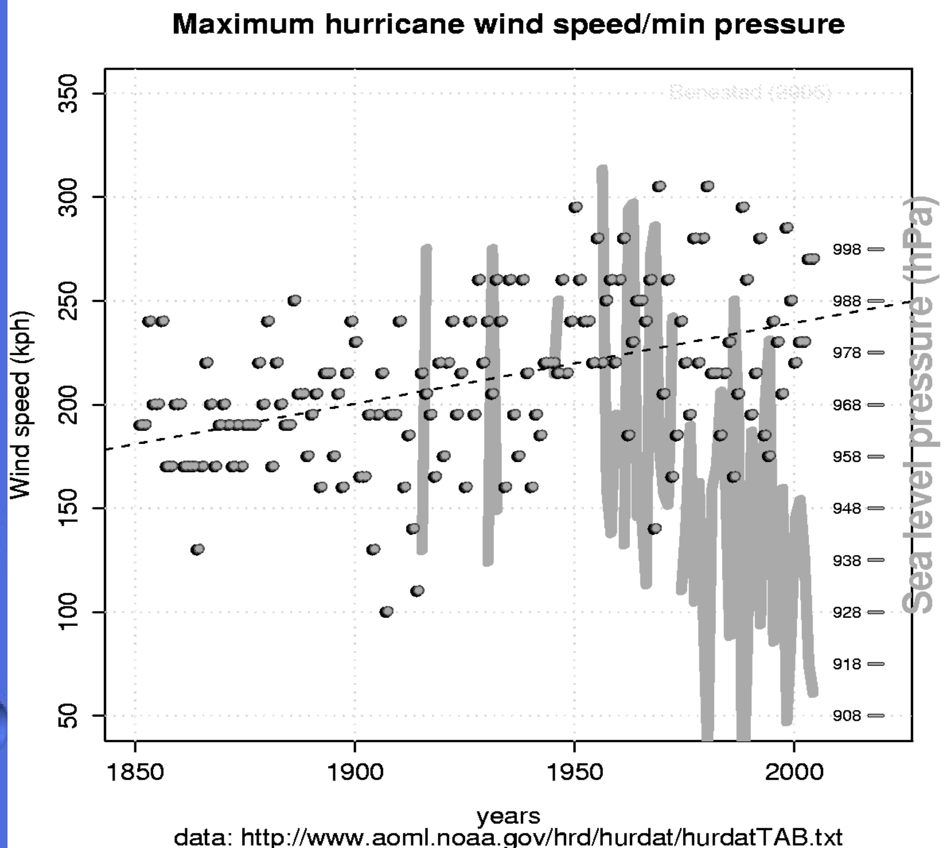

Intensity index of tropical cyclones

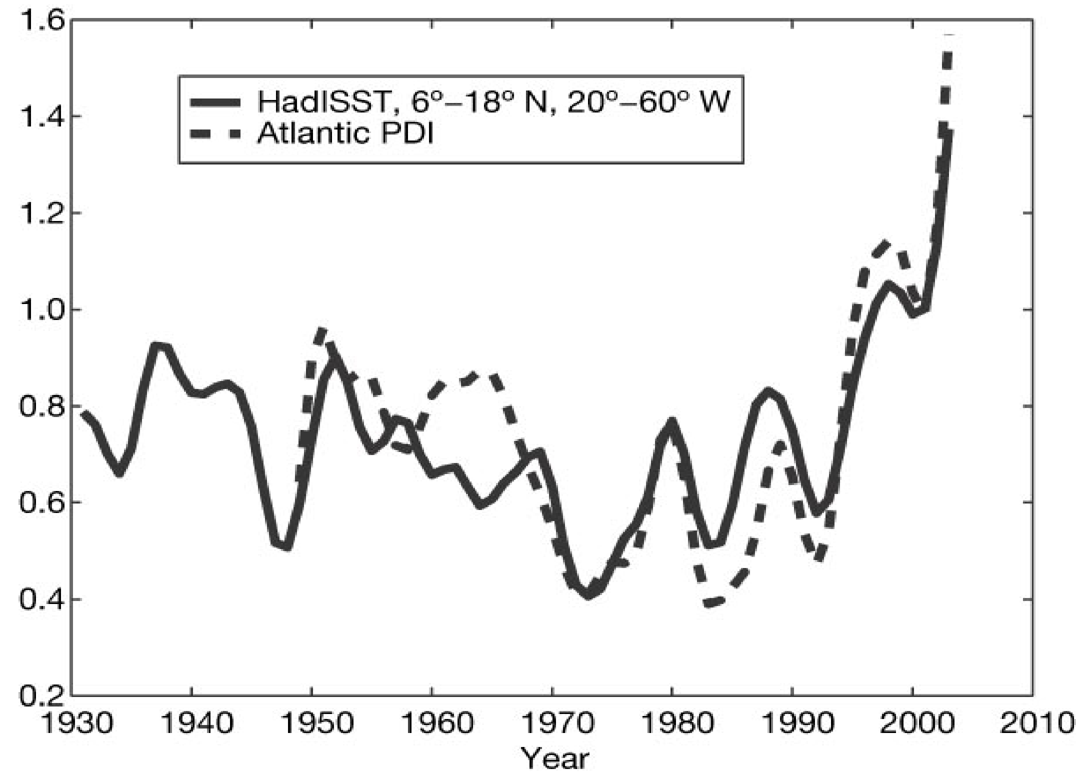

K. Emanuel, Nature, 2005

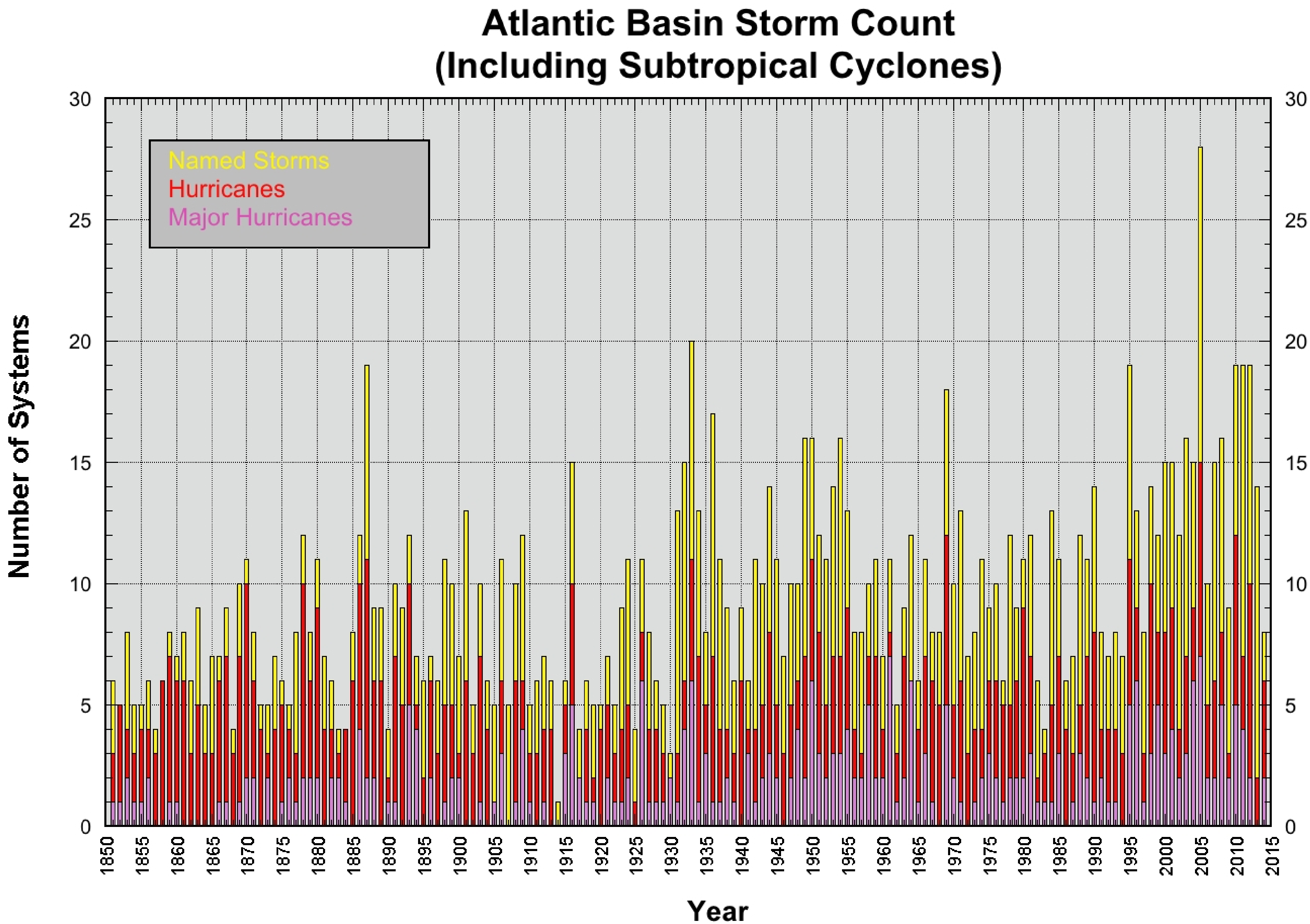

Atlantic Basin Storm Count
(Including Subtropical Cyclones)
Named Storms
Hurricanes
Major Hurricanes
Number of Systems
Year
0
5
10
15
20
25
30
1850
1855
1860
1865
1870
1875
1880
1885
1890
1895
1900
1905
1910
1915
1920
1925
1930
1935
1940
1945
1950
1955
1960
1965
1970
1975
1980
1985
1990
1995
2000
2005
2010
2015

Source NHC

CLIMATIC PROJECTIONS

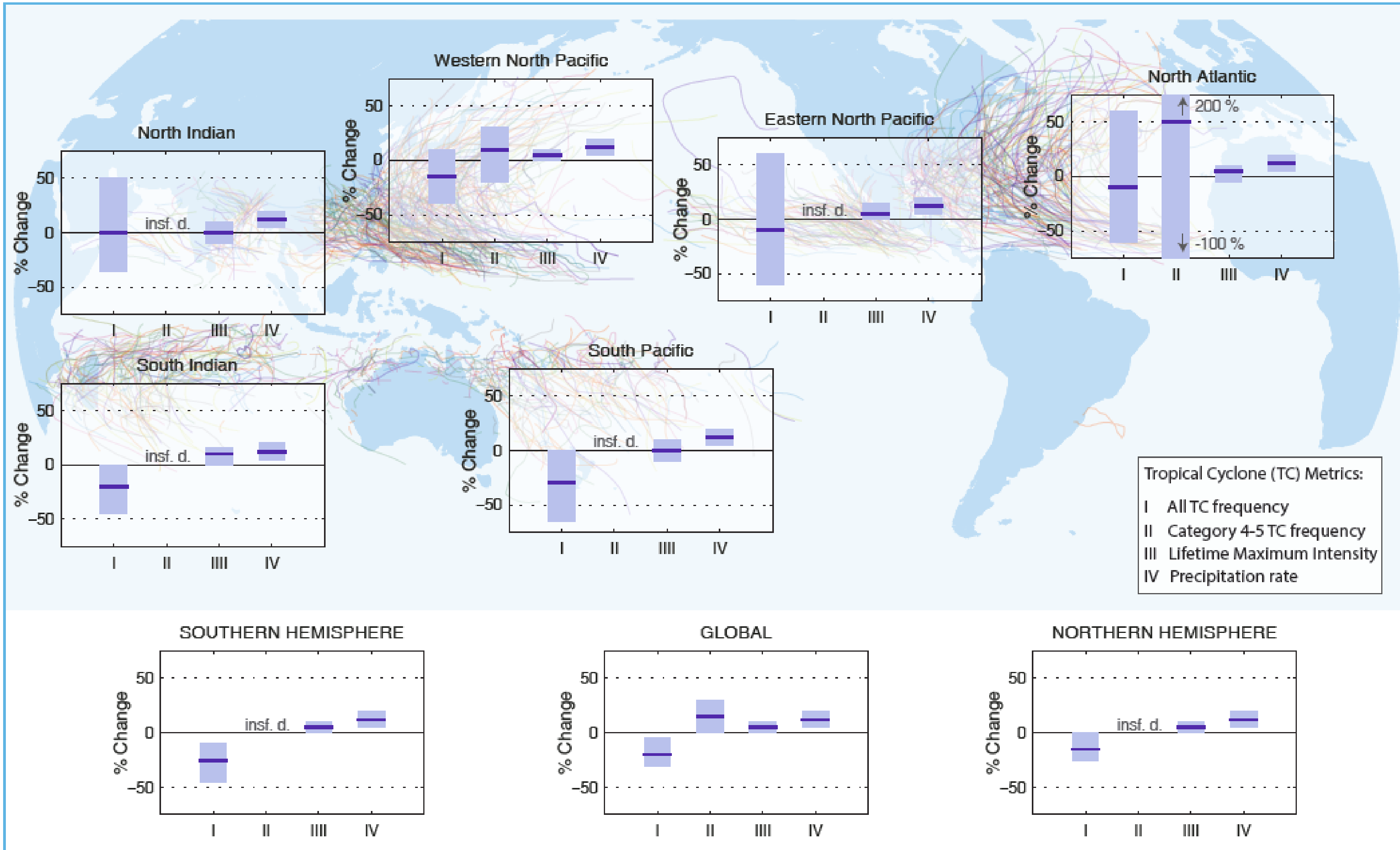

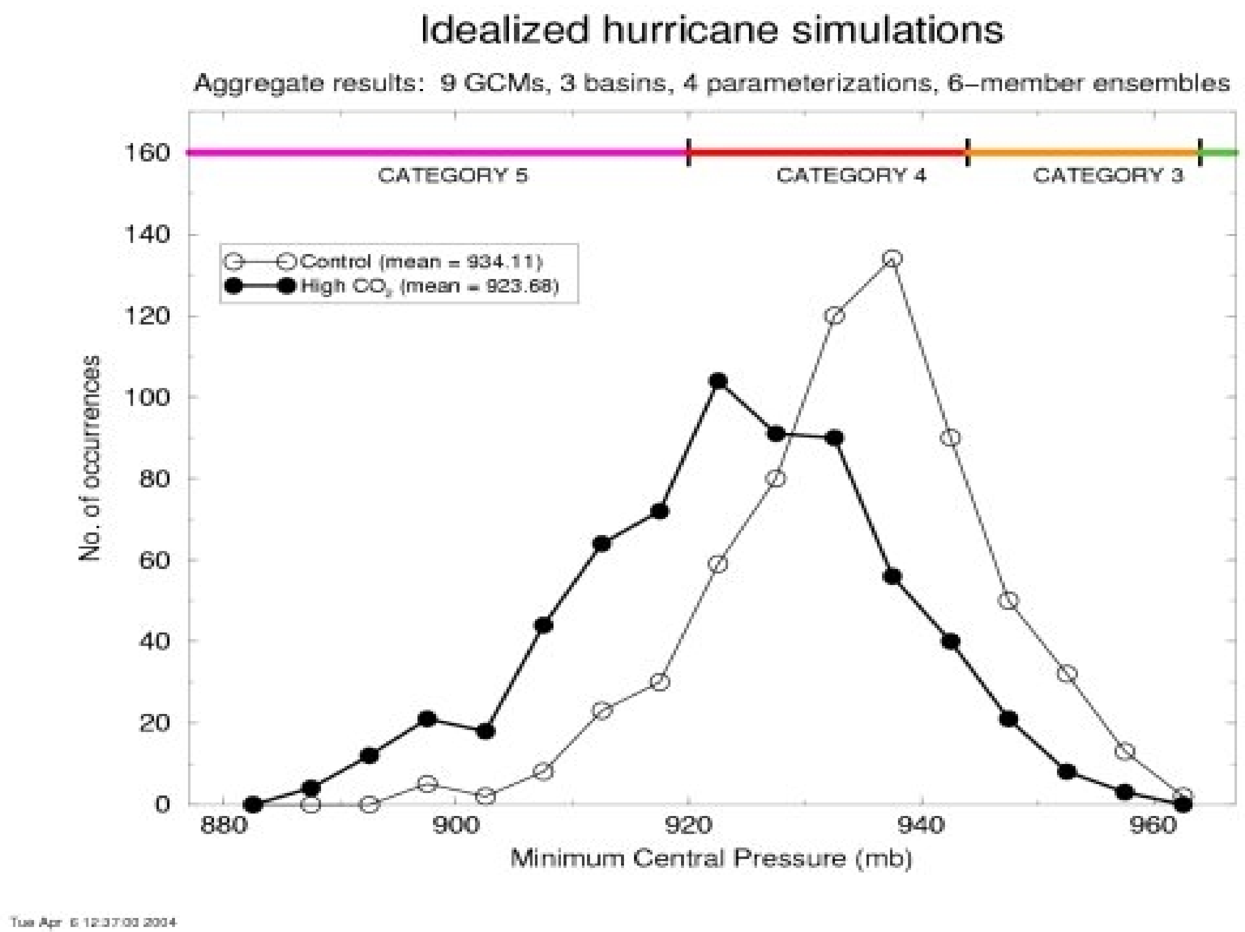

Knutson & Tuleya, J. Climate, 2004

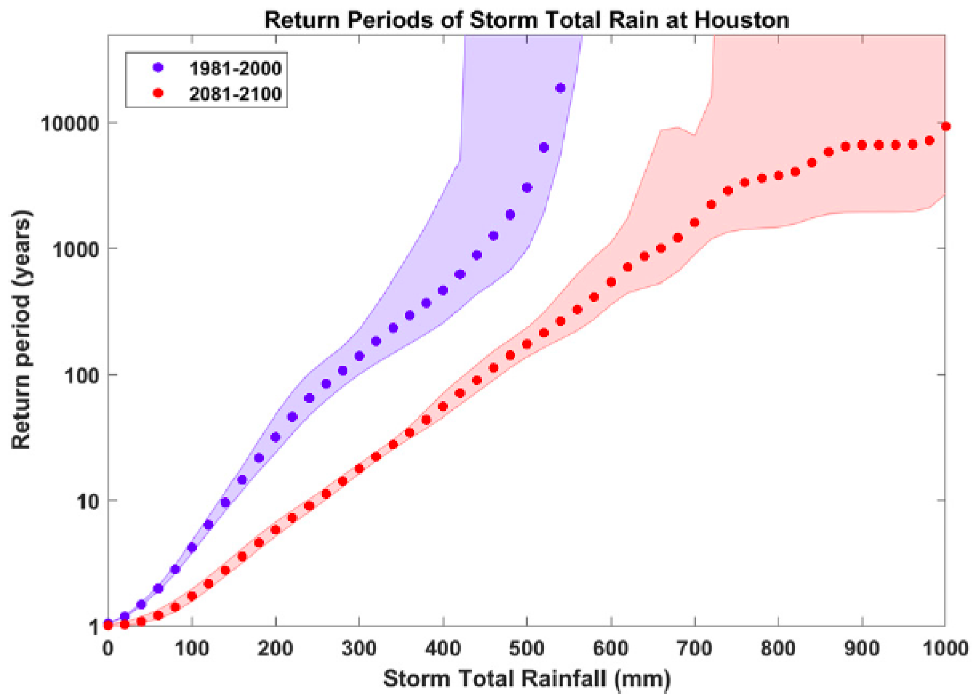

Fig. 4. Return periods of hurricane total rainfall (millimeters) at the single point of Houston, Texas, based on 3,700 simulated events each from six global climate models over the period 1981–2000 from historical simulations (blue), and 2081–2100 from RCP 8.5 simulations (red). The dots show the six-climate-set mean and the shading shows 1 SD in storm frequency, remapped into return periods.

Emanuel, 2017